Chem Soc Rev

RSC Publishing

REVIEW ARTICLE

View Article Online
View Journal | View Issue

Cite this: *Chem. Soc. Rev.*, 2013, **42**, 3033

Narrow bandgap colloidal metal chalcogenide quantum dots: synthetic methods, heterostructures, assemblies, electronic and infrared optical properties†

Stephen V. Kershaw,* Andrei S. Susha and Andrey L. Rogach

Received 10th August 2012

DOI: 10.1039/c2cs35331h

www.rsc.org/csr

The chemistry, material processing and fundamental understanding of colloidal semiconductor nanocrystals (quantum dots) are advancing at an astounding rate, bringing the prospects of widespread commercialization of these novel and exciting materials ever closer. Interest in narrow bandgap nanocrystals in particular has intensified in recent years, and the results of research worldwide point to the realistic prospects of applications for these materials in solar cells, infrared optoelectronics (*e.g.* lasers, optical modulators, photodetectors and photoimaging devices), low cost/large format microelectronics, and in biological imaging and biosensor systems to name only some technologies. Improvements in fundamental understanding and material quality are built on a vast body of experience spread over many different methods of colloidal synthetic growth, each with their own strengths and weaknesses for different materials and sometimes with regard to particular applications. The nanocrystal growth expertise is matched by a rapidly expanding, and highly interdisciplinary, understanding of how best to assemble these materials into films or hybrid composites and thereby into useful devices, and again there are many different strategies that can be adopted. In this review we have attempted to survey and compare the recent work on colloidal synthesis, film and nanocrystal composite material fabrication, concentrating on narrow bandgap chalcogenide materials and some of their topical applications in the solar energy and biological fields. Since these applications are attracting rising interest across a wide range of disciplines, from the biological sciences, device engineering, and materials processing fields as well as the physics and synthetic chemistry communities, we have endeavoured to make the review of these narrow bandgap nanomaterials both comprehensive and accessible to newcomers to the area.

1 Introduction

In the field of semiconductor nanocrystals (NCs), also termed colloidal quantum dots (QDs), research continues to grow apace with rapid advances in chemistry, materials and device physics and fabrication techniques worldwide. In the earlier years of NC research, much effort was focussed on materials with bandgaps positioned to give emission in the visible. In recent years, however, attention has increasingly turned to narrow bandgap NC materials active in the infrared (IR). These materials are of potential interest for optoelectronics (IR lasers, amplifiers, modulators); use in solar cells with extended IR absorption; as field effect transistor (FET) materials; and as fluorophores in connection with biological tissue studies to name but a few applications. We have taken the opportunity to review recent progress in a segment of this field, choosing to cover progress in the chemistry, processing and some applications (including solar energy and bio-sensors) of chalcogen containing narrow bandgap colloidally grown materials. We have not covered other types of colloidal semiconductors (groups III–V for example), in part to limit the size of the review, but also because these are already considered in several contemporary reviews, some of which are mentioned in the next section. Similarly, we have not explored the wealth of literature on the theoretical modelling (both optical and electronic) of narrow bandgap NCs in particular, though these aspects are covered to varying degrees in many of the references herein.

We have limited the scope of the materials discussed to those which emit from the near infra-red out to longer wavelengths,

Department of Physics and Materials Science & Centre for Functional Photonics (CFP), City University of Hong Kong, Hong Kong S.A.R. E-mail: skershaw@cityu.edu.hk; Fax: +852 3442 0538; Tel: +852 3442 9532

† Part of the Chemistry of Functional Nanomaterials themed issue.

though the short wavelength boundary has not been rigorously defined – in one or two cases materials are included which are in principle capable of IR emission, or which might be relevant in the case of alloys or heterostructures, even though the emission reported is mostly in the visible. The chalcogenides include CdE, HgE, PbE, Ag_2E, SnE, Bi_2E_3, $CuInE_2$ (E = S, Se or Te) and alloys and heterostructures of many of these materials. We have considered materials grown both in organic and aqueous media, and both grown directly and by ion-exchange starting with an alternate semiconductor (whether narrow bandgap or not) as a template. Ag_2E NCs and nanorods feature prominently in this latter category.

We have not included wide bandgap QD materials in which narrower intraband transitions can be created by forming n-type semiconductor QDs. Such IR transitions may in principle be obtained *via* impurity doping, or by electron transfer (*e.g.* by treatment with alkali metal compounds[1,2] or electrochemically[3,4]) or even simply transiently immediately after pulsed excitation.[5] However, to date these approaches do not yet appear to offer an alternative to interband transition materials for efficient luminescence.

Whilst many applications are mentioned in passing, we have described the use of narrow bandgap NCs in solar cells and in biological applications in more detail. Again this is in part a limitation of space and in part excused by the fact that other recent reviews (as mentioned below) cover some of the remaining applications in great detail already.

The review is written from a materials chemist's perspective – we have tried to bring out the many nuances of each groups' synthetic methods. For many years, differing properties have often been reported for nominally identical materials, and we have tried to put forward enough detail to help understand why this might be so, or at least to provide pointers to help the interested chemist look further. Here we have placed particular emphasis on reviewing and comparing synthetic methods to prepare NCs and the synthetic method/precursor materials' influence on the quality, particle size, size dispersion, overall performance, and the compatibility of the NCs with various applications. To this end we have drawn together almost 500 references in order to put together the full picture and to show the evolution of the synthetic methods rather than attempting to filter the literature to present a 'definitive' synthetic method for a given material. Whilst some methods unarguably lead to 'better' performance from particular points of view for certain materials, in some instances alternate approaches may have over-riding advantages for certain applications. For this reason, where multiple synthetic techniques can be used, we have tried to present the whole body of knowledge so that a newcomer to the field may be able to judge for themselves the better approach to take for compatibility with their intended application. As an example, it might be considered that for bio-labelling with near IR emitting QDs, water-soluble materials may be the better choice. These may be best synthesized in

Stephen V. Kershaw

Stephen V. Kershaw is a Research Fellow at City University of Hong Kong. He received his BSc in Physics and Chemistry (1980) and PhD in Physics (1984) from Manchester University, UK. Following postdoctoral research on Liquid Crystals at Manchester he joined British Telecom Laboratories (1989), working on optical materials including nanocrystals and integrated optoelectronic devices. His research continued on joining Corning's UK Research Labs in 2000 and in 2002 he co-founded a quantum dot applications startup company, acting as managing director until 2010.

Andrei S. Susha

Andrei S. Susha is a Research Fellow at City University of Hong Kong. He received his Diploma in Chemistry (1993, with honors) and PhD in Physical Chemistry (2001) from the Belarusian State University in Minsk, and worked at Max-Planck-Institute of Colloids and Interfaces in Potsdam, Germany during 1999–2003. During 2003–2009 he was a research fellow at the Department of Physics of the Ludwig-Maximilians-Universität in Munich, Germany.

Andrey L. Rogach

Andrey L. Rogach is a Chair Professor of Photonics Materials and the Director of the Centre for Functional Photonics at City University of Hong Kong. He received his Diploma in Chemistry (1991, with honors) and PhD in Physical Chemistry (1995) from the Belarusian State University in Minsk, and worked as a staff scientist at the Institute of Physical Chemistry of the University of Hamburg, Germany, from 1995 to 2002. During 2002–2009 he held a tenured position of a lead staff scientist at the Department of Physics of the Ludwig-Maximilians-Universität in Munich, where he completed his habilitation in Experimental Physics.

water in the first place, or if grown in organic media a solvent and ligand exchange process may be required. Conversely, for thin film electro-optic applications, spin-coating fabrication may be desirable and as such deposition from volatile organic solvents may lead to films with superior optical quality.

After first putting our review in context alongside other previous and contemporary reviews which either overlap or complement the narrow bandgap NC area, the Synthetic Methods section surveys methods of colloidal NC growth grouped by materials and includes in general both organic and aqueous colloidal chemistries. In many cases both approaches can be used, and for some materials one may have an advantage over the other. The reasons for favouring one approach may be historical, or it may prove to lead to better defined shapes, sizes or quantum efficiency, or the choice of ligands (*e.g.* their sizes, or functionalities) available by either method may be an advantage in a given application. For this reason we have tried to include *all* colloidal or related synthetic methods for each material, not just the current vogues. We have also tried to highlight some of the synthetic subtleties for each material, particularly for the hot injection approaches, where the choice of solvents, temperatures, precursors and method can have a marked influence on the quality of the NCs obtained.

The bandgap of a given semiconductor NC is blue shifted from that of the corresponding bulk material. The bulk bandgap of a ternary (or quarternary) alloy semiconductor is fixed by the bowing curve (bandgap *vs.* composition) for the combination of components and mostly lies between the limiting pure binary material cases *i.e.* for a ternary $A_xB_{1-x}C$ say, the bandgap would lie between that of AC and BC in most cases. In a few examples the bowing factor is large enough that the bandgap of the alloy may dip below that of the lower bandgap binary material. Armed with these facts, the bulk bandgap energies of various semiconductors (as listed in Table 1) can be used as a starting point to select likely narrow bandgap NC materials of interest.

Prior to reviewing applications we next survey physical and synthetic methods used to fabricate films of NCs, both as embedded colloidal particles within other types of host materials and as the network forming material itself. The main applications reviewed are various designs of solar cell (*e.g.* QD sensitized solar cells, NC heterostructure photovoltaics, *etc.*), and biological applications, and again this is approached from the chemical synthesis and material processing point of view, rather than the intricacies of the device physics, *etc.* One or two examples of other applications such as FETs, photodetectors and LEDs are mentioned in passing in the films and film formation sections but are not exhaustively summarised here.

Table 1 Representative bulk bandgap energies for narrow bandgap semiconductors and approximate[a] bandgap ranges for ternary alloys

Material	Bandgap/approximate bandgap range (alloys) (eV)
PbS	0.37
PbSe	0.27
PbTe	0.28
CdTe	1.5
HgS	0.5
HgSe	−0.06
HgTe	−0.3
$Hg_xCd_{1-x}Te$	−0.3–1.5
$Hg_xCd_{1-x}Se$	−0.06–1.9
$HgS_{1-x}Se_x$	−0.06–0.5
$CdS_{1-x}Se_x$	1.8–2.5
$CdS_{1-x}Te_x$	1.5–2.4
Ag_2S	0.93
Ag_2Se	0.15
Ag_2Te	0.06
Cu_2S	1.2
Bi_2S_3	1.7
Bi_2Se_3	0.3
Bi_2Te_3	0.16
SnTe	−0.5
SnS	1.0
$CuInSe_2$	1.0
$CuInS_2$	1.2
$AgInS_2$	1.2

[a] Assuming the alloy bandgap lies between the binary semiconductor extremes at $x = 0$, $x = 1$. Note in some cases bowing may cause intermediate compositions to have slightly lower bandgaps than the range given.

2 Reviews, overviews and perspectives

Whilst this review is limited to the synthesis and some of the properties and applications of colloidal narrow bandgap NCs, there have been numerous recent reviews and perspective articles which overlap in some areas or which centre on other aspects or cover wider or different NC material classes. Here we briefly list some of these articles which may be helpful where the reader may want to go beyond our purview or needs to see the work on narrow bandgap materials in a more general context.

Eychmüller's[6] feature article in 2000 neatly summarised the work up to that point on the structural and photophysical characterisation of a wide range of semiconductor NCs, including both narrow bandgap and wide bandgap materials, and also reviewed some of the latest optical measurement techniques. Cushing *et al.*[7] reviewed a wide range of synthetic methods to form inorganic nanoparticles in general, whilst Burda *et al.*'s[8] review focussed much more on semiconductor nanoparticles, how their shapes affected their optical and electronic properties, and excitation and relaxation mechanisms in such materials.

In 2007 we gave a review[9] of the status of IR emitting colloidal NCs, describing their synthesis, assembly into films and ordered solids, spectroscopic assessment and some of the emerging applications for these materials. The present review reflects the expanding range of narrow bandgap materials, synthetic methods and applications. The ever broadening range of electro-optic and electronic applications was covered in Talapin *et al.*'s[10] review of these aspects of the NC application area in 2009. Gaponik and Rogach[11] reviewed the status of thiol capped CdTe colloidal NCs, discussing the influence of and choices of ligands and how these could be used to optimise

performance in a range of applications that benefited from this primarily water-based synthetic approach. To mollify both the left-hand and right-hand sides of the NC congregation it is worth mentioning here that Yang *et al.*[12] addressed the topic of phase transfer of nanoparticles from aqueous to organic solvents and *vice versa* in their recent Chemical Society Critical Review Article.

Regulacio and Han[13] recently surveyed the field of composition tuned alloy semiconductor NCs, both wide and narrow bandgap, and including composition gradient and core–shell materials. Zhuang *et al.*[14] have given an overview of not just colloidal, but also other solution or liquid phase growth methods for NCs in general, and how such materials may be (chemically or otherwise) assembled further into more complex meso- or macrostructures.

The synthesis and properties of hybrid nanostructures such as core–shell NCs and nanorods, and how they can be assembled into hetero-dimers (and oligomers) of NCs and structures such as tetrapods were reviewed by Cozzoli *et al.*[15] Donegá[16] has also recently given a thorough review of the field of heterostructured NC growth for a wide range of materials, exploring the growth kinetics and epitaxy considerations in great detail. The organisation of NCs (including *e.g.* II–VI materials) into much larger (~100 nm scale), less organised but yet often highly monodisperse supraparticles has recently been reviewed by Xia and Tang.[17]

Ghosh Chaudhuri *et al.*[18] gave a very wide ranging review of applications and synthetic methods for core–shell nanoparticles including not only semiconducting materials but also metal and dielectric (silica, other glasses and organic) materials for both core and shell.

To make good quality optoelectronic devices it is important to minimise light scattering in composite materials. Althues *et al.*[19] described methods to combine inorganic nanoparticles and polymers whilst still retaining the good transparency of the host polymers. Combination of organic materials and inorganic semiconductor NCs at the dot/molecular level has been discussed by Holder *et al.*[20] They covered the combination of a wide range of semiconducting conjugated polymers and colloidal NCs to produce highly emissive hybrid materials for LED and solar cell applications.

Afzaal and O'Brien[21] gave a short review on II–VI and III–VI semiconductors and applications in solar cells which included activity at that time in NC versions of those materials. More recently Yang *et al.*[22] surveyed the use of semiconducting NCs in QD sensitized solar cells, including several of the narrow bandgap materials referred to in this review. This also formed a major part of our recent Perspective article on progress in NC based solar cells in general,[23] whilst the article by Debnath *et al.*[24] focussed more exclusively upon progress with solid film NC junction photovoltaic devices and the prospects for further enhancement of performance of these types of solar cell.

The synthesis of magnetic and magnetic–fluorescent hybrid nanoparticles for biological applications has recently been reviewed by Blanco-Andujar *et al.*[25] and includes references to II–VI NCs and methods to apply further shells to reduce cytotoxicity. Wang and Su's[26] Minireview also covers this topic, including organic fluorophores coupled to magnetic nanoparticles. Sperling and Parak's[27] recent Royal Society of London Review is a comprehensive tour de force of synthetic methods of surface modification and bioconjugation of colloidal inorganic nanoparticles of all kinds. Sortino's[28] Feature Article focuses on the use of nanomaterials to bring about photoactivated release in biological applications, in the sense of drug release and also to trigger the generation of biological agents such as nitrogen oxide or oxygen radical species for *in situ* phototherapy treatments. In some aspects there is overlap here with some of the energy transfer technology used in LED and solar cell hybrid NC materials.

3 Synthetic methods

Very brief outlines of reactions are given in the following sections to allow readers to determine the *type* of reaction involved *e.g.* organic/aqueous/hot injection/low temperature/*in situ*/in-host medium/ion exchange, *etc.*, and the types of materials (*e.g.* precursors, ligands and solvents) used. Details are given in brief, bullet point-like format to limit space, whilst retaining the differentiation of each group's approach and whilst trying to cover all classes of materials and syntheses.

3.1 Pb chalcogenides

PbS. Based on the hot injection growth technique given by Murray *et al.*,[29] shown schematically in Fig. 1, the most commonly cited method to prepare PbS QDs with particle sizes giving emission (or absorption) in the IR is that of Hines and Scholes.[30] This synthesis reliably yields good quality material in an organic solvent with a clear pronounced excitonic absorption spectrum, (Fig. 2) and well defined size distributions are easily obtained. The long chain ligands (oleic acid–oleylamine)

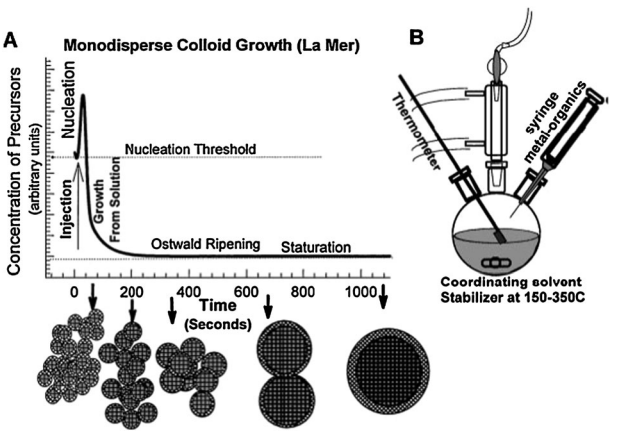

Fig. 1 (A) Cartoon depicting the stages of nucleation and growth for the preparation of monodisperse NCs in the framework of the La Mer model. As NCs grow with time, a size series of NCs may be isolated by periodically removing aliquots from the reaction vessel. (B) Representation of the simple synthetic apparatus employed in the preparation of monodisperse NC samples. Republished with permission of Annual Reviews Inc., from C. B. Murray *et al.*, *Annu. Rev. Mater. Sci.*, 2000, **30**, 545–610 (ref. 29); permission conveyed through Copyright Clearance Centre, Inc.

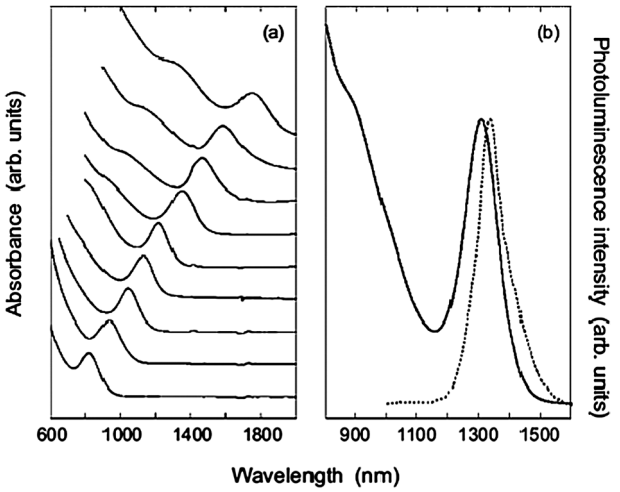

Fig. 2 Room temperature optical characterization of toluene solutions of PbS NCs. (a) Absorption spectra spanning the range of tuneable sizes. (b) Band-edge absorption and PL peaks for a sample ~6.5 nm in diameter. Reproduced from ref. 30, M. A. Hines and G. D. Scholes, *Adv. Mater.,* 2003, **15**, 1844–1849, © 2003 WILEY-VCH Verlag GmbH & Co. KGaA, Weinheim. With permission from John Wiley & Sons, Inc.

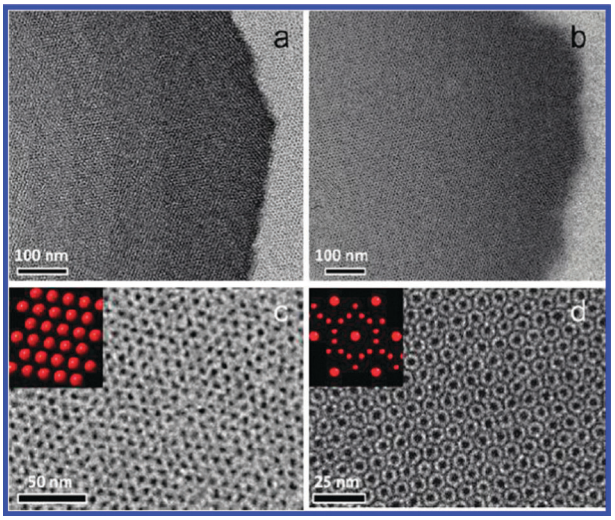

Fig. 3 TEM images at different magnifications of the assemblies obtained by drop cast from toluene solution on a copper grid of monodisperse size distribution PbS NCs (a and c), schematized in the inset of (c). (b and d) bimodal sized distribution PbS NCs, schematized in the inset of (d). Reprinted with permission from M. Corricelli *et al.*, *J. Phys. Chem. C*, 2012, 116, 6143–6152. Copyright 2012 American Chemical Society (ref. 31).

are used even where the target application requires injection or extraction of charge into/from the QDs, and good carrier mobility in NC films or composites. However the long chain ligands appear to be relatively easy to remove post-synthesis and replace with alternate shorter surface molecules or groups, at least to sufficient degree to allow the nanoparticles to function as intended.

Corricelli *et al.*[31,32] and Altamura *et al.*[33] synthesized both monomodal and bimodal size distributions of IR emitting PbS nanoparticles. They used the lead oxide precursor/hot injection method with hexamethyldisilathiane as the sulfur precursor in octadecene (ODE). Their lead precursor was dissolved in ODE with oleic acid and trioctylphosphine (TOP) as the coordinating ligands. They obtained differing size distributions by varying the Pb–S molar ratios (24 : 1 and 50 : 1 in their two syntheses) and reaction times. Their size control was sufficient to allow them to form superlattices (as shown in Fig. 3) with their well defined particle size distributions.

Asunskis *et al.*[34–36] have studied the nonlinear optical properties of PbS QD-doped polymer composites using NC material grown following the earlier methods of Hines[30] and the Bawendi[37] group. More recently they have adopted the hot injection method[38] using lead acetate and squalene/oleic acid as the metal precursor and ligands, respectively, and thioacetamide in dimethylsulfoxide to furnish the sulfur source. In electrical conductivity studies, Baik *et al.*[39] prepared films from PbS QDs synthesized by the standard hot injection method.

Acharya *et al.*[41,42] have grown PbS, PbSe and PbTe QDs directly on TiO_2 substrates by a hetero-epitaxial hot injection route. They have also extended the method to CdS and Cu_2S by first growing PbS on the substrate followed by a cation exchange. PbO was dissolved in oleic acid (OA)/ODE as the lead source, and elemental sulfur dissolved in ODE as the chalcogen source. In the selenide and tellurium cases the chalcogen sources were elemental selenium or tellurium dissolved in TOP at room temperature. The prepared TiO_2 film substrates were added to a flask containing degassed olylamine and injection of the lead and chalcogen precursor solutions initiated growth of PbE NCs both in solution and directly on the TiO_2 surface.

In a number of articles concerning fabrication and characterisation of PbS QD-based IR active films and devices (telecom wavelength emitters, electro-absorption devices and enhanced absorption wavelength range solar cells) Sargent[43–50] and co-workers have consistently cited the Hines synthetic method, with OA ligands used for the NC growth. For devices requiring charge extraction or injection they then exchange the original octadecyl ligands for shorter chain molecules to facilitate charge access and transport.

Heiss and colleagues and collaborators also consistently favour the same Hines and Scholes route. In studies of near and mid IR active materials[51,52] and film based devices (solar cell,[53] IR photodetectors,[54,55] QDs coupled to other optical materials[56] or devices[57]) they again generally start from OA stabilised PbS NCs grown in ODE or other organic solvents by the hot injection method.

Luther *et al.*[58] recently reported the synthesis of PbS QDs used in PbS–ZnO QD heterojunction solar cells using the Hines method, and Talapin and co-workers[59,60] have also used the same method to prepare PbS NCs with tightly defined size distributions for studies of PbS NC superlattices. Talapin's group has also extended the Hines synthetic method: initially PbS NCs are grown using the usual OA stabilizer but this is exchanged post-synthesis for molecular metal chalcogenide ligands such as K_4SnTe_4 *etc.*,[40] as depicted in Fig. 4.

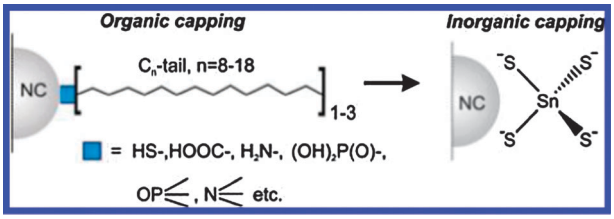

Fig. 4 Schematics of the ligand exchange process used for the preparation of all-inorganic NCs. Reprinted with permission from M. V. Kovalenko *et al., J. Am. Chem. Soc.*, 2010, **132**, 10085–10092. Copyright 2010 American Chemical Society (ref. 40).

Krüger *et al.*[61] reported a modified version of the hot injection method, using lead acetate as the precursor, heated in the presence of OA, diphenyl ether, OA and TOP to form lead oleate. The injected sulfur source was bistrimethylsilyl sulphide (TMS) mixed with thioacetamide and TOP in this case.

Liu *et al.*[62] have investigated the effect of using the usual Hines and Scholes hot injection reagents and solvents as well as other sulfur sources, metal salts and stabilizer combinations where the reactants are mixed (initially at room temperature) and growth carried out at lower temperatures than usual. They find that smaller nanoparticles with bandgap energies as high as just over 2 eV can be grown rather than <1 eV typical with faster hot injection schemes.

Li *et al.*[63] simply used sulfur dissolved in ODE as the chalcogen precursor and lead oxide dissolved in ODE along with mixtures of OA and olylamine as the ligand species.

OBrien's group reported a number of alternate organic injections routes[64] to IR emitting PbS with bandgap energies in the range of 0.88 eV to 1.72 eV. PbO was dissolved in olive oil (regular domestic grade) with OA and ODE. A sulfur source solution consisting of either elemental sulphur or TMS dissolved in olive oil and octadecene was rapidly injected at around 60 °C to form PbS NCs, with the reaction being carried out under oxygen-free conditions. The same group has also synthesized PbS by single precursor, soft hydrothermal routes, but with thiol stabilizers present.[65] Their precursors have the advantage of being air-stable, obviating the need for inert atmosphere for reactions. Precursors such as [2,2′-bipyridyl-$(Pb(SC(O)(C_6H_5)_2)]$; $[Pb(S_2(P(C_6H_5)_2)_2N)]$]; or [2,2′-bipyridyl-$(Cd(SC(O)(C_6H_5)_2)]$]) were added to vials containing 1-thioglycerol and NaOH and the mixtures treated with steam in a pressure vessel to bring about decomposition of the single source precursors to form PbS NCs. The nanoparticles obtained were typically larger and more structured than those that can be obtained by regular colloidal methods and ranged from around 10–50 nm in size. Earlier related work by Trinidade *et al.*[66] using lead(II) dithiocarbamato complexes ($Pb(S_2CNRR')_2$) yielded smaller ($\sim$6 nm) nanoparticles when lower temperature growth (100 °C) was used, but the corresponding absorption spectra did not show the type of strong excitonic band-edge features commonly observed with colloidally grown materials.

Early work by Bakueva *et al.*[67] on PbS NCs emitting in the 1.3 μm and 1.55 μm optical telecom wavelength ranges involved an aqueous synthesis route. Lead acetate with either thioglycerol or the latter mixed with dithioglycerol were used as the metal source and ligands, respectively, and sodium sulfide was used as the sulfur source. Growth was carried out under alkaline conditions (pH $\sim$11) using triethylamine to adjust the pH.

Fernée *et al.* have used a number of approaches to synthesise both PbS NC solutions (aqueous and organic solvents) and PbS nanoparticles grown *in situ* in (conducting) polymers *via* a single step stabilizer-less reaction scheme. In their earlier work, PbS NCs were grown as nanoparticle (few nm diameter) suspensions in aqueous polyvinylalcohol solutions using lead acetate as the metal precursor and injection of H_2S gas to provide the sulfur,[68,69] the approach being based on earlier reports by Nenadovic *et al.*[70] Subsequently, the group turned their attention to PbS loaded conducting polymer composites and an organic method using a mixture of lead acetate and poly-(3-hexylthiophene-2,5-diyl) (P3HT), dodecanethiol, and dimethylsulfoxide in toluene, into which a hot solution of elemental sulfur dissolved in additional toluene was injected. Having the polymer present during the reaction was intended to avoid NC aggregation during mixing of the polymer and NCs.[71] A similar approach was adopted for poly(2-methoxy-5-(20-ethyl-hexyloxy)-*p*-phenylene vinylene (MEH-PPV)–PbS composites, using dichlorobenzene as the solvent rather than toluene (the former permitting higher reaction temperatures).[73,74]

Biswas and Rao[75] have used ionic liquids (which have wide temperature ranges compared with many regular organic solvents) as the growth media for PbS QDs. They reported the use of 1-*n*-butyl-3-methylimidazolium borontetrafluoride, ([BMIM][BF_4]) to grow $\sim$10 nm diameter PbS nanoparticles.

Although the growth of PbS QDs in aqueous media using Pb salts with water soluble short chain thiols (thioglycerol, mercaptoacetic acid, *etc.*) and Na_2S as the precursor has been known for many years,[76] the detailed reaction kinetics of the aqueous route have only recently been studied in full detail. Brazeau and Jones[72] have recently probed the relative contributions to the growth process (nucleation, oriented attachment of smaller particles and Ostwald Ripening) on various time scales after the start of reaction using stopped flow optical spectroscopic techniques (as shown in Fig. 5). Cornacchio and Jones[77] have also followed the dynamics of the size distributions by dynamic light scattering during growth and the surface chemistry especially in connection with O_2 activity and its impact on the use of PbS QDs for biological labelling applications.[78]

Jiang *et al.*[79] have produced isolated PbS nanoparticles on top of self-assembled monolayers of long chain thiols (mercapto-undecanoic acid lead salts) by exposing the films to H_2S gas and have used STM tips to probe single electron tunnelling effects in individual PbS particles in the 3 nm size range.

Hens *et al.*[80] have investigated the influence of NC shape on the optical and electronic properties of PbS QDs by fabricating 'flattened' nanoparticles of the material on 1,4-dithiane self-assembled monolayers (SAMs) on single crystal gold and graphite substrates. They used an electrodeposition synthesis, with an aqueous solution of $Pb(NO_3)_2$ and $Na_2S_2O_3$ precursors at a solution pH of 2.8 to form particles with diameters ranging from 10–100 nm and thicknesses of a few nm.

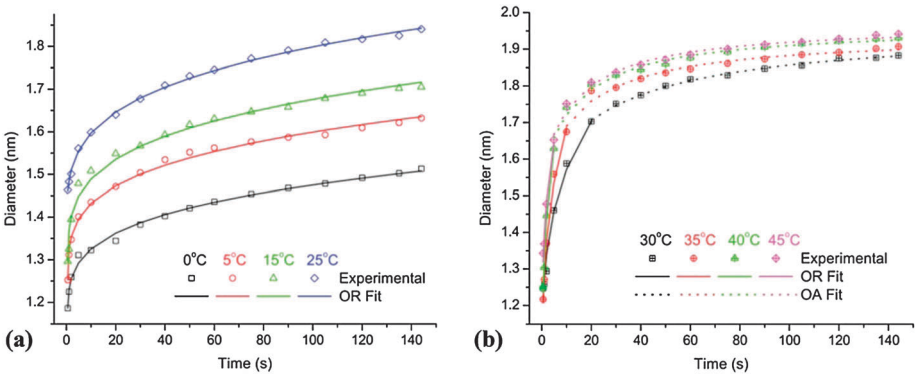

Fig. 5 Variation in approximate average particle radius (calculated from absorption data) with time for thiolate-capped PbS NCs grown by bottom-up reactions of Pb^{2+} and S^{2-} in water over the temperature ranges (a) 0–25 and (b) 30–45 °C. Symbols represent experimental measurements, while lines refer to theoretically derived values for Ostwald Ripening (OR) and Oriented Attachment (OA) mechanisms. Reprinted with permission from A. L. Brazeau and N. D. Jones, *J. Phys. Chem. C*, 2009, **113**, 20246–20251. Copyright 2009 American Chemical Society (ref. 72).

Jia *et al.*[81] described a method to form PbS nanoparticles with functionalization suitable for inclusion in photolithographically defined 3-D photonic nanostructures based on sol–gel materials. Based on a modification of their earlier method[82,83] they took a solution of lead acetate, acetic acid and mercaptohexanol dissolved in methanol to provide the lead precursor whilst a solution of thioacetamine in methanol acted as the sulfur source. After purification of the NC product and isolation as a dry powder, the NCs were subsequently suspended in ethanol and treated with mercaptopropyltriethoxysilane to make the particles compatible with subsequent (silica) sol–gel chemistry.

Narrow PbS rods with controlled diameters of 2.5 nm and under have been prepared by Khan *et al.*[84,85] by the simple addition of lead hexadecyl xanthate (see Clark *et al.*[86] for examples of a range of suitable xanthates), to hot (65 °C) trioctylamine. Metal xanthates are also cited as precursors for PbS NCs which were subsequently conjugated to secondary antibodies in immunoassay applications by Liu *et al.*[87]

Choi *et al.*[88] have grown PbS NCs with lead acetate and Na_2S to furnish the precursors and DNA fragments as the coordinating ligands to form IR emitting materials for bio-imaging applications. Deng *et al.*[89] have synthesized aqueous PbS from Pb salt, Na_2S, and the vitamin dihydrolipoic acid ($H_SCH_2CH_2CH(SH)(CH_2)_4COOH$). In related syntheses Turyanska *et al.*[90] have also grown PbS NCs in aqueous solution, capped with either thioglycerols[91] or dihydrolipoic acid ligands.

There have also been a number of articles that address the problem of loss of quantum yield when transferring organically grown PbS (*e.g.* using oleylamine/OA and hot injection) into water. Often the emission brightness drops by anything from 30–60% upon transfer due to loss of surface ligand/surface damage. Zhao *et al.*[92–94] and Li *et al.*[95] have each used amphiphilic polymers (poly(maleic anhydride-*alt*-1-octadecene)-*co*-poly(ethylene glycol) and poly(acrylic acid) respectively) as replacements for the initial organic ligand prior to the solvent transfer process. The amphiphiles remain on the surface during the transfer and the surface of the inorganic NC need not be disturbed.

9 nm to 16 nm diameter organic solvent soluble PbS NCs are reported by Si *et al.*[96] Lead acetate dissolved in water was injected into a stirred solution of elemental sulfur dissolved in oleylamine. The NC product was extracted in toluene from the resulting mixture.

Surfactant assisted solvothermal[97] and microwave syntheses[98–100] using ethanol and ethylene glycol as solvents have also been reported. Whilst these techniques in general tend to yield larger diameter PbS particles with less regular shapes, the inclusion of surfactants (*e.g.* thiols) may yield NCs more similar in size and shape to those obtained by regular colloidal syntheses. Templated growth of PbS NCs within porous structures[101] (very uniform matchstick-like 10 nm × 50 nm), montmorillonite interlayer cavities,[102] layered double hydroxides[103] and molecular cages without surface stabilizers has also been reported.

PbSe. As in the previous section on PbS NC growth, Acharya *et al.*[42,105] prepared PbSe–TiO_2 composites and Hens *et al.*[106,107] and Grandidier[108] grew PbSe on crystalline gold surfaces in directly analogous fashions. Koole *et al.*[104] prepared high quality PbSe with absorption spectra clearly displaying many features which they have assigned to transitions with higher energy states, as shown in Fig. 6. Following Murray's earlier paper,[109] a lead acetate, diphenyl ether and OA and TOP solution were heated to form lead oleate. The cooled solution was mixed with a solution of elemental selenium and TOP and the whole injected into hot diphenyl ether to initiate NC growth. The same method was used by Law *et al.*[110] (and in part by Luther *et al.*[111]) and Liljeroth *et al.*[112] to grow PbSe NCs which were subsequently self-assembled on hexanedithiol layers for measurements of NC densities of states. Law *et al.*[113] used a similar approach, but injected TOP–Se solution into a hot lead precursor solution containing diphenylphosphine rather than TOP.

Many groups cite the original works by Murray[109] *et al.*, Steckel *et al.*[37] and Hines *et al.*[30] as the basis for their hot injection PbSe syntheses.[114–119] For narrow size distribution studies the technique was modified by Murphy *et al.*[120] after the approach of Yu *et al.*,[121] originally used to produce narrow size range CdSe NCs. Some focussing of the size distribution was obtained by injecting the TOP–Se precursor in two tranches separated in time by around 3 to 9 minutes.

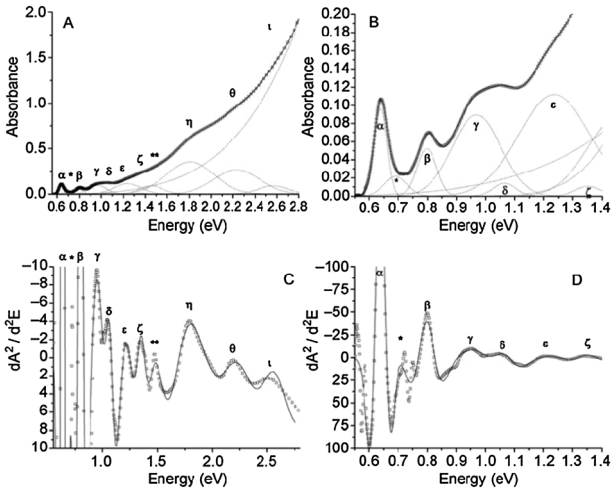

Fig. 6 (A) Optical absorption spectra of a dispersion of 6.8 nm quasi-spherical PbSe NCs in tetrachloroethylene. The open squares represent the experimental spectrum, the solid line is a fit to Gaussian components and a background that increases with E^4 (dotted lines). The low-energy part of the same spectrum and corresponding fit are shown in (B). The second derivatives of the experimental spectrum and the fit are shown in (C) and (D) as the open squares and solid lines, respectively. Reproduced from ref. 104, R. Koole *et al.*, *Small*, 2008, **4**, 127–133, © 2008 WILEY-VCH Verlag GmbH & Co. KGaA, Weinheim, with permission from John Wiley & Sons, Inc.

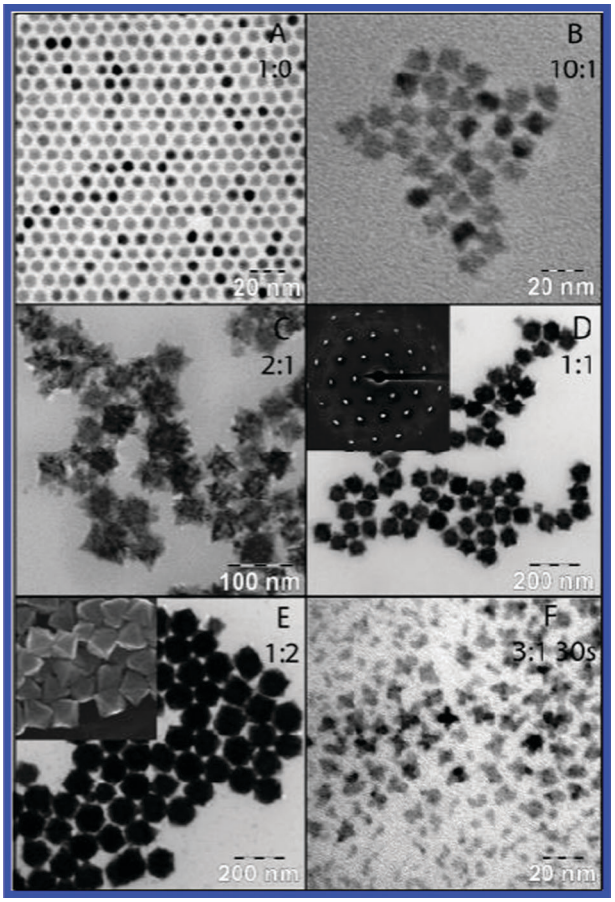

Fig. 7 TEM images of PbSe crystal shapes grown at different concentrations of acetate. (A–E) PbSe NCs grown under identical reaction conditions with a Pb : Ac ratio as indicated in the images. Insets are a diffraction pattern of a single octahedron (D) and a SEM image (E). (F) PbSe NCs after 30 s of growth, in the initial stage of oriented attachment toward octahedrons. Reprinted with permission from A. J. Houtepen *et al.*, *J. Am. Chem. Soc.*, 2006, **128**, 6792–6793. Copyright 2006 American Chemical Society (ref. 122).

Houtepen *et al.*[122] closely examined the effect of incompletely removing acetic acid and water by-products when forming lead oleate for the hot injection syntheses. If the product was completely dried (by vacuum drying as well as by evaporation) good quality near spherical PbSe NCs could be obtained whereas partially dried material most often resulted in faceted shapes *e.g.* octahedral, star-like, *etc.* as shown in Fig. 7.

Joo *et al.*[123] have carried out detailed comparative studies of hot injection synthesis methods (including kinetic modelling work). They comment upon the well-known but not always well-documented fact that TOP impurities such as dialkylphosphines are acknowledged to be responsible for batch to batch variations in PbSe (and other) NC syntheses. Their study compares the effect of using TOP alternates, diphenylphosphine or 1,2-hexadecanediol. They conclude that whilst both lead to higher product yields, the diol produces higher photoluminescence (PL) quantum yields (especially for larger particle sizes) due to slower growth rates relative to the phosphines.

A number of articles by the Klimov group in the last decade, addressing carrier multiplication,[124] phonon relaxation dynamics,[125] Auger relaxation,[126] amplified spontaneous emission,[127] and hot carrier transfer[128] effects in PbSe generally cite a TOP based hot injection synthesis by Pietryga.[129]

Ma *et al.*[130] have used a variant of the hot injection TMS route usually used for PbS (as illustrated in the previous section) with TMSe (bis(trimethylsilyl) selenide) replacing the sulfur source. With this approach they were able to grow good quality small diameter PbSe NCs with diameters of around 1 nm for use in photovoltage studies with regard to solar cell performance.

In a series of recent papers Yu and co-workers[131–134] have further developed Yu's[135] initial hot injection/TOP–Se method and studied the stability and behaviour of the PbSe NC product with respect to the chemical environment, temperature and exposure to light. The same injection technique is reported by many other groups.[136–143] In related work on PbSe nanowires (with some relevance to nanorod growth) Foos *et al.*[144] have varied the Yu synthesis, including strongly coordinating tetradecylphosphonic acid (TDPA) as a co-ligand to foster anisotropic growth.

Sliem *et al.*[145] recently modified the hot injection method by using selenourea in *N*,*N*-dimethylformamide (DMF) and phenyl ether as the selenium precursor that was injected into the hot lead oleate solution.

As for PbS, Li *et al.*[63] reported the growth of PbSe QDs using elemental Se as an alternate to TOP–Se for their hot injection method. They use OA and oleylamine in ODE with PbO heated to form the metal oleate and a prepared solution of Se–ODE which remains stable in air prior to use.

Chen *et al.*[146] reported a high temperature, non-injection synthesis that does not require an inert atmosphere, based on the use of SeO_2 as the selenium precursor. They take a solution of

SeO_2 and the metal myristate in ODE. Heating to temperatures around 250 °C initiates the nucleation of PbSe nanoparticles. Inclusion of oleylamine and TOP (or TOP alone) gave better stabilization of the NC product and tighter size distributions, leading to particle sizes of 4.6 nm and ~16 nm respectively.

PbSe nanowires, nanorods and anisotropic growth. Kim *et al.*[147] have used a modified version of the OA/ODE, TOP–Se method to grow PbSe nanowires. The usual lead acetate, OA, diphenyl ether solution was first prepared and then cooled to 60 °C. At this temperature TOP–Se was added but did not start nucleating at such a low temperature. Nucleation and rapid anisotropic growth of wires were initiated by injecting the combined solution into a hot (250 °C) TDPA diphenyl ether solution.

Shi *et al.*[148] described growth of PbSe dots, rods and branched rods starting with seed particles consisting of Au NCs embedded in (but with a facet at the surface of) Fe_3O_4 nanoparticles. The shape obtained depended upon the growth duration and proportion of seed to precursors. A similar approach has also been reported by Zeng *et al.*[149] and bare noble metal nanoparticles have also been used by the Prasad group.[150]

Bartnik *et al.*[151] have grown PbSe nanorods according to an earlier method by Acharya *et al.*[152] Using a modified version of the hot injection Pb oleate/TOP–Se route they also add tris-(di-ethylamino) phosphine to promote anisotropic growth.

In earlier work on the growth of both PbSe and PbSe–PbS core–shell NCs Sashchiuk *et al.*[153] used an alternate Se–phosphine precursor: a solution of elemental selenium and tributylphosphine was prepared and then mixed with a solution consisting of lead(II)-2-ethyl-hexanoate in toluene. Reactions were allowed to proceed at room temperature.

Wehrenberg *et al.*[154] modified the Murray synthesis to control size and size distributions by varying the injection temperature (by injecting hot solutions of precursors into hot reactant mixtures) and subsequent growth temperatures.

Talapin and coworkers have studied the growth and properties of PbSe nanowires in a number of articles. They take the hot TOP–Se injection method to form PbSe NCs a stage further, investigating the conditions to encourage oriented attachment of NCs to form straight nanowires (as illustrated in Fig. 8) and closed rings of NCs. They have systematically studied the use of different conditions and ligands (combinations of OA, hexadecylamine (HDA), TOP, TDPA, *etc.*) and solvents to form various nanostructures.[155,156] PbSe NCs with size distributions suitable for superlattice growth were also prepared using hot injection with a TOP–Se chalcogen precursor and squalene as the solvent.[157]

Preparation of water soluble PbSe NCs. Etgar[158,159] grew PbSe QDs by an organic hot injection method followed by 1-aminothiol exchange in water for biotagging applications, citing the earlier work of Brumer *et al.*[160] on PbSe core–shell systems as the basis for their synthesis.

Mahmood[161] has grown a broad range of PbSe particles with mean sizes up to around 5 nm. Lead acetate and Na_2SeO_3 were the respective water soluble precursors, and various molecular weight poly(vinyl alcohol) polymers were used as the size regulating ligand. PbSe QD-embedded polymer films were obtained by drying the solution.

Cui *et al.*[162] have produced PbSe nanocubes with sizes down to around 10 nm using a biological reaction system often used in the reduction of Na_2SeO_3. They used glutathione reductase (GR) to reduce SeO_3^{2-} to GSSeH (a Se derivative of glutathione (GSH) and then to H_2Se which could subsequently react *in situ* with dissolved lead salts to form PbSe NCs.

Kumar *et al.*[163] have produced PbSe NCs in water at relatively modest temperature (~90 °C) using RNA extracted from a yeast as a biocompatible ligand.

PbTe. PbTe NC growth in glasses and optical characterization of such materials had been extensively explored from the early 1990's by groups at various Corning research labs.[164,165] Grown by other methods and in nanoscale heterostructures with other narrow bandgap tellurides (*e.g.* SnTe or PbSe) the material is currently attracting a great deal of interest for its thermoelectric properties.[166] The first accounts of colloidal synthesis of PbTe NCs did not start to appear until 2000 with our report of PbTe NCs grown in water.[168] The first hot injection synthesis appears to have been reported by Cho *et al.*,[169]

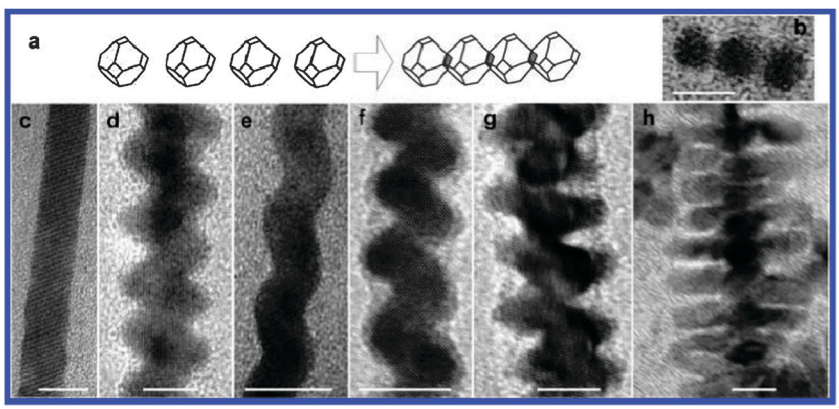

Fig. 8 PbSe nanowires synthesized by oriented attachment of PbSe NCs. (a) Schematic representation of the oriented attachment process. (b) High-resolution TEM image of a trimer formed in the early stage of reaction. TEM images of PbSe nanowires with (c) straight, (d) zigzag, (e–g) helical, and (h) branched morphologies. Scale bars are all 10 nm. Reprinted with permission from D. V. Talapin *et al.*, *J. Phys. Chem. C*, 2007, **111**, 13244–13249. Copyright 2007 American Chemical Society (ref. 155).

and was followed by an account by Lu *et al.*[170] They used a lead acetate/TOP–Te solution which was injected cold into a hot phenyl ether–OA solution to initiate NC growth.

Murphy *et al.*[171] adapted their previous PbS QD synthetic method, preparing lead oleate first from lead oxide and OA in hot ODE. Into the resulting solution they injected TOP–Te, prepared separately. Urban *et al.*[172] used a modified version of the Talapin/Murray PbS, PbSe QD hot injection synthesis, preparing and drying and de-acidifying their solution of lead oleate in squalene first before injecting a TOP–Te solution chalcogen precursor solution into the hot oleate solution.

There have since been a number of other reports of PbTe NCs using variants of these basic hot injection methods:

Zhang *et al.*[173] prepared PbTe QDs for NC monolayer studies with a lead acetate/OA/oleylamine lead precursor solution and TOP–Te injected into the hot metal precursor solution. Franchini *et al.*[174] used the methods of Lu[170] and Urban[172] to prepare PbTe NC starting materials for further modification with Au dopants. Kovalenko *et al.*[167] cited the Urban[172] method to prepare their PbTe starting material (Fig. 9) on which they based mixed tellurides and telluride alloys for thermoelectric studies.

Ko *et al.*[176] cited the Urban[172] route when preparing PbTe NCs of various sizes to measure Fermi level energies and densities of states in PbTe films. Likewise Lin *et al.*[177] grew their PbTe materials for photoconductivity studies following Urban[172] and Murphy.[171] Fafarman *et al.*[178] also used the Urban[172] method to produce oleyl capped PbTe NCs but added methods to replace the long alkyl chain ligands, both in solution or in deposited NC films, with far more compact ammonium thiocyanate ligands, thereby improving charge mobility and injection/extraction efficiencies.

As for other lead chalcogenides, Acharya *et al.*[42] have also synthesized PbTe nanoparticles in and on the surface of nanocrystalline TiO_2 films using the hot injection growth method with TiO_2 films present in the growth solution.

Erk *et al.*[179] have produced 30–50 nm PbTe and PbSe particles embedded in polymer films by first spin coating films doped with single precursor (homoleptic chalcogenate) molecules such as lead(II) bis-[tris(trimethylsilyl)silyl-tellurolate] $Pb[TeSi(SiMe_3)_3]_2$ in the case of PbTe, which could subsequently be converted by thermolysis to form embedded NCs.

Although this review does not generally encompass hydrothermal syntheses, as these often produce relatively larger nanoparticles (often ~50 nm), the large Bohr radius of PbTe (46 nm) leads to some overlap between the colloidal and hydrothermal approaches in the synthesis of narrow bandgap NCs. Tai *et al.*[175] have grown 30 nm diameter PbTe NCs in the form of strings of nanoparticles linked by oriented attachment (as seen in Fig. 10), by transforming pre-prepared Te nanowires by hydrothermal reaction with the $Pb(NO_3)_2$ lead precursor.

Similarly, whilst ion implantation is not directly related synthetically speaking, Kaufmann *et al.*[180] have prepared PbTe nanoparticles embedded in a crystalline CdTe host that fluoresce strongly at 2.9 μm at room temperature, indicating particle sizes on a similar scale to those prepared by colloidal methods and perhaps give encouragement that PbTe–CdTe core–shells are a valid approach for high quantum yields.

Pb chalcogenide alloys, core–shells and heterostructures. Here we review materials made by direct synthesis, whilst NCs grown by ion exchange with other starting materials are

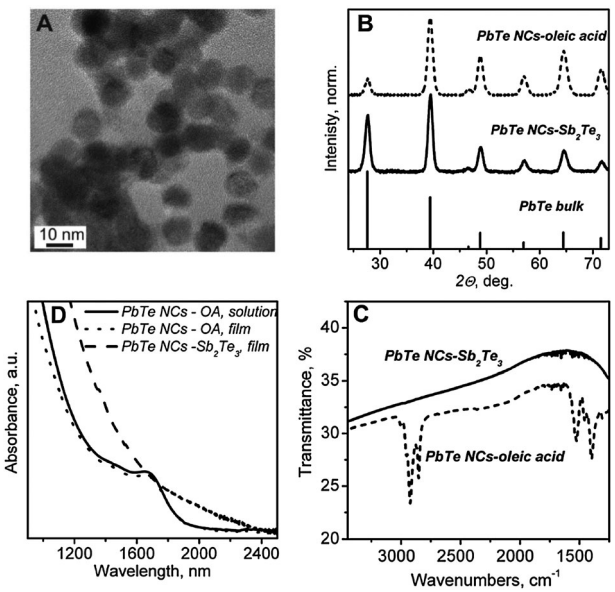

Fig. 9 (A) TEM image of PbTe NCs capped with Sb_2Te_3 Molecular Metal Chalcogenides (MCCs). (B–D) Comparative study of PbTe NC solids capped with original OA ligands and with Sb_2Te_3–MCCs using (B) powder XRD, (C) FTIR spectroscopy, and (D) near-IR optical absorption spectroscopy. Reprinted with permission from M. V. Kovalenko *et al.*, *J. Am. Chem. Soc.*, 2010, **132**, 6686–6695. Copyright 2010 American Chemical Society (ref. 167).

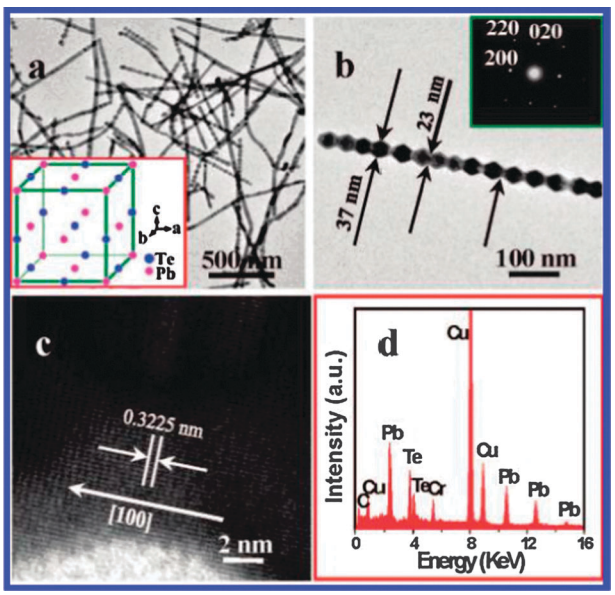

Fig. 10 (a) TEM image of the PbTe nanowires synthesized for 12 h at 453 K. Inset: Unit cell of PbTe (pink dots are Pb atoms; blue dots are Te atoms). (b) TEM image of a single pearl-necklace-shaped nanowire with diameters of about 23 nm in the junction section and about 37 nm in the bead section. Inset: SAED pattern indexed for cubic PbTe. (c) High-resolution TEM image taken from (b), which corresponds to the position referred by the downward-right arrow. (d) EDX spectrum of the nanowires. Reprinted with permission from G. Tai *et al.*, *Cryst. Growth Des.*, 2008, **8**, 2906–2911. Copyright 2008 American Chemical Society (ref. 175).

discussed later. Not restricted to lead-based materials, there are some general considerations that can make the choice of alloy NCs useful. Whilst the use of ternary or even quarternary alloys gives an additional degree of freedom in tuning the bandgap and therefore the emission wavelength of NCs, there are further benefits in adopting this approach. For example one can tune the emission energy for a given particle size, rather than being forced to accept the particle size dictated by the effect of quantum confinement on a simple binary composition semiconductor. This may be helpful for example when incorporating NCs into porous structures or maybe where self-organised packing may be desired in forming superlattices – in favourable cases it is possible to some extent to decouple the particle size and bandgap energy by trading alloy composition against the size-dependent confinement energy shift.

There are other possible advantages in the use of alloys: for example one may obtain better thermal stability in some cases (anecdotally for example, we have found $Cd_xHg_{1-x}Te$, to be more robust thermally than pure HgTe NCs); the alloy composition may be a more effective tool to tune material properties other than the bandgap energy, *e.g.* carrier effective masses (particularly the electron effective mass) and the degree of spin–orbit coupling (especially in the $Cd_xHg_{1-x}Te$ system). The latter effects are essentially identical in NCs to those observed in the bulk versions of the materials and are well documented in the literature.

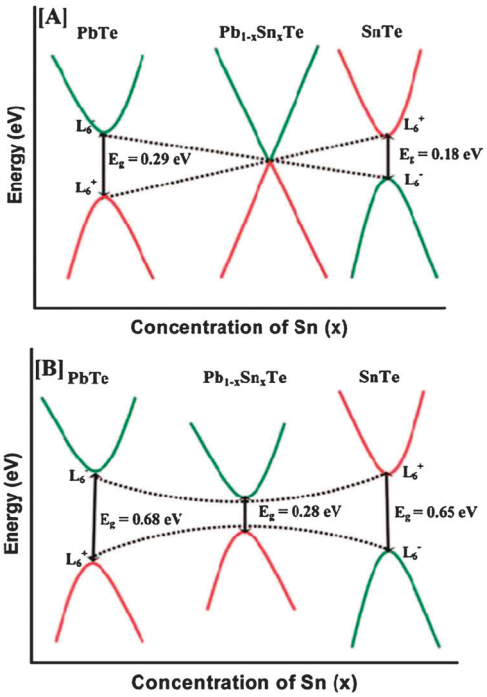

Fig. 11 Schematic representation of the band energy diagram of the $Pb_{1-x}Sn_xTe$ system where x = 0.67 at 300 K for (A) bulk materials and (B) the NCs showing the nature of band inversion. Reprinted with permission from I. U. Arachchige and M. G. Kanatzidis, *Nano Lett.*, 2009, **9**, 1583–1587. Copyright 2009 American Chemical Society (ref. 181).

Lead based chalcogenide alloys. Arachchige *et al.*[181] have synthesized and studied lead/tin telluride alloy NCs ($Pb_{1-x}Sn_xTe$). In the bulk this material exhibits a semi-metal range for some intermediate tin concentrations[182] (illustrated in Fig. 11). In their study, with bulk bandgap energies blue-shifted due to confinement, the material remained a semiconductor across the concentration range, with a minimum in the bandgap bowing curve which was lower than the PbTe or SnTe endpoints echoing the behaviour of the bulk. Alloy nanoparticles with diameters clustered in the range 4.4–5.1 nm and a series of compositions across the range x = 0.19 to x = 0.87 were synthesized by a variation of the hot injection/TOP–Te route using a mixture of freshly prepared lead oleate and bis[bis(trimethylsilyl)amino]tin(II) as metal precursors.

Ma *et al.*[183] synthesized PbS_xSe_{1-x} alloy NCs for photovoltaic studies using a mixed chalcogenide precursor hot injection method: lead oleate was first formed from lead oxide and OA in ODE and the prepared product heated to 150 °C. The chalcogenides were furnished by a mixture of TOP–Se and bis-(trimethylsilyl) sulfide with diphenyl phosphine in ODE and this was injected into the hot oleate solution. No evidence was found for phase segregation *e.g.* formation of a PbSe core within an alloyed shell as observed by Sashchiuk *et al.*[153]

$Pb_{1-x}Bi_xTe$ alloys with (x = 0.005, 0.010, 0.015, 0.020) have been grown by the hot injection method by Zhang *et al.*[184] These types of alloy are of significant interest for thermoelectric applications. A stoichiometric mixture of lead and bismuth alkanoates was prepared by dissolving lead acetate and OA, in ODE along with bismuth(III) 2-ethylhexanoate. After preparation the temperature of the mixture was raised to 150 °C and a solution of TOP–Te injected. Alloy particles in the 15–20 nm range were obtained.

Lead chalcogenide–semiconductor core–shell NCs. The Vanmaekelbergh group and their collaborators have extensively studied PbSe–CdSe core–shell heterostructures.[185–187] Starting with PbSe NCs grown by their previous methods,[122] they subsequently carried out a partial ion exchange of Cd^{2+} for Pb^{2+} in the outer shell by mixing the NC's with a cadmium oleate/toluene – 1-ODE solution at 100 °C. In one of these studies they have also observed the reconstruction of the core–shell structure into segregated PbSe–CdSe bi-hemispherical particles under thermal treatments[187] (as shown in the sequence of HRTEM movie stills in Fig. 12).

The Cd^{2+}–Pb^{2+} cation exchange route to PbSe–CdSe core–shells has also been used by Nguyen *et al.*[188]

There have been a number of articles describing the synthesis and characterisation of PbSe–PbS and PbSe–$PbSe_xS_{1-x}$ core–shell and core–alloy shell NCs by Lifshitz and co-workers.[153,189] In the earlier of these studies, a few nm layer of PbS was deposited on previously prepared PbSe NCs by adding a solution of sulfur dissolved in tri-*n*-butyl phosphine to a solution of the core nanoparticles. Alloy shell particles were grown by simultaneously injecting lead acetate, TOP–Se and TOP–S solutions into a hot solution of OA, TOP, and diphenyl ether at 180 °C. At this temperature PbSe NCs nucleate faster

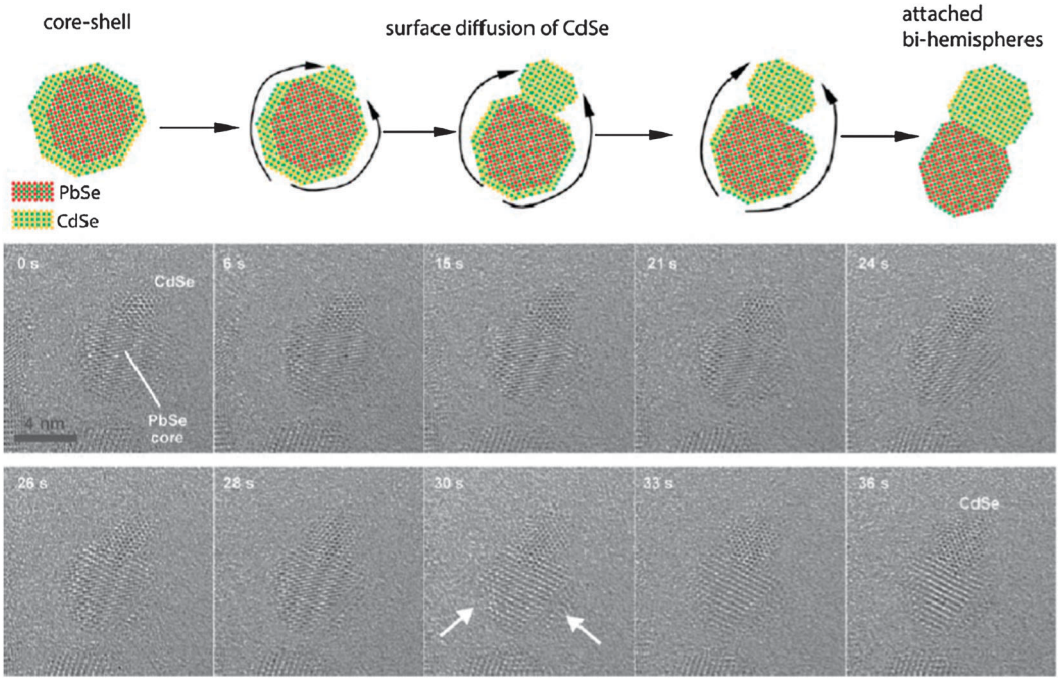

Fig. 12 Stills of a real-time *in situ* HR-TEM recording showing partially the transformation from core–shell to bi-hemisphere heteronanocrystal, at a constant temperature of 200 °C under vacuum (10^{-7} mbar). At the top-right of the PbSe–CdSe core–shell QD (0 s frame), there is a thicker part of the CdSe shell. During the following 36 s, this tiny CdSe NC grows at the expense of other parts of the CdSe shell. White arrows (at the 30 s frame) point to a few locations at the CdSe shell where the surface becomes discontinuous, while the shell becomes thinner. After 36 s, the top right CdSe NC has considerably grown in volume, thereby approaching the hemisphere configuration. The mechanism of the thermally induced structural transformation from core–shell to bi-hemisphere heteronanocrystal is schematically depicted in the top panel. Reproduced from ref. 187.

than PbS would, leading to PbSe cores surrounded by $PbSe_xS_{1-x}$ shells (probably with a concentration gradient, $dx(r)/dr < 0$ through this region).

PbSe–CdSe, PbS–CdS, and PbSe–CdSe–ZnS core–shell structures have been synthesized by Pietryga *et al.*[190] Lead chalcogenide core NCs prepared by hot injection methods (see above) were treated with hot cadmium oleate solutions (in either toluene or diphenyl ether, depending on the reaction temperatures required for either selenide or sulfide reactions respectively) and cation exchange was allowed to occur for given periods of time to control the thicknesses of the exchanged layers. For the double shell structure, a layer of ZnS was added to PbSe–CdSe core–shell nanoparticles after the latter had been purified and redispersed in hexane. The latter solution was added to a mixture of OA, TOP and phenyl ether and heated to remove the hexane. To the resulting hot solution a mixture of TMS–TOP and diethyl zinc was added to deposit the second shell layer of ZnS.

The Cd oleate ion exchange synthesis has also been used by Zhao *et al.*[191] to prepare PbS–CdS core–shell NCs. They synthesized both thin and thick shell particles to investigate the influence of the outer layer thickness on fluorescence quantum yields. Thin shells were prepared using a short (30 min) exchange in a toluene based solution at 100 °C. To obtain thicker shells this first stage was followed by a further higher temperature exchange stage with durations up to 48 hours. PL quantum yields up to 67% were reported.

The Alivisatos group has demonstrated two-stage cation exchange methods[192] to form PbSe NCs embedded in PbS nanorods. The starting material was an analogous Cd based structure which was first transformed to a Cu_2Se–Cu_2S heterostructure before exchanging the Cu^+ ions for Pb^{2+} ions.[193] They also confirmed that the anion heterostructure remained undisturbed throughout the exchange processes. Similar strategies are also adopted with Ag_2E starting and intermediate nanoparticles – these methods are discussed in later sections.

Monolayer precision coating of PbSe NCs with PbS shells has been reported by Xu *et al.*[194] using a form of the SILAR (successive ion layer adsorption and reaction) method adapted from that used by Li *et al.*[195] with wider bandgap NC systems. A hot pre-prepared and purified solution of PbSe NCs dissolved in ODE was alternately injected with precise doses of lead oleate and sulfide solutions. Amounts were carefully calculated to just coat the surface of the PbSe NCs with monolayers of each precursor with no excess left to form an independent population of PbS particles. The lead oleate was formed from lead oxide and OA in ODE and injected at 80 °C into the PbSe NC core containing solution held at 140 °C. The TOP–S/ODE precursor solution was allowed to cool to room temperature before injection.

Water soluble PbS–CdS core–shell nanoparticles were reported by Warner *et al.*[196] Aqueous colloidal PbS core particles were first prepared[70] and then treated with further H_2S gas to fully saturate the surface layer with sulfur. A sodium hexametaphosphate solution was added before injecting a further $CdCl_2$ solution to

form the shell layer. Subsequently increasing the pH to 10.5 (where the respective free metal ions have negligible solubility) enhanced the luminescence of the NCs.

An alternate route to water soluble PbS–CdS core–shell NCs has been given by Zhao *et al.*[93] They started with PbS grown using a $PbCl_2$–oleylamine precursor in organic solvents, followed by the cation exchange method given above to displace surface lead ions in favour of cadmium ions. After the exchange reaction they cleaned the product and re-dispersed the NCs in chloroform prior to a ligand exchange process where they displaced the oleylamine ligand with an amphiphilic polymer poly(maleic anhydride)-*alt*-1-octadecene-*co*-poly(ethylene glycol) (PMAO–PEG) also dissolved in chloroform. After adding water the chloroform was gradually removed over several hours to leave a water soluble core–shell solution.

Lead chalcogenide–metal heterostructures. Falqui *et al.*[197] have prepared PbTe NCs which were then treated with a solution of $AuCl_3$ in toluene and after depositing as a dry film, subsequently irradiated with an electron beam *in vacuo.* The treatment led to the formation of a mixture of several types of nanostructure: PbTe NCs coated with an amorphous layer of oxide, core–shells of crystalline gold coated with amorphous $Pb_xTe_yAu_z$ material, and gold particles attached to PbTe NCs. The group[174] has also studied the same system using solution based reactions – PbTe NCs prepared by hot injection and re-dissolved in toluene were mixed with a gold precursor solution prepared freshly prior to reaction. The latter was a mixture of two solutions: $AuCl_3$–tetraoctyl ammonium bromide in toluene and dodecylamine in toluene were mixed together just prior to addition to the NC solution. Subsequent reaction was carried out for a range of times and at a range of temperatures. Again a range of different heterostructures including Au–PbTe core–shells were observed.

Several groups have attempted to combine gold with PbS nanoparticles. Yang *et al.*[198] have grown small (2–4 nm) gold particles on the surface of larger PbS NCs prepared previously. The coating solution was a solution of chloroauric acid ($HAuCl_4$) and tetraoctylammonium bromide (TOAB) in toluene, treated with a small volume of dodecylamine. The freshly prepared gold solution was added to the PbS NC solution at 80 °C. They observed that as well as gold decoration on the PbS surface, the gold salt was also found to be responsible for some etching of pits into the PbS NC substrate, leading to partially hollowed out heterostructures, as seen in Fig. 13.

Au–PbS core–shells have been grown by Lee *et al.*[199] The usual lead oleate solution (lead oxide/OA/ODE) was first prepared and the solution cooled to 100 °C. At this point pre-prepared Au NCs capped with dodecanethiol in toluene were added and the toluene removed by distillation. Injection of TMS in ODE triggered the growth of the PbS shell on the surface of the Au NCs. The crystallinity of the PbS shell was strongly influenced by the shell growth temperature – low temperature growth led to polycrystalline shells whilst growth at over 150 °C yielded monocrystalline near spherical shells with size uniformity good enough to form long range ordered superlattices.

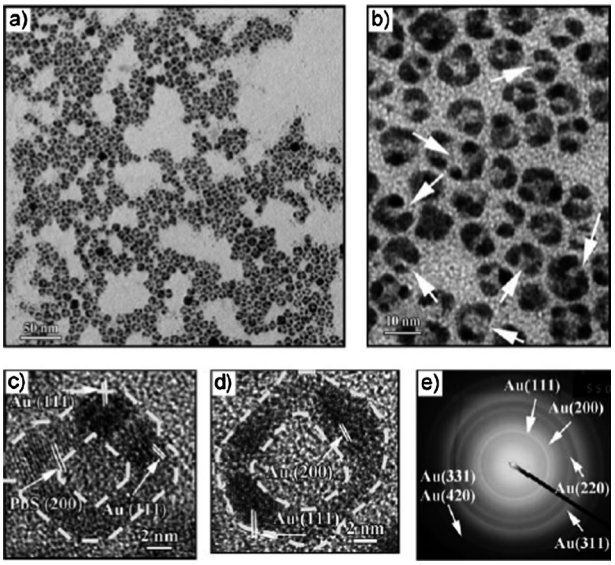

Fig. 13 (a and b) TEM images, (c and d) HRTEM images, and (e) SAED pattern of the hollow PbS–Au hybrid nanostructures. The reaction conditions are PbS (4 mL), dodecylamine (2 mL, 50 mM), gold precursor (0.3 mL comprising 20 mM $HAuCl_4$ and 50 mM TOAB), 80 °C, 1 h. The arrows in (b) indicate a typical structural feature of a pit, suggesting that the voids are connected to the surface. Reproduced from ref. 198, J. Yang *et al.*, *Angew. Chem.*, 2009, **121**, 4051–4055, © 2009 Wiley-VCH Verlag GmbH & Co. KGaA, Weinheim, with permission from John Wiley & Sons, Inc.

Other lead chalcogenide nanostructures. Mukherjee *et al.*[200] have fabricated PbS nanoparticles on CdS nanowires by using a two stage cation exchange process. First Ag^+ ions were introduced into surface sites on previously prepared CdS nanowires to form nanoscale Ag_2S regions. A subsequent treatment with Pb^{2+} containing solution converted the Ag_2S fraction to PbS, leading to CdS nanowires surface decorated with many PbS NCs. The cations were complexed with tri-*n*-butylphosphine which allowed the exchange processes to be carried out in organic solutions.

3.2 Cadmium and mercury chalcogenides

CdTe. Cadmium telluride has a bulk bandgap at room temperature of around 1.5 eV and so its emission may in principle be tuned by quantum confinement from around 850 nm in the IR into the mid-visible region of the spectrum. In NC form it is most often used as a visible (green to red) emitter,[201] but it has been included here as a near IR emitting material (at larger NC sizes) and because it is often encountered in connection with narrow bandgap heterostructure and alloy nanoparticles. The aqueous synthesis of CdTe NCs has long been known[202,203] and Gaponik *et al.*[204] have also demonstrated how NCs such as CdTe can be efficiently extracted from an aqueous phase into organic solvents and the ligands changed from short chain ionic stabilizers such as thio acids, to long chain steric stabilisers such as dodecanethiol.

After reports of high quantum yields (up to 65%) in organically grown CdTe QDs by Wuister *et al.*[205] and Talapin *et al.*[206] using modified versions of their previous organic method

(*e.g.* dodecylamine, TOP, and dimethyl cadmium as the metal precursor and TOP–Te as the chalcogen source), Shavel *et al.*[207] revisited the aqueous CdTe NC synthesis technique and found that by systematically optimising the reagent proportions and reaction conditions they could increase the PL quantum yields from typically less than 10% up to around 50%. For high quantum yields they used $Cd(ClO_4)_2$ with thioglycolic acid (TGA) as the stabilizer in a 1 : 1.3 molar ratio and growth was carried out at pH 12. The Te precursor was obtained as H_2Te gas generated by the action of mineral acid on Al_2Te_3 granules under a flow of nitrogen. The initial room temperature addition of H_2Te was followed by further nucleation and growth at 100 °C under reflux for periods of time ranging up to several hours.

The underlying chemical mechanisms involved in organic/hot injection CdSe and other Cd chalcogenide NC syntheses (including CdTe) have been studied in detail by Liu *et al.*[208] with particular focus on the evolution of the precursor species prior to growth.

Lifshitz and Eychmüller[209] described a modified aqueous synthesis using NaHTe(aq) as an alternate method to introduce the tellurium precursor. Preparation of NaHTe by reduction of elemental tellurium and other methods to prepare H_2Te are given in the comprehensive account of aqueous CdTe synthesis by Rogach *et al.*[210] They also describe how the aqueous synthesis of CdTe NCs can be extended to form larger (~6 nm diameter) particles with emission in the IR to 800 nm (*i.e.* close to the bulk bandgap limit) by the use of mercaptopropionic acid (MPA) as an alternative to TGA. Fig. 14 shows representative examples of absorption and emission spectra and PL lifetime measurements for these types of CdTe NCs.

Zhao *et al.*[211] gave a related hydrothermal synthesis using *N*-acetyl-L-cysteine (NAC) as an alternate ligand for NIR (~800 nm) emitting CdTe QDs. They prepared a solution of $CdCl_2$, NAC, and NaHTe (freshly made by $NaBH_4$ reduction of elemental Te) held initially at 0 °C to stall reaction between the precursors. The solution was then swiftly transferred to a sealed Teflon reactor and autoclaved at 200 °C for around 1 hour. The product was CdTe QDs capped with a thin shell of CdS, the sulfur originating from partial decomposition of the ligand at the high temperature during synthesis.

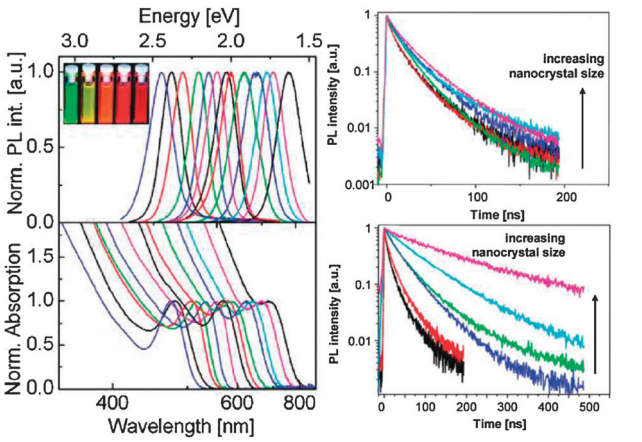

Fig. 14 Left – sets of typical PL (top) and absorption (bottom) spectra of TGA-capped and MPA-capped CdTe NCs demonstrating their tuneability over a broad spectral range in the visible and near-infrared. Excitation wavelength is 450 nm. The inset shows a photograph of brightly emitting CdTe NCs of different sizes taken under UV-lamp excitation. Right – PL decays of TGA-capped (top) and MPA-capped (bottom) CdTe NCs of increasing sizes. Reprinted with permission from A. L. Rogach *et al.*, *J. Phys. Chem. C*, 2007, **111**, 14628–14637. Copyright 2007 American Chemical Society (ref. 210).

Xu *et al.*[212] used an aqueous colloidal approach similar to earlier accounts, employing $CdCl_2$/thioglycerol at pH 10.5 and injection of a NaHTe precursor. In previous work Zhang *et al.*[213] also investigated the role of the carboxylate functional group of the alternate thioacid stabilizers commonly used. Their synthetic method was also cited by Wang *et al.*[214] Recently Liu and Yu[215] surveyed the use of TGA, thiopronin, and glutathione as stabilizers for high quantum yield (up to 83% reported for the latter), though their article reported only visible emitting materials.

In the recent perspective article by Gaponik and Rogach[11] the relative merits of a wide range of water soluble thiol, amine and carboxylate containing ligands, including MPA, are discussed with regard to CdTe and II–VI NC growth in general. Li *et al.*[216] have also recently surveyed the techniques to synthesize highly fluorescent aqueous CdTe NCs and their use, particularly in biological applications for these materials.

Lesnyak *et al.*[217] have recently added 5-mercaptomethyltetrazole to the range of ligands suitable for high quantum yield aqueous CdTe NCs (QY up to 60%) with the added benefit that the ligand is also highly suited to facile hydrogel formation.[217,218]

Kloper *et al.*[219] have demonstrated still higher PL quantum yields, up to 80% in the visible, in organically grown CdTe NC solutions. In their version of the Cd–oleate/TOP–Te injection synthesis (carried out in ODE) the Cd–oleate forming solution of cadmium oxide and OA in ODE was heated in the usual way to first form the oleate. Then, just prior to injection of the TOP–Te precursor, the solution was heated further to 310 °C at which point Cd(0) nanoparticles (of around 100 nm size) began to form as a gray precipitate. Within 30 seconds the TOP–Te solution was injected. The fortuitous increase in the QY of the CdTe product was explained as a partial removal of Cd stock in the initial nucleation and growth stages, followed by a gradual re-introduction of available metal precursor for reaction (from the Cd(0) particles) after the remaining oleate complexed cadmium had been depleted.

Piepenbrock *et al.*[220] have studied the growth dynamics of CdTe QDs synthesized by hot injection (TOP–Te injected into a previously prepared cadmium acetate–dodecylamine–trioctylphosphine oxide (TOPO) solution) in the early stages of particle growth. They found that at small diameters the particles are liquid and will grow even at room temperature until they reach a diameter at which the NCs become solid. Furthermore, they found that higher PL quantum yields were obtained when particle surfaces were cadmium rich *i.e.* starting with low initial Te : Cd precursor ratios or conditions chosen to lead to Te depletion at the end of the growth stage.

Notwithstanding some of the above reports of very high quantum yields reported for CdTe NCs, grown both by organic

or aqueous methods, it should be pointed out that in both cases, as the particle diameters increase and the bandgap energy approaches that of the bulk material, the quantum yields inevitably drop. It is not uncommon to find that a synthesis yielding material with a QY of say 50% emitting in the visible will result in NCs with only 1–5% when continued to give emission shifted to say 700–800 nm. It isn't clear if this is solely a simple consequence of the reduction in quantum confinement, or perhaps also related to the quality (shape and defects) of the NCs at larger diameters.

HgS. We first reported the colloidal synthesis of (zincblende) HgS NCs in water in 2000[168] though the material had poor thermal stability, and weak PL. In a number of papers Kuno and co-workers[221–223] describe the synthesis of small clusters (1–2 nm) and larger NCs (up to 10 nm after heat treatment) of HgS in the β- or zincblende modification. In the bulk several modifications are known with the α-form being trigonal and larger bandgap (2.1–2.3 eV) than the inverted, semi-metal β-form. As in the following section for HgSe they used a surfactant mediated growth with each precursor dissolved in an otherwise immiscible pair of solvents. Mercury acetate and thioglycerol in water were brought into contact with a $(TMS)_2S$–hexane solution, along with the surfactant AOT in cyclohexane. Brij-30 was also alternately used[222] as the surfactant.

Mahapatra *et al.*[224] reported the growth of α-HgS NCs of around 10 nm diameter using a room temperature synthesis. They took an aqueous solution of mercury chloride and thiourea, adding dilute poly(vinylalcohol) solution as a steric ligand. NC growth was triggered by the addition of a 3 M ammonia solution.

Patel *et al.*[225] grew β-HgS NCs of around 15 nm diameter by an electrochemical method (electrolysis of acidified $HgSO_4$ and $Na_2S_2O_3$ solutions) and characterized the phonon modes by Raman spectroscopy. They observed two different phonon modes in different regions of their sample, both shifted from the bulk value (245.3 cm^{-1} and 246.9 cm^{-1}, compared with the bulk 1LO phonon mode of 253 cm^{-1}).

Several groups have produced polymer films containing HgS NCs: Winiarz *et al.*[226] synthesized photorefractive polymer films of HgS in poly(vinylcarbazole) by spin coating substrates with a mixture of the polymer and mercury acetate in organic solvent. The dried films were then exposed to H_2S gas and NCs were formed *in situ.* Nair *et al.*[227] formed HgS NCs in a polystyrene co-polymer host by copolymerizing a mixture of styrene and mercury acrylamide and likewise subjecting the mercury doped product to H_2S gas to form the composite.

Zhang *et al.*[228] described a novel inorganic co-ordination polymer method to form HgS nanowires. They used the linear chain forming properties of the $Cd(NCS)_3^-$ ion to form a template alongside which HgS NCs formed and merged into nanowire bundles. However the wire diameters were relatively large, of the order 60 nm and above.

Polyacrylamide has also been used as a host for HgS nanoparticles grown by microwave solvothermal methods. Zhu *et al.*[229] have synthesized several types of metal sulfide NC doped polymer composites by this method, using elemental sulfur as the chalcogen source and ethylene glycol as the weakly coordinating solvent. However this resulted in relatively large diameter (several tens of nm). A number of other microwave and solvothermal syntheses of HgS have also been reported using variously ethanol[99] (6 nm diameter NCs) and poly(ethyleneglycol)[98,100] (20 nm diameter NCs) as the coordinating solvent/mild reducing agent.

Accounts of high temperature organic solvent growth of HgS nanoparticles by colloidal methods are relatively few. Xu *et al.*[230] recently used such an approach, but could only obtain relatively broad size distributions and nanoflower aggregates (see Fig. 15). This contrasts with other lead chalcogenides by hot-injection routes. Excitonic features were observed in the 700–800 nm size range but only a relatively narrow growth temperature range produced good quality NC materials. They started with mercury oxide and OA in ODE solvent to form the mercury oleate precursor, by analogy with lead chalcogenide syntheses. Their preferred sulfur precursor, elemental sulfur and

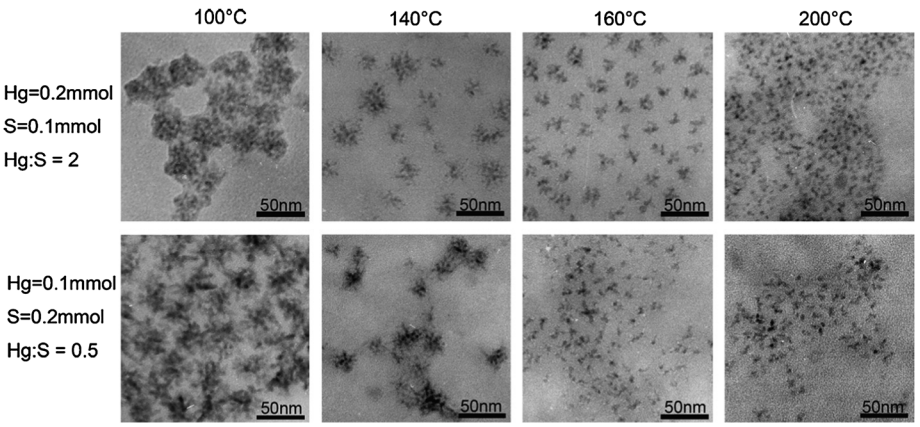

Fig. 15 TEM images of as-prepared HgS nanoflowers samples obtained in 1 h after the injection of S precursor. The corresponding temperature to prepare S precursors is marked above the pictures. The reaction system was set to 100 °C for the injection of S precursor and then lowered down to 80 °C for NC growth. Reprinted from W. Xu *et al.*, Moderate temperature synthesis of flower- and dot-shaped HgS nanocrystals, *Colloids Surf., A*, **341**, 68–72 (ref. 230), Copyright 2009, with permission from Elsevier.

octadecylamine dissolved in ODE, was injected at a range of reaction flask temperatures and 100 °C injection with subsequent growth at slightly lower temperature found to give best results.

HgSe. Recent reports of new (direct) syntheses for HgSe NCs are sparser than for other mercury chalcogenides, though it was reported by aqueous methods alongside HgTe and CdHgTe alloys during early work.[168] Although not a colloidal method, Pejova *et al.*[231] used a chemical bath technique to deposit HgSe films on polymer sheets (alongside similar work on copper selenides) for solar applications and attributed the bandgap energy blue shift to the formation of ~8 nm nanoparticles in the deposited layer. Crouch *et al.*[232] synthesized mercury chalcogenide complexes including imino-bis(diisopropylphosphine selenides), which could be pyrolysed to form mercury selenide films and possibly NCs, though related work with similar lead based systems tended to lead to large nanoparticles.[65]

Kuno and co-workers[222,223] used a mixed water–organic solvent method to grow HgSe clusters with small diameters which exhibited strong excitonic absorption spectra and clearly visible multiple higher excited state transitions. They used an aqueous mercury precursor (mercury acetate and thioglycerol aqueous solution). The chalcogen precursor was $(TMS)_2Se$ dissolved in hexane, which is not water miscible. The reaction between the two solutions is mediated by use of a surfactant – they used either Brij-30 (a polyoxyethylene ether surfactant also known as C12E4 where E = OCH_2CH_2), or the alternate AOT dispersed in TOP. In the case of AOT higher reaction temperatures (100 °C) were needed to give sufficient solubility. There was some evidence that particles with complete shells (magic numbers) of atoms might be formed by this method. Small HgSe clusters were also synthesized and studied by Abeykoon *et al.*[233] using a CVD growth method within sub-nm pore size zeolites.

Howes *et al.*[234] had limited success growing HgSe NCs in an alcoholic solution using mercury acetate and TOP–Se as the respective precursors at room temperature. They obtained 4.9 nm particles with a relatively broad size distribution but reported that they decomposed relatively easily in storage.

Jang *et al.*[235] recently fabricated *n*-channel thin film transistor (TFT) films based on HgSe NCs synthesized according to our earlier paper.[168] They used mercury perchlorate as the metal precursor, stabilised with 1-thioglycerol as the ionic ($R–S^-$) stabilising ligand in alkaline solution. H_2Se gas in N_2 was the selenium precursor, formed by the action of a mineral acid on Al_2Se_3. Sodium selenide is an alternate source, less prone to surface oxidation when stored.

HgTe. Our earlier work on aqueous HgTe synthesis[236–239] led to remarkably strong (around 40% PL QY) and readily tunable IR luminescence in the 1–2 μm region[9,240] (shown in Fig. 16). In addition, by using an Ostwald ripening treatment, holding the initial synthesis product at around 70 °C for up to several hours, the average NC diameter could be increased further and the emission shifted out to 3.5 μm, as also shown. It should be pointed out that as with CdTe earlier, the highest PL QYs were obtained for the smaller sized particles and that the emission efficiencies declined on heating (see Fig. 17 and below,[243] for example). The synthesis originally used mercury perchlorate

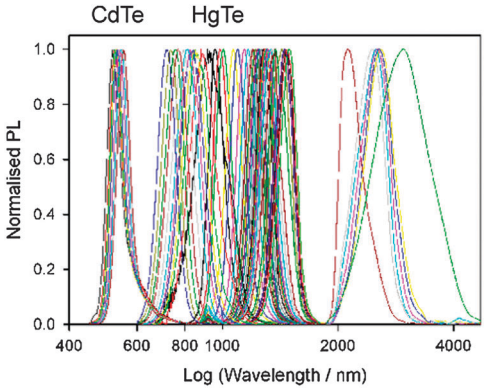

Fig. 16 Reliably narrow PL spectra obtained by aqueous synthesis of HgTe QDs. On the left part for comparison we show spectra of aqueous, size-fractionated CdTe QDs. Authors' previously unpublished data.

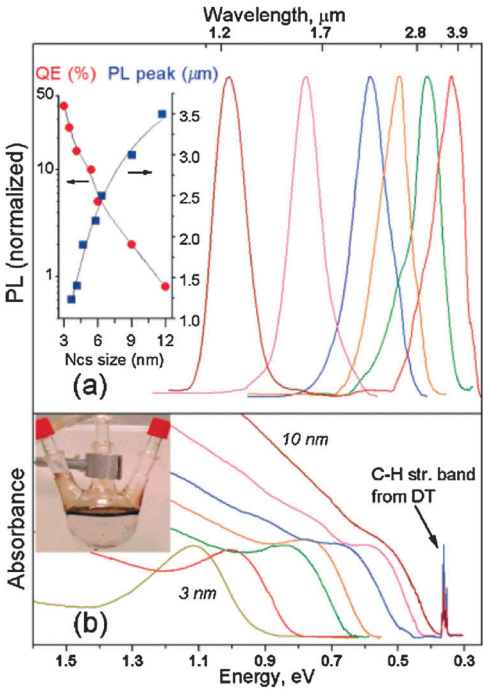

Fig. 17 Representative room temperature PL (a) and absorption (b) spectra of dodecanethiol-capped HgTe NCs in CCl_4. The insets show the size dependence of the PL peaks with the corresponding quantum efficiencies (a) and illustrate the phase transfer completeness for MEA used as initial stabilizer (b). Reprinted with permission from M. V. Kovalenko *et al.*, *J. Am. Chem. Soc.*, 2006, **128**, 3516–3517. Copyright 2006 American Chemical Society (ref. 243).

complexed with a water soluble short chain thiol, with a negative charge in alkaline solution (typically pH 10–11) and tellurium added as H_2Te in a flow of nitrogen. The hydride was generated in a second connected flask *e.g.* by the action of acid on Al_2Te_3. A more convenient generation method for slow syntheses which can yield narrow size distributions (corresponding to PL peaks with $<10\%$ FWHM/λ_{max}) is the electrolysis of 50% sulfuric (or *e.g.* phosphoric) acid with a tellurium cathode.[241,242] Best results for 1300 nm to 1500 nm emission were obtained using 1-thioglycerol as the ligand.

Gaponik *et al.*[204] subsequently demonstrated that such aqueous HgTe NCs could be readily and efficiently transferred into polar organic solvents with dodecanethiol as a ligand to replace the short chain thiolate using acetone to reduce the interfacial surface tension between the two phases and facilitate exchange.

Zhang *et al.*[244] reported quantum yields of around 50%, growing HgTe NCs by the aqueous route using dihydrolipoic acid (made by reduction of lipoic acid with sodium borohydride) as a stabilizer. The latter was chosen as it was not only compatible with a further synthetic step to add a CdS shell, but was also a good, strongly charged ligand (compared with thioglycerol) suitable for the deposition of polyelectrolyte/NC films using a layer by layer coating method.

Green *et al.*[245,246] were one of the first to use an organic route to HgTe NCs. Using TOPO and $HgBr_2$ in ODE as their metal precursor, and injecting TOP–Te at 70 °C they grew HgTe NCs without the use of highly toxic mercury alkyl starting material. However the materials were not observed to be strongly luminescent on this occasion and had relatively poor stability.

Kovalenko *et al.*[243] developed the aqueous synthesis method further in order to grow larger sized HgTe NCs with emission ranging from 1.2 μm up 3.5 μm (corresponding to diameters from 3 nm to 12 nm). In their version of the synthesis H_2Te was generated and passed into the reaction flask rapidly at room temperature and after absorption in the reaction mixture the flask was heated to 75–80 °C and maintained at this temperature for several hours to Ostwald ripen the NCs to give the size and emission wavelengths required. They also compared the rates of growth for several water soluble mercapto ligands, finding that mercaptoethylamine (MEA) gave not only the highest rate of shift, but also the highest PL efficiencies, as shown in Fig. 17, though these fell rapidly as the NC size increased. MEA capped HgTe was also easiest to extract into organic solvents (after Gaponik[204]) with dodecanethiol–acetone, and in fact addition of acetone was often found to be superfluous in this case.

Recently Keuleyan *et al.*[247,248] have synthesized HgTe NCs with better optical properties in the mid-IR, that show excitonic absorption features, and narrow size distribution and emission to over 5 μm. Their approaches are organic: in one they first prepared a TOP–Te solution with an amount of butanol in addition. Their mercury precursor solution was mercury acetate dissolved in a butanol–pyridine mixture. The latter solution was injected into the TOP–Te solution which was maintained at a particular temperature between 0 and 90 °C, the temperature controlling the final particle size. If growth was allowed to continue for several minutes, precipitation eventually occurred and particles could not be re-dissolved, whereas early removal and quenching in dodecanethiol–ethanol solutions halted growth and gave a precipitate that was recoverable, after decantation of the supernatant, by re-dissolving in organic solvents. In a second version[248] they dissolved mercury chloride in oleylamine to form the metal precursor and into this they injected a TOP–Te solution. Size was determined by the reaction flask temperature at the time of injection and this ranged from 60–100 °C. Again immediate quenching in dodecanethiol–solvent solution after a few minutes reaction time was necessary to preserve solubility and halt continued growth.

Kim *et al.*[249] have also recently adopted a similar organic method (to grow particles with absorption edges in the 1–2 μm range), using a mercury acetate/oleylamine/dodecanethiol metal precursor. After heating the latter under vacuum the flask was cooled to room temperature and diphenyl ether added. TOP–Te in a further amount of TOP was injected at various temperatures between 60 and 100 °C, according to the particle size required.

Piepenbrock *et al.*[250] have reported a *low temperature* organic method to produce HgTe NCs with diameters around 3.4 nm emitting in the 1.3 to 1.5 μm range. They prepared a solution of mercury acetate in ethanol and HDA and after heating to give a clear solution, the flask was cooled in dry ice. A TOP–Te solution was injected into the flask whilst it was being cooled and NCs started to form. Eventually a precipitate was formed which could later be collected, washed and redissolved in organic solvent (*e.g.* toluene). The authors reported substantial Ostwald ripening of their NC solutions on standing, emissions red-shifting by several hundred nm over a number of days.

A room temperature version of the organic synthesis method for HgTe was reported by Li *et al.*[251] They used mercury oxide with oleylamine in ODE to furnish the metal precursor. Cooling the solution to room temperature after preparation, they added dodecanethiol which is a stronger coordinating ligand than oleylamine alone, and this presumably was the primary reason why they could grow with control at room temperature rather than below zero degrees Celcius. Their tellurium precursors were either TOP–Te or tellurium dissolved in tributylphosphine and were injected into the mercury solution at room temperature. HgTe NC solutions were extracted and growth quenched by dilution in toluene. The authors reported a steady progression of clearly defined band edge features (though there was no strong excitonic peak). They observed no strong progression of the PL, though it is highly likely that this was masked by the long wavelength cut-off of their spectrometer's photodetector at around 850 nm. Almost certainly their emission peak *was* progressing unobserved.

Priyam *et al.*[252] have grown HgTe NCs in water-compatible polyamidoamine dendrimers without the need for small molecule stabilizers, using mercury chloride and NaHTe as the respective precursors. With generation 7 dendrimers they were able to grow slightly oblate nanoparticles with 2.6 nm diameter minor axes, a size distribution width of around 10% and band edge in the 900–1000 nm region.

Song *et al.*[253] have prepared HgTe nanowires of ~15 nm diameter and lengths around 200 nm by a sonochemical method with 1-thioglycerol present to stabilize the product and regulate growth.

Rath *et al.*[254–256] have published a number of articles on electrochemically deposited HgTe NC films. Galvanostatic deposition from acidified mercury chloride–tellurium tetrachloride

solution at room temperature yielded 5.35 nm average diameter particles (by TEM) with PL reported at various wavelengths in the visible, *in contrast to* infrared emission at these and smaller diameters for colloidally grown materials reported by most others. With DNA template material the same authors grew 1.59 nm diameter conjugated NC's[257,258] and report very narrow fluorescence spectra, again at visible wavelengths. More recently the same group reported 2 nm diameter HgTe NCs claiming emission in the UV at around 360 nm using a non-electrochemical growth method.[259] A solution of mercury chloride and L-cysteine ethyl ester hydrochloride stabilizer in water was de-aerated and a second solution of NaHTe prepared from tellurium powder and $NaBH_4$ in water. The two solutions were mixed at 90 °C and stirred at that temperature for 6 hours to yield a fine *black powder precipitate*. No mention is made of the solution pH and no reason given why Ostwald ripening at this temperature would not lead to HgTe particles far larger than 2 nm.

CdE and HgE alloys. In addition to the recent short review on alloy composition QDs by Regulacio and Han[13] mentioned in the introduction, there are also several comprehensive works on narrow bandgap bulk semiconductors and their alloys that are useful sources of reference for cadmium and mercury telluride related systems. The reviews by Dornhaus and Nimtz[260] on $Hg_xCd_{1-x}Te$ materials, and by Rogalski,[261] more centered on optoelectronic applications, are highly recommended starting points for those working on NC versions of these materials.

HgCdTe. The tendency of mercury telluride and cadmium telluride heterostructures in contact with each other to undergo interdiffusion of the two metal cations is well known and was observed in HgTe–CdTe superlattices[262,263] well before the advent of colloidally synthesized NC variants. Our earliest work on CdHgTe systems[236,238] was originally intended to mirror previous work on CdS–HgS–CdS core–multishell heterostructures by Schooss *et al.*[264] by forming the analogous Te heterostructures. However it rapidly became clear that in fact alloying of the metal cations was occurring at least to some degree. The synthetic route was based on the aqueous HgTe route and emission was observed to shift across the 700 nm to 1200 nm range, depending on the Hg/Cd ratio. The emission efficiency was also observed to remain high, in contrast to some reports for other ternary II–VI alloy nanoparticles. This may in part be due to the fact that in our early work the Hg ion addition was done in several small stages rather than by co-dissolving the metal precursor salts and attempting to grow rapidly with disparate metal reactivities.

Haizhu *et al.*[265] also reported HgCdTe alloy NC formation by a variation of our earlier aqueous route. Taking a mixed metal salt solution with MPA as the ligand in alkaline solution, they introduced a solution of NaHTe prepared by reduction of tellurium using $NaBH_4$. The resulting alloy NC solution was additionally annealed at 40 °C for 30 min. The group points out that for approximately equal metal ion starting concentrations, nucleation and growth will be faster initially for HgTe because of the 20 fold lower solubility product compared to CdTe.

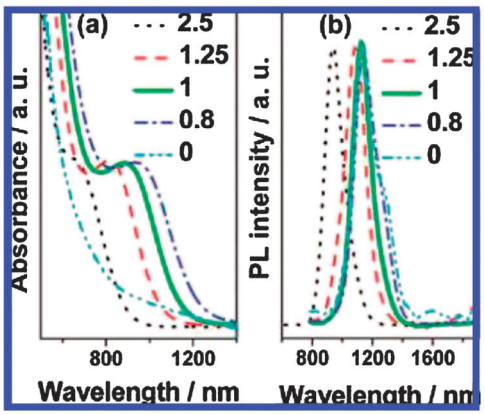

Fig. 18 (a) UV-vis absorption and (b) PL spectra of CdHgTe NCs with different Cd–Hg feed ratios of 2.5, 1.25, 1, 0.8, and 0, corresponding to $Cd_{0.46}Hg_{0.54}Te$, $Cd_{0.29}Hg_{0.71}Te$, $Cd_{0.23}Hg_{0.77}Te$, $Cd_{0.14}Hg_{0.86}Te$, and HgTe NCs, respectively. The CdHgTe NCs with the highest QYs are the bold traces. Reprinted with permission from S. Haizhu *et al.*, *Chem. Mater.*, 2008, **20**, 6764–6769. Copyright 2008 American Chemical Society (ref. 265).

Thus they deduced that single step mixed aqueous salt syntheses will result in Hg-rich cores and Cd-rich shell regions, which appears to be beneficial in terms of both emission spectrum shape *i.e.* relatively narrow and with peak wavelengths tunable to 1150 nm as shown in Fig. 18. Quantum yields up to 45% were measured.

Lesnyak *et al.*[266] developed the aqueous 'one-pot' synthesis still further. Taking around 1 : 19 ratios of mercury to cadmium salt starting molar ratios, to take account of the differing solubilities, they synthesized alloy NCs with MPA and also with TGA ligands. Further heat treatment at much higher temperatures than Haizhu *et al.* (refluxing at 100 °C) efficiently red-shifted the band gap absorption features and the fluorescence maxima. In the case of TGA the reflux treatment moved the emission out to around 1600 nm after 22 hours, whereas with MPA the red shift was limited to just under 800 nm.

Yang *et al.*[267] used an aqueous ion exchange method to form HgCdTe alloy particles starting with mercaptoethylamine stabilized CdTe NCs grown in water. This was followed by partial ligand removal by precipitation with alcohol and separation of the precipitate by centrifugation and re-dissolution in an aqueous mercury salt solution. Whilst this removed any excess cadmium ion from the original CdTe synthesis, and may facilitate the exchange process, a further consequence was the tendency of the alloy NCs produced to form into chains and eventually alloy composition wires. This is not uncommon with other tellurides when precipitated from aqueous solutions in this way.

HgCdTe nanorods emitting at up to 830 nm with good quantum yields (around 18%) were grown in aqueous solution by Tang *et al.*[268] Initially CdTe nanorods were synthesized in aqueous solution using a mixture of TGA and cysteine ligands. Partial cation exchange was carried out by treating the nanorod with aqueous mercury acetate solution.

Smith and Nie[269] synthesized HgCdTe NCs by ion exchange of organically grown CdTe QDs (hot injection growth with

mixed ligands of oleylamine, tetradecyl phosphonic acid and TOP). The exchange used mercury salts dissolved in chloroform and yielded emission red-shifted from the visible to around 1000 nm. The emission spectra remained reasonably narrow and the corresponding absorption spectra retained the excitonic band edge shape in the range of NC size and composition studied. Taniguchi and Green[270] have also produced HgCdTe NCs by a similar method to that of Smith, performing their cation exchange with mercury bromide in a toluene–methanol solution. Taniguchi *et al.*[271] followed up their initial findings with more detailed discussion and analysis of the mechanism of their exchange process, focussing on the increased anisotropy of the product. They attributed this to a molecular 'welding effect' of mercury telluride formed during exchange, effectively joining CdTe NCs together, leading to alloy nanoparticles with inhomogeneous distribution of the cations. The authors also discussed the role of the methanol (used to help solvate the mercury salt) in this process and this may be a common factor with Yang's findings.[267]

HgCdS. Korgel *et al.*[272] grew $Hg_xCd_{1-x}S$ nanoparticles by precipitation of mixed cadmium and mercury chloride salts absorbed within vesicles with ammonium sulfide as the sulfur source. Prior to the addition of the sulfide, the excess metal ions external to the vesicles were removed by passing the solution through an ion exchange column. They observed weak emission in the 435–440 nm range, relatively weakly dependent on composition, and a more strongly composition dependant absorption feature which was assigned to deep trap state emission from Hg centres acting as impurities in CdS rather than a direct excitonic transition. The absorption spectrum features ranged in energy from 4.5 to 3.15 eV, far higher than would be expected for simple excitonic emission from 4 nm particles, given the bulk bandgap energies of the respective constituent binary semiconductors.

HgCdSe. Doll *et al.*[273] have grown zincblende HgCdSe extensions onto the ends of wurtzite CdSe seed nanoparticles that had been pre-treated to oxygen passivate the side walls of the seed CdSe particles. No fluorescence data were reported, but diameters and overall heterostructure lengths are in a size range in principle relevant for narrow bandgap emission, *etc.* However defects at the interface between cubic and hexagonal regions are likely to lead to substantial trapping and low emission efficiencies.

Taniguchi and Green[270] formed HgCdSe nanoparticles starting with previously prepared CdSe QDs and nanorods (in organic solvents) treated with mercury ions to partially replace cadmium ions in the structures by an ion exchange process. The mercury ion source was mercury bromide prepared in a methanol–toluene solution. The visible CdSe emission peak and absorption band edge were replaced by longer wavelength features in each case, with far weaker fluorescence. For the QDs, the absorption profile became less pronounced but with excitonic features still clearly visible, red-shifted by around 100 nm, but with very weak corresponding fluorescence. For the nanorods, the absorption was less substantially affected, but the emission was a little more visible, having broadened substantially and red-shifted to between 700 and 900 nm. This may have been due to either trap states (as the authors suggest) or localised composition variation forming a segmented heterostructure, leading to separation of holes and electrons which then recombine less readily. However no time resolved data were given to corroborate this hypothesis – recombination across such an interface would be expected to be somewhat slower than bandedge recombination.

Very recently Prudnikau *et al.*[274] have examined the same system in detail, introducing mercury by ion exchange into zincblende and wurtzite QDs and wurtzite nanorods. Each of these starting materials were synthesized by various hot injection methods in organic solvents. The mercury ion source mercury(II) benzoate was prepared in tetraethyleneglycol dimethylether and the exchange carried out in toluene solution in a sealed flask. In this case stronger near IR emission but with the same characteristic broad profile in the 700–900 nm range was observed after the partial exchange process. The structure type was seen to have a bearing on the efficacy of the exchange process, but in both QD cases a zincblende alloy nanoparticle was eventually obtained, with some time for rearrangement in the wurtzite to zincblende case. In the wurtzite nanorod exchange process the authors saw evidence that the mercury exchange was localised in the rod *i.e.* in mercury rich regions, transformation to zincblende ordering occurred, whilst adjacent regions remained more like the original CdSe wurtzite structure until later in the exchange process.

HgSeS. Alongside their work on HgSe 2–3 nm diameter clusters cited above, Kuno *et al.*[222] also made $HgSe_{1-x}S_x$ clusters in the same size range using their surfactant mediated two phase (water–organic solvent) synthesis method. The small size range resulted in alloys with emission limited to the visible at the lowest x values studied, though this could extend into the near IR for larger particle sizes.

Turner *et al.*[275] attempted to address the differences in chalcogen precursor reactivities by using a single mixed chalcogen source $Me_3Si–SeS–SiMe_3$ for their pyrolysis route to $HgSe_xS_{1-x}$ NCs. The metal source was mercury acetate with tributyl phosphine as ligand. Again 2–3 nm diameter particles were reported as the product, but absorption spectra shapes and the solution colour cited suggest that there was probably a broad distribution of sizes with a tail extending to large sizes. However there were no PL measurements given to confirm this.

CdSeTe, CdSTe. There have been several reports of CdSeTe alloy NC syntheses which include compositions extending the emission range into the near IR. Bailey and Nie[276] first synthesized a range of CdTe and CdSe based structures including homogeneously alloyed CdSeTe and CdSeTe gradient composition structures with Te rich core regions emitting in the 700 to 900 nm region. Gurusinghe *et al.*[277] and Piven *et al.*[278] followed with further similar reports – in the former case the authors

synthesized CdSTe alloy NCs by hot injection (with Cd oleate as the metal precursor) and in the latter CdSeTe was prepared by an aqueous synthesis.

Bailey and Nie's synthesis was a mixed chalcogenide precursor hot-injection method, with cadmium oxide HDA and TOPO as the metal containing part of the reaction mixture. The chalcogenide precursor was a selenium–tellurium TOP mixture with the ratios weighted to compensate for the 2 fold difference in reactivities between Te and Se and both in large excess relative to the amount of cadmium. Gurusinghe *et al.* make the point that for some alloy compositions, the bowing constant (a parameter in the bandgap energy *vs.* composition relationship) is sufficiently large enough to yield alloy bandgaps lower than either of the binary end-point compositions, *e.g.* CdS or CdTe in their case. Again their materials had emission energies in the near IR, up to around 800 nm and both homogeneously distributed and radial gradient compositions were shown (see Fig. 19).

Piven *et al.* used simultaneous injection of NaSeH and NaTeH precursors into an alkaline cadmium salt solution with TGA as ligand. Again emission in the near IR was observed and a bowing constant derived, but emission was found to be much weaker than the corresponding CdTe and CdSe endpoint materials. Significant differences were also observed in the reactivity of the two chalcogen precursors.

CdE and HgE core–shells. The earliest synthesis and characterisation of core–shell and multilayer (sometimes termed quantum dot quantum well) NC structures were reported by Weller's group[279–283] and others using the Weller group synthesis method.[284–286] CdS–HgS–CdS multilayer particles were prepared by aqueous synthesis, varying the solution pH at key stages to balance nucleation of fresh nanoparticles against additional growth on the surface of existing QDs. CdS was first grown in an aqueous solution of cadmium ions with hexametaphosphate as the stabilizer and H_2S as the sulfur precursor. Nucleation was started at high pH, and growth continued at progressively lower pH, effectively stopping additional nucleation. Addition of mercury ions to the NCs for the first shell was done by surface ion exchange at neutral pH (step change), with the amount of mercury added calculated to just cover the available CdS surface. Returning the pH to a lower value caused the further deposition of Cd ions (along with sulfur from the H_2S) to resume and the presence of this outer stabilizing layer is cited as the reason why the mercury interlayer did not simply diffuse into the CdS core.[284]

The quantum dot quantum well concept was extended to make structures with many additional layers and with varying shell thicknesses (as shown schematically in Fig. 20[287]) by Dorfs and Eychmüller,[288] Braun *et al.*[289] and Dorfs *et al.*[290] again using the same basic synthetic approach. Schill *et al.*[291] modified the synthesis to prepare CdS–HgS–CdS multilayers in poly(vinylpyrollidone) (PVP) composites by carrying out the synthesis with relatively low molecular weight (50 kD) PVP as the ligand, water/methanol as the solvent and metal chlorides as the respective metal precursors. Korgel and Monbouquette[272] produced HgS–CdS core–shell structures without ligands using the vesicle (restricted growth) method described earlier for alloy structures.

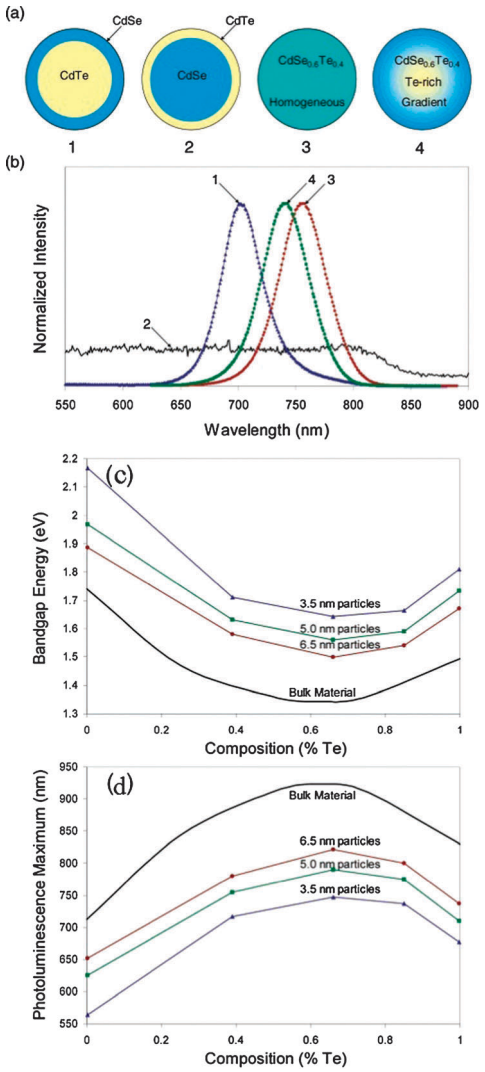

Fig. 19 Internal structures and optical properties of core–shell and alloyed $CdSe_{1-x}Te_x$ QDs: (a) schematic drawings of four different types of QDs; (b) their corresponding fluorescence emission spectra. (1) Traditional core–shell CdTe–CdSe dots; (2) reversed core–shell dots; (3) homogeneous alloyed dots; and (4) gradient alloyed dots. All dots were synthesized to have a mean diameter of 5.9 nm (core plus shell) and an overall composition of $CdSe_{0.6}Te_{0.4}$, with relative standard deviations of *ca.* 10%. Within each batch of NC samples, the standard deviations for both size and composition were approximately 5%. (c) The absorption onset energy (in eV) as a function of tellurium content; and (d) the emission peak wavelength (nm) as a function of tellurium content. Note that the absorption onsets are slightly lower in energy than the emission maxima. Reprinted with permission from R. E. Bailey and S. Nie, *J. Am. Chem. Soc.*, 2003, **125**, 7100–7106. Copyright 2003 American Chemical Society (ref. 276).

The Weller group's pioneering work on multilayer heterostructures triggered a great deal of interest from other groups. Whilst the CdS–HgS–CdS system is (in principle at least) epitaxial, Cd^{2+} and Hg^{2+} ions having almost identical radii, it has proved to be the case that NC multilayers do not have to be perfectly lattice matched and a number of multilayer and simple core–shell structures have been successfully synthesized. In some cases the purpose is simply to passivate the core surface (remove traps) or isolate the core electronically from the

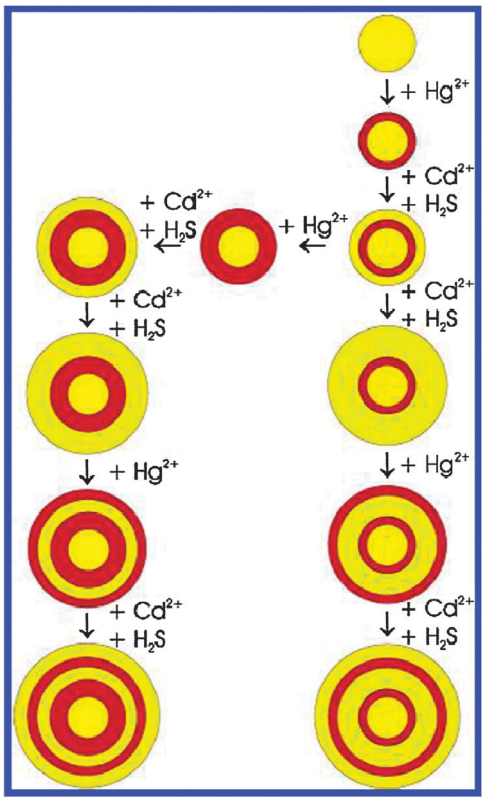

Fig. 20 Synthetic route for different CdS–HgS structures. Reprinted with permission from D. Dorfs *et al.*, *J. Phys. Chem. B*, 2004, **108**, 1578–1583. Copyright 2004 American Chemical Society (ref. 287).

surrounding environment. In other cases the differing energy levels of holes and electrons in core and shell are advantageously aligned to form type II heterostructures so that excited electrons and holes may be spatially separated within the particles.

HgTe–CdS. Harrison *et al.*[292] grew HgTe NCs capped with a thick layer of CdS, simply by adding washed HgTe nanoparticles grown in a previous aqueous synthesis to a cadmium salt–thioglycerol solution (at high pH) and adding H_2S gas (see Fig. 21 for HRTEM image). The solution could also be refluxed at this stage, but this did not appear to affect the optical properties of the capped NCs. Zhang *et al.*[244] have recently revisited the HgTe–CdS core–shell synthesis using their dihydrolipoic acid ligand in place of the thioglycerol used by Harrison. Interestingly, when they refluxed their capped material after adding the CdS shell they observed a substantial red-shift that was reflux time dependent and which is difficult to explain in terms of continued growth of the CdS shell thickness. It may possibly be the case that a concentration of unreacted mercury ion from the core synthesis was present in the capping reaction solution and the shell composition and size were both changing during reflux. In addition, their TEM images do not appear to show any contrast between core and shell regions, whereas the contrast between the two was clear in the images from Harrison *et al.*

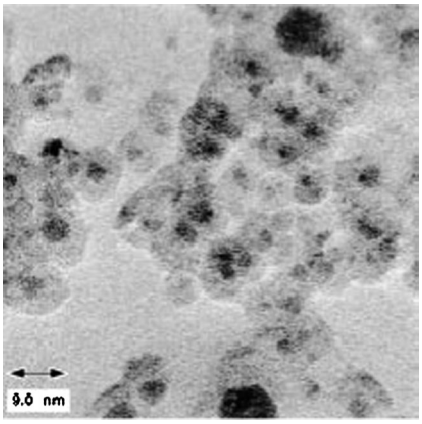

Fig. 21 HRTEM image of a 30 min refluxed HgTe–CdS composite material. Reproduced from ref. 292, M. T. Harrison *et al.*, *Adv. Mater.*, 2000, **12**, 123–125.

CdTe–CdS. There have been a few accounts of red to near IR emitting CdTe–CdS core–shell syntheses. Schöps *et al.*[293] synthesized CdTe NCs partially coated with a CdS shell showing emission between 700 nm and 800 nm. They used a two stage organic method, CdTe core NCs were first prepared by hot injection using dimethylcadmium in TOP into a solution of TOPO, HDA and ODE. The resulting NCs were then purified in toluene and injected into a (hot) fresh TOPO–HDA solution and cadmium precursor (cadmium ethylhexanoate) and sulfur source (thiourea) were added drop-wise.

Zhao *et al.*[211] prepared CdTe–CdS by a hydrothermal process with a *N*-acetyl-L-cysteine ligand present. NCs with emission between 600 and 900 nm were synthesized and it was claimed that the ligand also furnished sulfur to form a layer of CdS at the high reaction temperatures (200 °C) used in the process. A range of reaction temperatures were used to vary the particle size and thereby the emission wavelengths and it is claimed that the surface was passivated by a thin layer of CdS in each case. It is not clear how the formation of a graded CdSSe (perhaps sulfur rich at the outside) structure was avoided.

HgTe–CdTe–HgTe. Our attempts to synthesise HgTe–CdTe–HgTe analogues of the original CdS–HgS–CdS Weller heterostructures led instead to (graded) alloy heterostructures.[294] Similar work by Kim *et al.*[295] starting with a CdTe core also led to core–graded alloy shell heterostructures (CdTe–HgCdTe) with the composition in the shell varying radially. Kim *et al.*[296] claimed to produce the inverse CdTe–HgTe–CdTe heterostructure taking pre-synthesized CdTe NCs and adding them to an alkaline solution of Hg salt and thioglycerol. H_2Te gas was then passed through the solution. It isn't clear how this two stage growth process resulted in a three layer heterostructure, and the basis for the assumption of a discrete triple layer structure seems to rest heavily on comparisons of the spectral width of the emission with our alloy data from the literature, despite there being no discussion in either paper about respective size distributions. There is no strong indication of a multilayer structure in their TEM data.

HgCdTe–ZnS and other shells. In addition to synthesising HgCdTe alloy core NCs (see earlier) Tsay *et al.*[297] also added a further ZnS capping layer. Their organically grown ternary core NCs were washed and re-dissolved in chloroform and then added to a tributylphosphine–TOP mixture. Dimethyl zinc, $(TMS)_2S$, and tributylphosphine were then added drop-wise to complete the shell formation. Addition of the ZnS shell was seen to further red shift luminescence by up to 110 nm, depending on the shell thickness, whilst preserving the emission spectra's FWHMs.

Smith and Nie[269] took their ion exchanged HgCdTe synthesis a stage further by adding shells of CdTe and then CdZnS ternary outer shells to the alloy composition cores. Their shell synthesis was similar to that of Tsay *et al.*[297] but using mixed dimethyl zinc and dimethyl cadmium for the ternary outer layer. After adding the multilayer shell the emission was observed to be very similar to that of the original cores apart from a significant improvement in quantum efficiencies. The lack of an additional red shift on capping was attributed to the CdTe intermediate layer which avoided the formation of a stress induced type II structure.

HgTe–HgCdS. Building on our earlier synthetic work on HgCdTe alloys we extended our aqueous synthetic route to add CdHgS ternary shells on top of HgTe core NCs. With Fradkin *et al.*,[282,283] using PL and optically detected magnetic resonance spectroscopy, the nature of the ternary shell was established.

CdTeSe–CdS. Ternary core–binary shell NCs emitting in the near IR (to just over 800 nm) for biological applications were made by Jiang *et al.*[298] Mixed selenium and tellurium precursors (TOP–Te, TOP–Se) were injected into a hot dimethyl cadmium–TOPO mixture to form the ternary cores. When the required size for a given chalcogen composition ratio was reached the NCs were capped by adding a mixture of TOP–$(TMS)_2S$ as a sulfur source, with the reaction flask temperature lowered from 325 °C to 280 °C.

More recently Pons *et al.*[299] have synthesized a similar ternary core–ternary shell material, CdTeSe–CdZnS, also using a hot injection organic route. Their materials emit in the same near IR range, with biological tagging cited as the primary application. Rather than using highly toxic dimethyl cadmium and zinc compounds, they employed cadmium complexed with tetradecylphosphonic acid for the core NC synthesis and mixed cadmium and zinc oleates for the shell addition. A mixture of TOP–Se and TOP–Te was added to the metal precursor/TOP/ODE to form the core NCs. Before adding the ternary shell, the core material was collected and re-dispersed in a trioctylamine–TOP mixture, along with the mixed metal oleates. The sulfur precursor for the shell was TOP–S. Trioctylamine and metal oleate precursors for the shell were justified in terms of better shell quality and said to preserve the zincblende structure in both the core and shell, rather than tending to switch to wurtzite in the shell.

3.3 Silver chalcogenide (and copper sulfide) alloys

Earlier accounts of colloidal silver chalcogenide NC syntheses used techniques derived from commercial silver halide processes and microemulsion techniques using the surfactant AOT to regulate the contact between precursors in either phase. Buschmann *et al.*[300] reported Ag_2Se NCs in the 2–15 nm size range using the two techniques. Larger NCs of Ag_2S, Ag_2Se and Ag_2Te ranging from 21 nm to 40 nm were prepared by Jiang *et al.*[301] using a slow (72 hours) interfacial reaction between silver nitrate in the aqueous phase and triphenylphosphine chalcogenides in a toluene phase. Elongated nanoparticles (nanorods and nanotubes) of $Cu_{2-x}Se$, Cu_2Te, Ag_2Se and Ag_2Te were prepared by Jiang *et al.*[302] at room temperature, with CuO and AgCl as the metal precursors, ethylenediamine as a metal chelating agent, hydrazine as a reducing agent and elemental selenium or tellurium as the chalcogen source. NCs of 8 nm and 50 nm diameter on and within polydiacetylene (PDA) thin films were formed by Belman *et al.*[303] by exposing PDA monolayers on top of aqueous silver nitrate solutions to H_2Se gas. Liu *et al.*[304] used a reverse micelle microreactor approach similar to previous accounts but adding a perfluorinated surfactant alongside the AOT and replacing the regular organic solvent with supercritical CO_2. This yielded NCs with a narrow size distribution – 5.9 nm average diameter, FWHM 1.65 nm.

Shi *et al.*[305] described the use of commercial metal extraction compounds (such as (di(2,4,4-trimethylpentyl) monothiophosphinic acid) to coordinate with silver ions prior to reaction with H_2S to form NCs in the 10 nm size range in organic solvents.

A conversion method, using pre-prepared silver nanoparticles was given by Tan *et al.*[306] to produce either partially or fully selenized Ag_2Se particles. In the case of partial selenium absorption, silver–silver selenide core–shell particles were formed. Aqueous silver colloids were mixed with ethanolic solutions of CSe_2 and exposed to UV light to trigger the reaction to form the selenide NCs. The diameters of smaller particles ($\sim$10 nm) increased slightly on full selenization, but larger particles tended to crack and form hollow structures.

Tang *et al.*[307] synthesized thin films of $\sim$25 nm Ag_2S NCs by depositing solutions of a single source precursor Ag(SCOPh) dissolved in TOP onto a hot (160 °C) substrate.

As precursors for mesoporous materials, Ag, Ag_2S and Ag_2Se nanoparticles (4.7 nm, 7.3 nm and 8.5 nm respectively) NCs were synthesized directly in organic solvent by Wang *et al.*[308,309] Silver nitrate and the elemental chalcogen were simply added to octadecylamine and the mixture stirred at 180 °C for 10 to 20 min.

Several groups have used biologically compatible ligands in the synthesis of silver chalcogenide NCs. Kim *et al.*[310] prepared CuS, Cu_xS, and Ag_2S, the latter in the 20–50 nm size range. Metal salts were simply treated with sodium sulfide in the presence of dextran polymers to stabilize the NC product, and could be almost completely removed subsequently by treatment with a dextran digesting enzyme. Gu *et al.*[312] used glutathione in conjunction with sodium selenite and alanine to coordinate their silver ion precursor in the preparation of 1.5 nm to 2.4 nm diameter NCs with near IR emission ranging up to 820 nm.

There have been a number of reports of silver chalcogenide–metal heterostructures:

Yang and Ying[313] have grown gold on Ag_2S NCs (with gold deposited at single sites) and Ag_2S on gold as core–shell nanoparticles. Gold core–Ag_2S shell nanorods and nanoparticles (with lengths/diameters around 50 nm) with a void formed between the inner and outer components were synthesized by Zhu *et al.*[314] Partially Au coated Ag_2S particles have also been formed by Qu et al[315] who observed gradual coalescence of mixed Au nanoparticles and Ag_2S NCs over a period of several hours. Similarly 15–25 nm diameter particles of Ag_2S with single site Ag decoration have also been synthesized by Jiang *et al.*[316]

Sahu *et al.*[311,317] have successfully applied a modified hot-injection approach to the synthesis of Ag_2S, Ag_2Se and Ag_2Te, producing sub-10 nm diameter particles with low polydispersities (~5%, ~5%, 9% respectively). Silver nitrate and sulfur (or selenium or tellurium) were each dissolved separately in TOP and the chalcogen solution and then added to a flask containing OA, octadecylamine and ODE. At 160 °C the Ag–TOP solution was injected and the reaction continued for around 5 min at a slightly lower temperature. They obtained Ag_2S and Ag_2Te in monoclinic phases and Ag_2Se in a metastable tetragonal phase. In their later paper the authors refined their method, with a slightly lower growth temperature to fine-tune the synthesis of Ag_2Se, showing size control over the size range from 2.8 nm to 10.4 nm. This corresponded to a bandgap range from 0.89 eV down to 0.19 eV (see Fig. 22 for corresponding absorption spectra and bandgap data), the latter being one of the lowest yet reported NC bandgap energies.

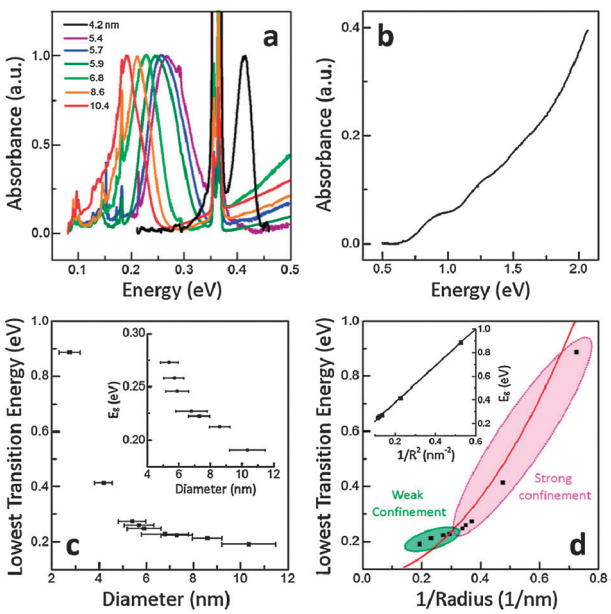

Fig. 22 (a) Room-temperature mid-IR absorbance spectra of films of Ag_2Se NCs of different sizes. The strong peak around 0.36 eV is due to C–H stretches in the organic surface ligands. (b) Room-temperature near-IR absorbance spectrum of 2.8 nm Ag_2Se NCs dispersed in tetrachloroethylene. (c) The energy of the lowest optical transition *versus* size for Ag_2Se NCs. The error bars represent one standard deviation. The inset is a blow-up for NCs larger than 5 nm. (d) The energy of the lowest optical transition *versus* 1/radius. The solid red line represents effective mass theory using literature parameters. The transition energy does not vary as 1/radius but rather $1/(\text{radius})^2$ for NCs ~6 nm, which are strongly confined (inset). The solid black line is a linear fit to the data with a coefficient of determination of 0.9998. Reproduced from ref. 311.

The drawback of having to conduct the hot injection reaction at lower than ideal temperatures to efficiently trigger nucleation in silver chalcogenide syntheses has been addressed by Yarema *et al.*[318] Building on their prior observation that Pb chalcogenide nucleation benefited from the presence of tin silylamide, the same approach was found to be useful in silver chalcogenide formation. However a different reaction mechanism was proposed in the latter cases. They found lithium silylamide to be a better choice, co-injecting the latter along with the chalcogen precursor (*e.g.* TOP–Se) into the metal precursor solution. For the latter they used a solution of silver trifluoroacetate and oleylamine as a coordinating solvent. By restricting the nucleation temperature to under 100 °C Yarema *et al.* were able to grow the monoclinic form of Ag_2Se, but the silylamide promoted nucleation at this low temperature, leading to monodisperse and small particle formation. The method was also found to be generally applicable to the sulfide and telluride and shells of ZnSe were also successfully added to such NCs.

Mesoporous silica shell coated silver sulfide particles emitting in the IR at 1275 nm were recently reported by Han *et al.*[319] First silver nanoparticles were formed in mesoporous silica shells, and this was followed by sulfidation *in situ* with sodium sulfide solution in a one-pot reaction scheme.

An alternate approach to hot injection (applied to many other metal sulfides) by Zhuang *et al.*[320] is termed 'dispersion-decomposition'. In their method, a metal salt (*e.g.* silver nitrate) is simply heated with a large excess of dodecanethiol as both a ligand and a sulfur source. Heating to 200–250 °C resulted in the decomposition of the intermediate metal thiolate to form relatively uniform metal sulfides. For silver and copper sulfides, particles in the few to 10 nm size range were obtained.

Silver chalcogenides in ion exchange reactions to form other II–VI and IV–VI NCs. The use of ion exchange processes in NCs (and nanorods, *etc.*) has recently been investigated as both a method to indirectly form silver chalcogenide NCs and conversely using the latter as templates to form other narrow bandgap metal chalcogenides.

Alivisatos' group has extensively studied ion exchange in silver chalcogenide systems. Starting with CdSe, CdTe or CdS NCs (as dots, rods or tetrapods) Son *et al.*[321] demonstrated exchange to corresponding (lower bandgap) silver structures and in a subsequent step could also show the reverse step. In the case of fluorescent materials, in some cases the recovered cadmium analogues showed some evidence of surface disruption (fluorescence from surface traps) but were otherwise, largely identical in form to the original structures. The forward exchange (Cd^{2+} replaced by $2Ag^{+}$) was initiated simply by mixing a toluene solution of the cadmium chalcogenides with an equivalent amount of silver nitrate solution and a small amount of methanol. The reversal was carried out by adding a 50–100 times excess of cadmium nitrate in a toluene–methanol solution with a small amount of tributylphosphine.

The fast (< few milliseconds) and complete nature of the forward exchange process was demonstrated by Chan *et al.*[322]

using millisecond resolution X-ray absorption spectroscopy in a microfluidic reactor chip. Sadtler *et al.*[323] examined and compared the spatial distribution of copper and silver in separate exchange reactions with CdS nanorods where the amounts of Cu^+ or Ag^+ ions added were calculated to be less than twice the cadmium equivalent. Cu exchange was observed by TEM to be concentrated on the end facets of the rods and could be asymmetrically distributed between the two facets. Silver uptake was initially more patchy along the rod, but the Ag_2S regions rapidly organised into discrete regular bands as the silver/cadmium ratio increased. The mechanism for localisation of Ag_2S was attributed by Robinson *et al.*[324] to be driven by strain with typical swings of +2% to −2% (of bond length) in regions along the rod axis on traversing each Ag_2S zone. Fluorescence from the rods in the 900 nm to 1500 nm range was observed and its tuning could be achieved according to the size of the Ag_2S zones.

The preparation of cubic silver selenide NCs (rather than the more often encountered orthorhombic form) by water-based ion exchange from zinc selenide NCs has been reported by Wang *et al.*[325] They used water-soluble, MPA stabilized NCs as the starting templates, and trisodium citrate and silver nitrate aqueous solutions to carry out the exchange. The authors also suggested that the same approach could be used to obtain copper and lead selenides in the same manner.

The exchange process of cadmium replacement by silver in CdSe nanowires has been monitored during the exchange process by Dorn *et al.*[326] A mat of such wires was deposited onto an electrode array and could be observed in the same locations, optically, by SEM and HRTEM before, after and at intervals during the process by temporarily removing the sample from the exchange medium. Furthermore, the sample's conductivity could be measured *in situ* during the exchange process, with a substantial increase observed as the silver content increased. As with the Alivisatos group's findings, they confirmed that the exchange was substantially topotaxial.

Mukherjee *et al.*[200] have also studied ion exchange starting with CdS nanowires. *Via* an intermediate stage with partial replacement of Cd^{2+} with Ag^+ they then went on to replace the silver with lead ions to form regions of PbS along the surface of the CdS wires, serving as p–n (PbS–CdS) nano-junctions. The first stage employed silver nitrate with methanol as the exchange agents, whilst for the second stage the authors used lead nitrate and examined the effect of various proportions of tributylphosphine in regulating the degree of exchange and the density of surface lead sulfide zones.

Zuo *et al.*[327] and Moon *et al.*[328] have described the formation of silver telluride nanowires and rods starting with tellurium nanowire templates. The latter group then described the further ion exchange to form CdTe, ZnTe and PbTe wires and in the case of CdTe nanowires a further exchange to form $PtTe_2$ nanotubes. Moon *et al.* rationalised the relative ease of ion exchange for a wide selection of binary metal chalcogenides in terms of their (aqueous) solubility products (though exchange is often carried out in alcoholic rather than aqueous solutions) and again considered the role of additional complexing agents such as tributylphosphine or TOP in assisting otherwise thermodynamically unfavourable transformations.

Silver–silver chalcogenide core–shell NCs have also been used as the starting templates for the formation of hollow metal chalcogenide and selenium–metal chalcogenide core–shell structures. Zhu *et al.*[329] grew hollow PbSe nanoparticles starting from Ag/AgSe NCs. Initially ethylenediamine is used to chelate elemental selenium and then nanoparticles of selenium formed by slowly adding the solution to water. After transfer to ethylene glycol the selenium nanoparticles were treated with silver nitrate to form the core–shell templates (stabilized with PVP). Ion exchange to form PbSe was carried out in methanolic solution using lead acetate, with tributylphosphine to assist the exchange. Although the hollow structures formed were relatively large (hundred nm or more diameter), the walls were relatively thin (around 20 nm), resulting in some quantum confinement relative to the bulk material. The same group extended the method to include zinc and lead selenide structures and also metal chalcogenide shells around iron oxide cores (Camargo *et al.*[330]).

3.4 Other related nanoscale metal chalcogenides

Most of the following materials (*e.g.* Bi_2E_3, SnE (E = S, Se, Te), *etc.*) have narrow bandgap energies but do not show significant fluorescence (SnTe is a direct gap semiconductor and so NCs show fluorescence, whilst the SnSe and SnS analogues are indirect). They are however of interest for hybrid nanomaterial solar cell and thermoelectric applications. Many of these materials have also been grown by solvothermal and hydrothermal methods, especially the bismuth chalcogenides, for thermoelectric studies. Generally such methods yield larger scale particles, wires and other structures with size scales of several tens to hundreds of nm. Here we focus on synthetic methods that yield smaller structures, though some hydrothermal methods, often those including ligand materials in the reactant mixture, produce materials in a similar size range. In some cases the materials are also of interest for cation exchange routes to other materials such as lead chalcogenides.

Nanoscale Bi_2S_3 was prepared as early as 1994 by Weller *et al.*[331] as a potential light harvesting material for use in conjunction with wide bandgap semiconductors for solar cells. Suarez *et al.*[332] later reported a simple synthesis using BiI_3 treated with H_2S in acetonitrile solution with particle growth restricted using a porous Nafion membrane. Foos *et al.*[333] produced Bi_2Te_3 with sizes below 10 nm, controlling the size by reacting $BiOClO_4$ with $(TMS)_2Te$ in a reverse micelle formed by sodium dioctylsulfosuccinate (AOT) and water/hexane. The NC product was dissolved in toluene and washed with TOP added during the work-up to stabilize the NCs.

Kovalenko *et al.*[167] recently produced both Bi_2S_3 and PbS nanoparticles capped with either Sb_2Te_3 or Sb_2Se_3 (antimony zintyl) ions in hydrazine as precursors to form thermoelectric films. By using inorganic rather than organic ligands they were able to sinter NC films without leaving any carbonaceous residues behind in the nanostructured film.

Very small tin sulfide clusters were also reported in the 1990s by Bowes and Ozin[334] who grew Sn_4S_6 particles using Zeolite-Y as a so-called supercage. In 2007 Kovalenko *et al.*[335] reported the synthesis of SnTe nanoparticles in the 4–15 nm size range. After some trial and error the authors settled on a hot injection method using bis[bis(trimethylsilyl)amino]tin(II) (Sn-[$N(SiMe_3)_2$]$_2$) rather than an oleate or chloride as the metal source, and TOP–Te with oleylamine as the chalcogen precursor and ligand respectively. The same group[335] also synthesized SnSe and found that the tin could readily and rapidly be displaced by lead ions in the SnTe and SnSe NCs. This observation led to a novel synthetic method to produce PbSe NCs[336] by carrying out the cation exchange in the reaction flask at the point when SnSe particles were nucleating. By including lead chloride with the previous reactants the authors were able to grow PbSe with an effectively much lower barrier to nucleation, leading to less asymmetric particles and faster onset of NC growth.

Ning *et al.*[337] also described a synthetic method to produce small ($\sim$4 nm) diameter SnTe NCs. They used $Sn_6O_4(OH)_4$ as their tin precursor with OA and oleylamine as ligand. The tin salt solution was dehydrated at 180 °C before TOP–Te was injected to form NCs. The same group reported an analogous method to produce SnSe with selenourea as the chalcogen source.[338]

Xu *et al.*[339] reported the synthesis of good quality SnTe particles with sizes tunable from 2 nm to 37 nm. They dissolved tin bromide in dimethylformamide with triethanolamine as the ligand. The tellurium source, NaHTe, produced by the reduction of tellurium by sodium borohydride, was injected into the metal salt solution at 50 °C. Additionally the solution could also be refluxed for a few minutes to increase particle sizes.

A number of groups have synthesized SnS NCs in recent years: Stavrinadis *et al.*[340] used hot injection (temperatures between 80–170 °C) of $(TMS)_2S$ into a tin oleate–oleylamine ODE solution to yield particles in the 3.6 nm to 9.6 nm size range. Hickey *et al.*[341] grew very good quality and low polydispersity (<10%) NCs using a similar approach to that of Kovalenko for SnTe mentioned above. (Bis[bis(trimethylsilyl)-amino]tin(II)) was used to form tin oleate by reaction with OA in ODE with TOP as the ligand. Into this prepared solution, thioacetamide with oleylamine and TOP were injected at 170 °C.

Copper indium disulfides–copper indium diselenides and related I–III–VI ternary compounds. There has been a great deal of interest in recent years in I–III–VI ternary compounds for solar applications in particular and NC versions of these and other closely related narrow bandgap materials have been investigated by several groups primarily with the view to extending the spectral harvesting range of solar cells, whilst trying to avoid the use of heavy metals such as lead or cadmium as the chalcogen's counterpart.

Prior to Allen and Bawendi's[342] report of CuInSe NCs grown by hot injection, previous syntheses had employed single precursor pyrolysis methods[343] that tended to yield NCs with no or weak fluorescence due to poor surface quality and difficulty controlling particle sizes. Mixed metal iodides dissolved in oleylamine and TOP were heated to between 280 and 360 °C. $(TMS)_2Se$ in TOP was injected as the selenium precursor yielding NCs emitting in the 600–900 nm range. Using the same approach the authors also synthesized $AgInSe_2$ with up to 15% PL quantum yields.

Xie *et al.*[344] addressed the poor air stability of the amine ligand capped CuInSe NCs with a modified synthesis using dodecanethiol as the ligand and indium stearate/copper acetates with OA as the metal precursors. $CuInS_2$ NCs were then grown by injecting sulfur/oleylamine in ODE. Passivation was achieved by adding a ZnS shell upon injection of a solution of zinc stearate/oleylamine in ODE yielding air-stable NCs with emission spectra ranging up to around 1000 nm. Again the silver version, $AgInS_2$, could be grown, replacing the copper source with silver nitrate.

$AgInSe_2$ nanoparticles have also been grown by Tian *et al.*[345] with a single source precursor, $(PPh_3)_2AgIn(SeC\{O\}Ph)_4$, with oleylamine and dodecanethiol present during the pyrolysis (at around 120–130 °C). However the particles were mainly large (lengths ranging from 15 nm to around 100 nm) and 'tadpole' shaped. Some fluorescence was observed at just over 800 nm.

$AgInS_2$ NCs and nanorods ($\sim$9 nm and 3 nm $\times$ 30 nm respectively) were grown by Peng *et al.*[346] using individual precursors by hot injection. For NCs, silver acetate and indium triacetate were heated with dodecanethiol and octadecane. Elemental sulfur in oleylamine was injected and reaction allowed to proceed for *e.g.* 2 hours (relatively long for a hot injection synthesis). Injection and growth at lower temperatures yielded nanorods.

Small $CuInS_2$ NCs (around 2 nm) emitting at 660 nm were recently synthesized by an aqueous method by Liu *et al.*[347] Whilst they used copper and indium chlorides as metal precursors, again they favoured a thiol, mercaptoproionic acid, rather than an amine as the coordinating ligand. As for many other thiol reactions involving mercapto acids, the pH was raised (to 11.3) to form the thiolate as a coordinating species. The sulfur precursor $CS(NH_2)_2$ was added with the solution still at room temperature. The reaction mixture was then transferred to an autoclave and reaction carried out for 150 °C for 21 hours. The reaction temperature was chosen to balance the reactivities of the two metal precursors. Lower temperatures favour the formation of copper sulfides (of various stoichiometries), but at higher temperatures (*e.g.* 150 °C) the indium also participates in the reaction.

Alloy NCs of $(ZnSe)_x(CuInSe_2)_{1-x}$ and $CuInSe_xS_{2-x}$ with composition dependent bandgaps as low as 0.96 eV have been reported by Li *et al.*[348] Cubic and pyramidal zincblende particles with sizes in the 20 nm range were obtained – the ZnSe component helping to stabilize the zincblende structure at room temperature. The synthesis was by hot injection, with selenium (or selenium/sulfur) dissolved in oleylamine heated in the main reaction flask. The metal precursors, chlorides of copper, and indium (and zinc) were dissolved in oleylamine

and heated to 220 °C prior to being injected into the main flask which was held at 300 °C. Their reaction times were around 5 min.

3.5 Synthetic method summary

The last few years in particular have seen great improvements in the synthetic methods used to produce narrow bandgap colloidal NCs and an expansion of the range of materials that can be grown by these methods. The range has been extended, not only in the semiconductor species, but also the diversity of heterostructures and shapes of NC particles that can be synthesized. These advances have been supported by more detailed understanding of the details of the growth mechanisms involved (*e.g.* the subtleties of the nucleation processes[219,318]) and by ever more sophisticated spectroscopic[104] and electronic measurement techniques. The influence of synthetic factors, *e.g.* reaction temperatures,[62] choice of reagents, by-products,[122,172] rate of addition of reagents *etc.*, upon the NC quality are becoming better understood, leading to better performance at the NC level at least, *e.g.* quantum yields of 60–80%[205,206,215] are commonplace for many materials, with core–shell and composition gradient[189] structures.

The choice of ligand(s) is not limited to those which optimise the synthesis. Better understanding of ligand exchange processes[12,204] allows the ligand used in growth to be readily exchanged for ones better suited to the target application: for photovoltaic (PV) and electronic applications long alkyl chain ligands can be exchanged for short chain molecules[45,110,111,120] or even small inorganic molecules[40] or atomic shells;[349] for organic solvent processing, ionic ligands can be replaced by solvent-soluble organic materials;[204] in biological applications, compatibility can be improved by coating with polymer or biomolecular species.[27,94] In the latter case, the great potential for narrow bandgap materials as fluorophores in the near IR tissue transparency window[350] is attracting interest from the biological sciences, not just from the optical penetration standpoint, but also the potential for multiplexing with several narrowly defined NCs and the useful gating characteristics[244] with typical NC fluorescence lifetimes in the one to a few 100 ns range to improve signal to noise.

Driven largely by the electronic (charge transfer) requirements of QD based FETs, and solar cell devices the use of small inorganic molecules or atomic anions as the final ligand applied to QDs after synthesis or even deposition has become increasingly popular and has led to useful improvements in performance. Pourret *et al.*[351] have deposited a few atomic layer thick films of ZnO on CdSe QD films previously treated with NH_4OH to remove organic growth ligands. Ihly *et al.* have used the same approach on narrow bandgap PbS QD films with Al_2O_3 as the inorganic layer capping layer.[352] Talapin and coworkers[353] and Kovalenko and co-workers[354,355] have pioneered approaches where growth ligands are exchanged in solution for so-called molecular metal chalcogenide complexes (*e.g.* zintyl ions above), chalcogenides such as As_2S_3 or chalcogenide ions. These approaches are all synthetically compatible with the vast majority of the narrow bandgap materials discussed herein and can be expected to improve both stability and performance in most applications.

In the case of low bandgap QDs such as HgTe, Ag_2Te and PbSe the influence of the vibrational spectra of the stabilizer ligands on QD PL quantum yield has been investigated, and the effect of organic ligands, rich in strong C–H overtone and combination bands (and of course those of other functional groups) points towards the eventual use of more suitable infrared materials hosts and ligands such as the zintyls and chalcogens above. Kovalenko *et al.*[243] pointed out the rapid decline of the PL efficiency of HgTe at longer emission wavelengths, and Semonin *et al.*[356] similarly correlated the drop in the quantum yields of PbS and PbSe QDs of various sizes to the proximity of vibrational levels in their oleic acid ligands at larger dot sizes. The probable influence of coupling to ligand vibrations was also remarked by Pietryga *et al.*[129] in earlier work on long wavelength PbSe QDs. Photoluminescence lifetime measurements on PbSe and PbSe–CdSe core–shell QDs with hydrocarbon and perfluorinated ligands by Liu and Guyot-Sionnest[357] also support the mechanism of dipolar transfer of energy from the QDs to the vibrational modes of the surrounding ligand molecules.

Ion-exchange growth methods[321] are becoming increasingly popular: in many cases a desired optimum shape, size and size distribution of NCs can be obtained using one type of semiconductor and the cation or anion structure exchanged to form an alternate semiconductor from the original template.[328] This opens up many possibilities – for materials which are difficult to grow with a particular shape or size, that may be first achieved with a more amenable template and the NC then converted to the required material by exchanging anions or cations. Some materials, for example, are difficult to grow as nanorods,[270] with no strong difference in surface energy in any given crystallographic direction, precluding the use of ligand mixtures to encourage anisotropic growth. Partial exchange may also lead to useful alloy compositions[269] or heterostructures.[324] In the former case this may be a more useful and controllable method of synthesis than direct growth with mixed (*e.g.* cation) precursors, especially where the two alloy components have widely differing reactivities or solubilities.

4 Coupled nanoparticles, films and self-assembly

4.1 Hybrids – NCs coupled with other nanoparticles

Perhaps the most basic form of nanoparticle assembly is the conjugation of NCs with other nanoparticles or substrates. The linking of narrow bandgap semiconductor NCs with wide bandgap nanoparticles has been particularly important in the development of QD sensitized solar cells. Mostly lead sulfide or selenide NCs have been combined with titania nanoparticles: Sun *et al.*[76] prepared PbS NCs in the presence of previously synthesized titania particles using $SHCH_2CO_2H$ as a stabilizer and a bifunctional linker, inferring coupling between the two types of nanoparticle at either end of the mercapto-acid.

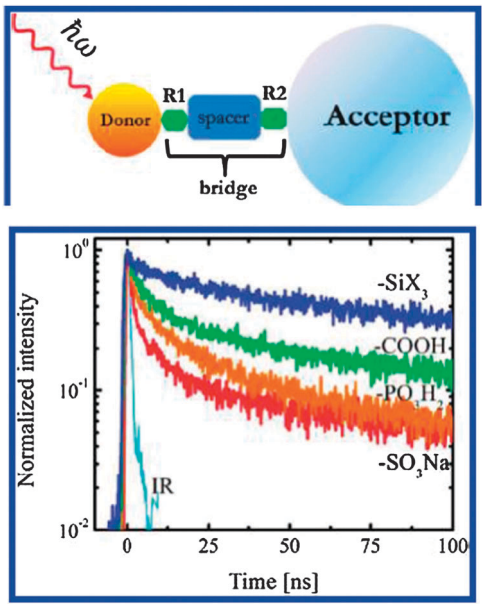

Fig. 23 Top – Schematic of a donor–linker molecule–acceptor system. In the present work, the donor is a PbS NC and the acceptor is a TiO_2 nanoparticle with a diameter of 25 or 50 nm. The linker molecule consists of functional groups R1 and R2 and a spacer (S). Bottom – Variation of fluorescence decay of PbS NCs coupled to TiO_2 with different anchor groups binding to the TiO_2. Aliphatic linker molecules have thiol (–SH) groups at one end to bind to the NC and different anchor groups at the other end to bind with TiO_2: MPTMS (HS–$(CH_2)_3$–$Si(OCH_3)_3$, solid blue line), MBA (SH–$(CH_2)_3$–COOH, solid green line), MBPA (SH–$(CH_2)_4$–PO_3H_2, solid orange line), and S3MPS (SH–$(CH_2)_3$–SO_3Na, solid red line). IR (solid cyan line) is the instrument response function. All linker molecules have a three carbon chain except the MBPA. 1/e decay times are 77 ns (silane group), 12 ns (carboxylic acid), 5.8 ns (phosphonic acid), and 2.5 ns (sulfonic acid), respectively. Reprinted with permission from B.-R. Hyun *et al.*, *Nano Lett.*, 2011, **11**, 2126–2132. Copyright 2011 American Chemical Society (ref. 358).

The coupled particles were then deposited by electrostatic interaction onto a substrate coated with layers of polyelectrolytes. MPA has similarly been used recently by Wang *et al.*[359] to link PbS to copper decorated TiO_2 nanoparticles to form a photocatalyst for the reduction of CO_2 to CH_4, with the PbS acting as an electron donating sensitizer. Turyanska *et al.*[90] similarly combined PbS with titania in Schottky type solar cells using thioglycerols, though they grew the NCs separately in water and then absorbed them into porous titania layers from solution.

The Wise group[358] has made a comprehensive study of the effect of the linker molecule between NC and titania particles upon electron transfer rates as a function of the linker length, functional groups within the linker molecule and specifically also the functional groups at the ends of the linker anchoring to the respective particles. Interestingly, as shown in Fig. 23, whilst the choice of anchor functional group was found to have a substantial influence on transfer rate, the length of the intermediate section of the linker molecule rather than its chemical structure was found to be a more significant factor.

Etgar *et al.*[360] have investigated PbS/titania nanosheet based heterojunction solar cells. They took PbS QDs grown organically with an OA ligand and replaced the latter with a MPA ligand. Rather than combining PbS and titania intimately, a layer of MPA capped PbS NCs was deposited upon a layer of TiO_2 nanoplatelets in their solar cell structures, with contact (*via* linker molecules) only along the layer interface.

Acharya *et al.*[105] have avoided the use of linker molecules by growing PbSe NCs directly onto the surface of TiO_2 nanorods. The latter were grown first and PbSe NCs formed by a hot injection method, decorating the surface of the wide bandgap nanorod substrate. The two materials were in intimate contact, quasi-lattice matched along the interfaces between them. The use of the hot injection method was also extended by Acharya *et al.*[42] to grow not only lead sulfide, but also lead selenide, and lead telluride on titania nanoparticles. Using cation exchange they were also able to add CdS and Cu_2S to the selection of intimately contacted NCs.

Apart from wide bandgap oxides, NCs have also been used in combination with carbon nanostructures (C_{60} and graphene) in solar cell studies. Dissanayake *et al.*[361] combined C_{60} with PbS capped with OA and (in view of the thermal stability of the two respective nanoparticles) used pyrolysis to remove the organic ligand in the composite film to improve electron transfer. Graphene flakes have also been used as a substrate during PbS growth by hot injection using TOP ligands. Manga *et al.*[362] combined the two nanomaterials, finding that the PbS was directly contacted on the graphene substrate, with only outward facing PbS surfaces capped with the ligand. The authors then went on to grow titania nanoparticles on the surface of the composite by including the hybrid particles in a further synthetic step, hydrolysing titanium alkoxide in alcoholic solution to first form a titania sol–gel and subsequently pyrolysing the product to convert the titania component to form anatase particles.

4.2 NC doped polymer films, NC gels and photonic crystals

There are many examples of narrow bandgap NC–polymer composites, both for film fabrication and as a method to encapsulate or stabilize the NCs themselves. In the latter case, NCs were usually grown *in situ* either in solid polymer hosts or in polymer solutions. Composites have also been formed post-NC synthesis. Sometimes this was a relatively trivial step, the only requirement being mutual solubility of the ligand stabilized NCs and polymer in a common solvent and miscibility of the two components after removal of the solvent in the case of solid composites. In early work Gao *et al.*[363] prepared PbS in methacrylate–styrene copolymer matrices using lead methacrylate precursors to form an intermediate organosol. Exposure to H_2S formed PbS QDs within the sol and thereafter the latter could be further cross-linked to form a solid. The nature of the surface leads to polymer bonding and the effect on the luminescence was further studied.[364] Lead sulfide QDs have also been prepared in polyacrylonitrile[365] and polymethyl methacrylate,[366] whilst silver sulfide QDs have been grown *in situ* in polyvinylpyrrolidone films,[367] and Ag_2S, Cu_2S and HgS have been grown in polyacrylamide by direct microwave heating of both the NC precursors and the monomer. Whilst these direct methods to form NCs in organically soluble polymers can result in quite

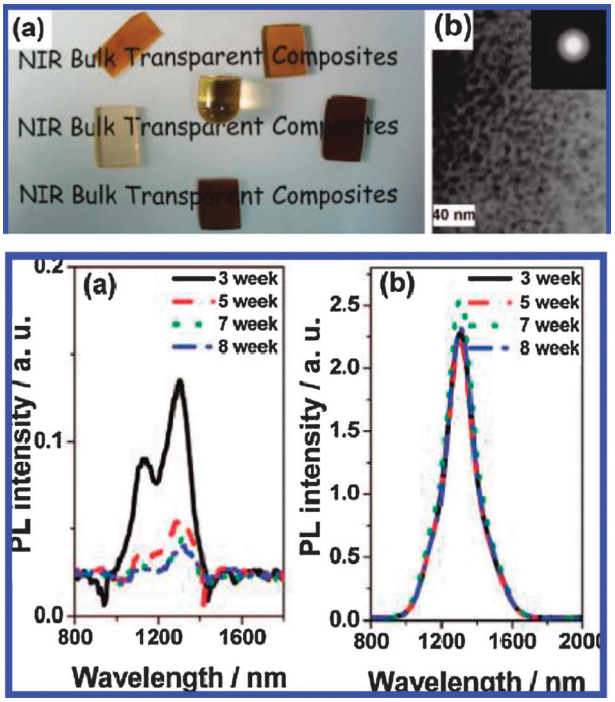

Fig. 24 Top – (a) Optical photographs of CdHgTe NC–polymer bulk composites in various shapes. (b) TEM image of a $Cd_{0.23}Hg_{0.77}Te$ NC–polymer composite based on the microtome method. Inset is the SAED pattern. Bottom – PL spectra after heat treatment at 100 °C of (a) CdHgTe NCs in aqueous solution and (b) the NC–polymer composites. Reprinted with permission from H. Sun *et al.*, *Chem. Mater.*, 2008, **20**, 6764–6769. Copyright 2008 American Chemical Society (ref. 368).

high loading (*e.g.* 50% or more inorganic content) and good dispersion, the control over size distribution and particle shape is relatively poor, leading to lower than optimum PL quantum efficiencies.

Sun *et al.*[368] adopted a more sophisticated approach, first synthesising HgCdTe alloy NCs with strong (up to 45%) QY and reasonably narrow size distributions by the aqueous route and then transferring the aqueous NC product into an organic solution containing a cross-linkable ligand, octadecyl-4-vinylbenzyl dimethylammonium chloride, which allowed incorporation into a thermally driven copolymerization with styrene and methylmethacrylate monomers. Composites with good transparency and stable luminescence (with respect to time and temperature) were obtained (see Fig. 24).

For relatively low loading (few % inorganic volume fraction) HgTe NC/PMMA films we and other groups[369] have found that it is relatively straightforward to use an organically soluble long chain thiol such as dodecanethiol (DDT) and simply co-dissolve the NC solution along with commercial PMMA polymer in a convenient polar solvent *e.g.* chloroform, toluene, chlorobenzene, *etc.*, depending on the application. Ketones will also act as a solvent, but tend to slowly destabilize the ligands, leading to gradual aggregation of the NCs. Shorter chain alkanethiol ligands may also be used, but the shorter homologues tend to be somewhat unpleasant to work with. This approach can be used whether organically or aqueous grown HgTe NCs are used, as it is relatively straightforward to extract aqueous material (*e.g.* with short chain thioglycerol or mercapto-acid ligands) into an organic solvent–DDT mixture. For many optoelectronic applications that involve propagation along the plane of the film rather than perpendicular to it (*e.g.* planar or single mode channel waveguide devices, *etc.*), low NC loading may be preferable in any case.

An equally straightforward approach was used by Choudhury *et al.*[137] to prepare a photorefractive poly(vinylcarbazole)/optically nonlinear dye (4-(*N*,*N*-diethylamino)-β-nitrostyrene) film sensitized with PbSe NCs. The latter were produced by hot injection with OA stabilizer and all the composite film ingredients were co-dissolved in toluene which allowed thin films to be prepared by either spin coating or drop casting.

HgTe NCs have also been grown within polyamidoamine (PAMAM) dendrimers, both within the interior voids and between adjacent dendrimer particles. Priyam *et al.*[252] have synthesized NCs emitting at 950–970 nm, *i.e.* fairly tightly regulated by the dendrimer dimensions, although particle size distributions were similar to those that can be obtained by regular colloidal aqueous synthesis. Bronstein and Shifrina[370] have recently given a comprehensive review of the use of dendrimers as size controlling media (*i.e.* as both cages and surfactants) for inorganic NC growth in general.

For biological applications, or in the case of NCs grown by aqueous methods where transfer to organic solvents and organically soluble ligands is either difficult or inconvenient, water soluble polymers such as polyvinylalcohol (PVA) or amphiphilic polymers have been used. They can also be useful for the reverse case, where organically grown material must be transferred into an aqueous environment, functioning as both a transfer agent and a stabilizer in the aqueous phase. Mahmood[161] has recently revisited the synthesis of PbSe NCs in PVA, correlating the NC size with polymer molecular weight and conversely investigated the effect on the polymer's degree of crystallinity due to the PbSe NC loading, and the consequent effect on the composite films' photovoltaic response. Zhao *et al.*[92–94] have explored the use of amphiphiles such as poly(maleic anhydride-*alt*-1-octadecene-*co*-poly(ethylene glycol)) to transfer or stabilize PbS and CdS capped PbS NCs in aqueous media. In their initial work, they found that transfer of oleylamine stabilized organically grown PbS using their amphiphilic polymer led to the initial narrow and monomodal size distribution splitting into a bimodal distribution due to etching of some NCs and Ostwald ripening of others, and the emission quantum yield also decayed dramatically. This was improved upon by the use of CdS capped PbS: organically grown materials had QYs up to 67% in organic solvents, whilst post-transfer, QYs in the 26–33% range were obtained in aqueous buffer solutions. The choice of initial stabilizer was also found to have a strong bearing on the size fidelity and colloid stability of the transferred material. PbS NCs without a CdS capping layer could be successfully transferred without significant degradation of the optical properties when grown with OA or OA–TOP ligands during the hot injection synthesis.[94]

Jia *et al.*[81] successfully incorporated hydrophilic PbS NCs into a commercial or Mercer photoresist formulation using

mercaptopropyl trimethoxysilane as a stabilizer to give compatibility with the ethanol based solvents. NC doping levels up to 0.04 wt% were used whilst still retaining the photolithographic sensitivity required to produce 1 μm periodicity photonic structures.

4.3 NC/polyelectrolyte layer by layer films/coatings

An alternate approach to the formation of high loading, thin NC/polymer films from aqueously grown materials is known as Layer by Layer (LbL) deposition,[371] using alternate immersion of substrates in polyelectrolytes and ionically charged NC solutions. Examples include the deposition of HgTe NC/polyelectrolyte multilayers on the surface of polystyrene spheres and opals and inverse opal structures derived from these,[372] and the deposition of planar multilayers on glass and ITO coated substrates.[373,374] Fig. 25 shows a typical quartz microbalance, frequency *vs.* dip cycle plot and corresponding sample photographs, indicating the good coating uniformity and linearity that can be obtained by this method. Rinnerbauer *et al.*[375] produced high quality HgTe/polyelectrolyte LbL planar films of 1–10 bilayer thicknesses and determined the dispersion relationship of the NCs by spectroscopic ellipsometry measurements. They were able to quantify confinement blue shifts not only for the bandgap transition, but also for higher energy transitions, along with transition strengths *vs.* NC diameters[376] (Fig. 26).

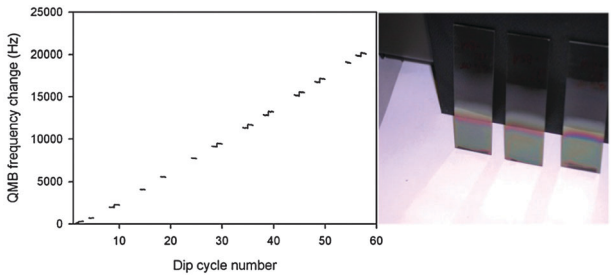

Fig. 25 Left – The quartz microbalance (QMB) frequency change during LbL coating with HgTe–PDDA multilayers (measured at dip cycle intervals and for several minutes at each measurement stage). Right – Photograph of HgTe/PDDA LbL coating on glass slides showing uniformity of layers distribution. Authors' previously unpublished data.

As a prelude to later work by others, Olk *et al.*[377] investigated the emission characteristics of single latex spheres coated with HgTeNC/polyelectrolyte LbL films emitting in the 1200 to 1800 nm range, finding that emission lifetimes were shortened as the number of layers deposited was increased. The conformal nature of the LbL coating process allows good quality (low surface roughness) coatings to be applied to other types of curved optical surfaces without too much degradation of their optical quality. This was exploited by Shopova *et al.*[379] who coated larger diameter silica microspheres (*e.g.* 650 μm diameter) with HgTe and HgCdTe alloy/polyelectrolyte LbLs. Such microspheres have resonant circumferential surface optical modes (termed Whispering Gallery Modes – WGMs) with very high finesse. NCs deposited in the surface region experienced very strong excitation electric fields due to the pump laser used and the high Q-factor structure. The emission spectrum of the NCs was also substantially modified due to the spectral resonances of the WGMs, with narrow emission modes obtained near 1250 nm.

Roither *et al.*[378] fabricated planar HgTe LbL microcavities, enclosing their resonator between a silica/titania multilayer Bragg reflector on a transparent substrate and a silica/metal reflector on top of their LbL film. They observed tuning of cavity modes in the 1400 to 1750 nm region with cavity length and with temperature, and moreover found the emission to have a low divergence, with the emission cone half-angle varying between 2.6 and 4.6 degrees (Fig. 27).

4.4 NCs with conjugated polymers

The combination of narrow bandgap NCs with conjugated polymers as composites has attracted a continuing high level of

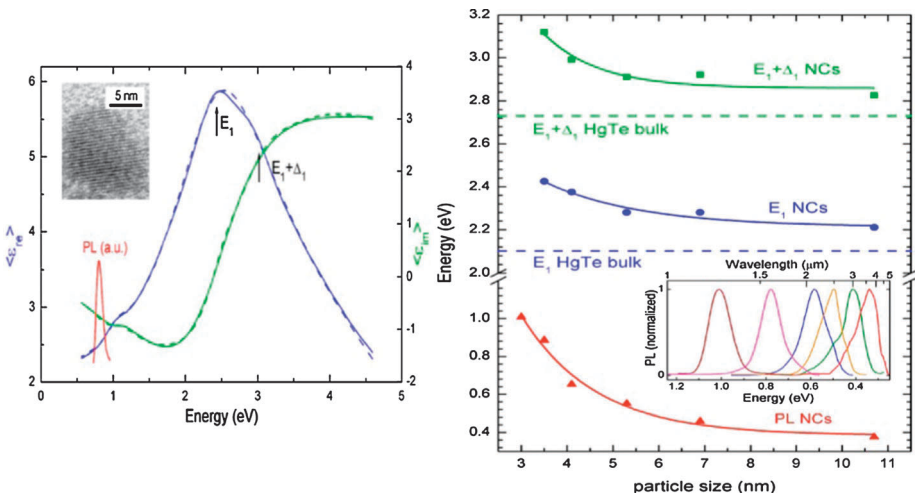

Fig. 26 Left – Spectroscopic ellipsometry measurement (straight line) and fit (dashed line) as well as PL measurement of a sample with ten bilayers of HgTe NCs–polyelectrolyte with a diameter of 3.5 nm on glass. Inset: TEM picture of a NC with a diameter of 9 nm. Right – Dependence of PL peak energy and higher transition energies on the size of HgTe NCs (lines are a guide for the eye). Reprinted with permission from V. Rinnerbauer *et al.*, *Appl. Phys. Lett.*, 2006, **89**, 193114 (ref. 376). Copyright 2006, American Institute of Physics.

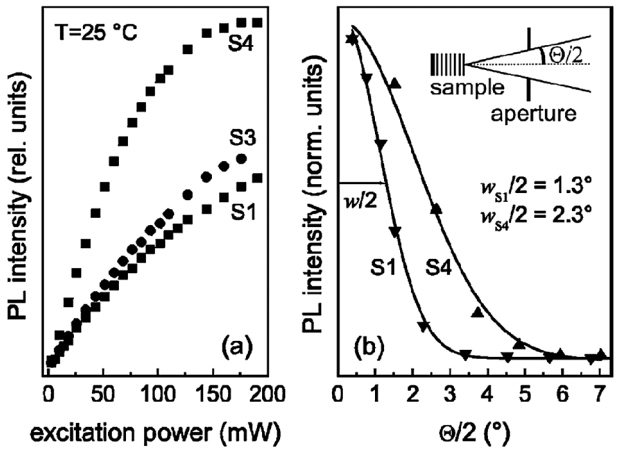

Fig. 27 (a) Power dependence of PL peak intensity for a number of different planar microcavity structures S1, S3, and S4 based on HgTe NCs. (b) PL intensity as a function of the half divergence angle. The fitted Gaussian function results in a total beam divergence of 2.6° for S1 and 4.6° for S4. Reprinted with permission from J. Roither *et al.*, *Appl. Phys. Lett.*, 2005, **86**, 241104 (ref. 378). Copyright 2005, American Institute of Physics.

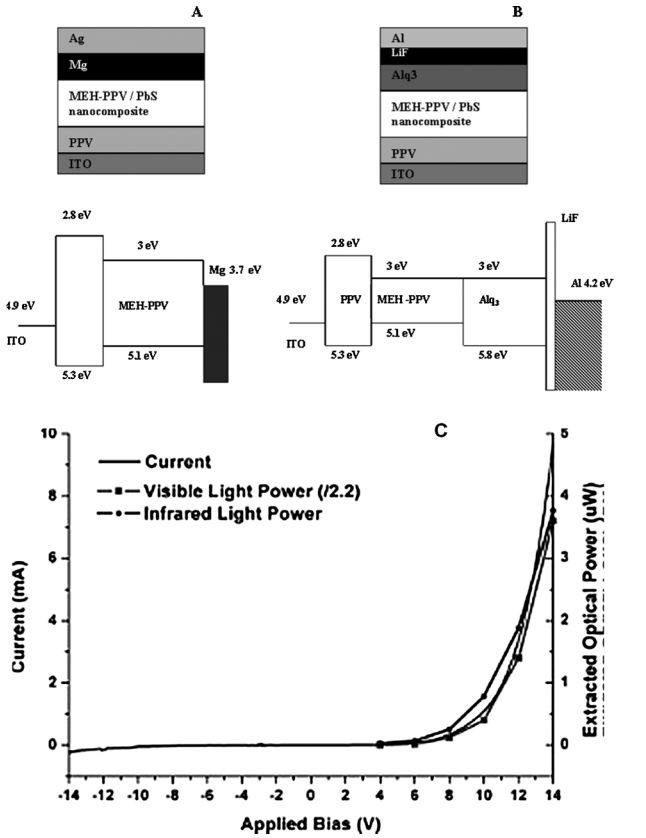

Fig. 28 MEH-PPV/PB based device structures. (A) The Mg-cathode device and the corresponding band diagram in flat-band conditions; (B) an Alq_3/LiF/Al-cathode device by comparison. (C) The light–current–voltage (L–I–V) characteristics of the 1 : 1 polymer/NCs Alq_3/LiF/Al device. The rectification is obviously improved compared to the Mg-cathode device. Reproduced from ref. 45, G. Konstantatos *et al.*, *Adv. Funct. Mater.*, 2005, **15**, 1865–1869, © 2005 WILEY-VCH Verlag GmbH & Co. KGaA, Weinheim, with permission from John Wiley & Sons, Inc.

interest for several applications (light emission, solar cells) due to the great potential for charge or energy transfer between the two species, with emission or absorption spanning the near IR region. Watt and co-workers have investigated PbS NC and nanorod blends with poly(2-methoxy-5-(2′-ethylhexyloxy)-*p*-phenylene vinylene) (MEH-PPV). With OA capped PbS they observed the signature of Förster energy transfer from the conjugated polymer to the PbS NCs,[380] and this is anticipated to be a means to improve the excitation of the PbS emitters, making use of the easier injection characteristics of the polymer. The carrier transport properties of MEH-PPV–PbS composites with NCs grown without ligand stabilizers were studied and the presence of the PbS NC has been found to dramatically improve both hole and electron mobilities and to give a better balance between the two relative to the case in the pure polymer.[381] The group used the same synthetic method to form nanorod–polymer composites by adding a post-synthetic treatment with alcohols, which led to oriented attachment of nanoparticles to form nanorod structures.[73]

The Sargent group is one of several that have pioneered the use of narrow bandgap NC–conducting polymer composites for solar cell and light emission devices.[382,383] They have also fabricated PbS NC/MEH-PPV electroluminescent devices and NC–Alq_3 hybrid devices (see Fig. 28) emitting in the IR (1000–1600 nm) region with external efficiencies of 0.27%.[45] This was 1–2 orders of magnitude higher than generally reported at that time for other IR emitting NCs dispersed in non-conjugated host polymers. Characteristic of the Sargent group's approach is the post-synthetic exchange of NC ligands to replace the oleate groups used during the hot injection synthesis.

Chambers *et al.*[384] have also investigated the use of PbSe NCs with MEH-PPV as potential gamma radiation detectors. Förster resonance energy transfer from NCs to polymer results in visible emission which is linearly proportional to the gamma radiation dose.

In addition to MEH-PPV, several groups have investigated lead chalcogenide NC blends with oligothiophenes and poly(thiophenes). Asunskis *et al.*[36] described a vapour phase and a solution based method to produce PbS–thiophene blends where the NCs were grown without an organic ligand layer. Tan *et al.*[385] and Itskos *et al.*[53] have studied poly(3-hexylthiophene) (P3HT) with PbSe and PbS NCs, respectively, as photovoltaic/photodetector materials. Tan *et al.* incorporated a layer of P3HT–PbSe NC blend into their planar-bulk heterojunction structure, to form a photovoltaic cell which showed an extended IR response and a power conversion efficiency of 0.26%. The Heiss group[53,55,386] combined P3HT and fullerenes in ternary blends with PbS NCs as extended IR range sensitizers. The inclusion of the fullerene molecules improved charge transfer between the respective polymer and NC components, acting as an intermediate in the transfer process (Fig. 29) with more efficient charge transfer at the fullerene–polymer and fullerene–NC interfaces compared to polymer–NC interfaces. This led to the demonstration of a photovoltaic response under reverse bias with an external quantum efficiency of 51% (with cut off around 1200–1300 nm). Ternary blends with larger diameter PbS (*e.g.* 5.2 nm) extended the range to around 1800 nm,

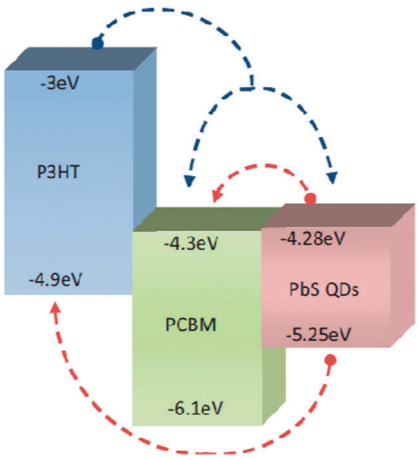

Fig. 29 Diagram of the energy band offsets for P3HT–PCBM–PbS NC blends. Interfacial carrier transfer channels potentially responsible for emission quenching of P3HT (blue dotted lines) and QD (red dotted lines) are also depicted. Reproduced from ref. 53, G. Itskos *et al.*, *Adv. Energy Mater.*, 2011, **1**, 802–812, © 2011 WILEY-VCH Verlag GmbH & Co. KGaA, Weinheim, with permission from John Wiley & Sons, Inc.

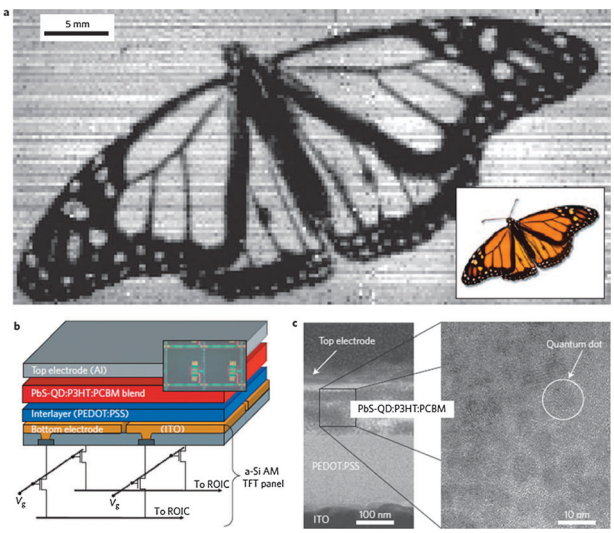

Fig. 30 PbS QD-sensitized organic NIR imager. (a) Infrared shadow cast at 1310 nm of a slide showing a monarch butterfly (the original slide is shown in the inset for comparison). (b) Schematic of the imager with an a-Si AM backplane and an unstructured inorganic–organic hybrid front plane. The inset shows an optical micrograph of two active matrix pixels with a pixel pitch of 154 μm. (c) TEM cross-section of the hybrid diode layer stack. The high-resolution TEM image shows colloidal QDs distributed in the P3HT:PCBM matrix. a-Si AM, amorphous silicon active matrix; ROIC, readout integrated circuits; TFT, thin-film transistor; P3HT, poly(3-hexylthiophene); PCBM, [6,6]-phenyl-C61-butyric acid methyl ester; PEDOT:PSS, poly(3,4-ethylenedioxythiophene):poly(styrenesulphonate). Reprinted by permission from Macmillan Publishers Ltd: T. Rauch *et al.*, *Nat. Photonics*, 2009, **3**, 332–336, copyright 2009 (ref. 386).

but with lower efficiencies. Their ternary blend was incorporated with a silicon TFT backplane to form an imaging device as shown in Fig. 30.

4.5 Cross-linked NC networks

Im *et al.*[387] and Hanrath *et al.*[143] respectively have produced PbS and PbSe films formed by networks of the particles themselves *i.e.* without the use of a host polymer to give the film its structure. In the former case, multiple coatings of a mesoporous titania photoanode with alternate PbS NCs and an ethanedithiol solution was used to fabricate a PbS layer in a hybrid photovoltaic cell structure with up to 3.4% power conversion efficiency. The bifunctional thiol linker molecule was used to bind the PbS NCs into a dense cross-linked layer that accumulated in thickness with multiple spin coating cycles. In the process of characterising NC–polymer blends and the effect of removing oleate ligands from PbSe NCs, Hanrath *et al.* found that the smaller, ligand-stripped PbSe NCs tend to show oriented attachment to form large, crystallographically connected nanoparticle networks. This is an example of a quite common phenomenon after treatments to remove ligands (*e.g.* Warner,[388] Sliem *et al.*[145]) and often occurs to some degree, in particular when precipitating NCs from aqueous solutions using alcohols.

4.6 NC close packed arrays, dense films and solids

For many applications it is desirable to have NCs more densely packed than in composite films or in randomly linked NC networks. NCs with narrow monomodal or bimodal size distributions may form regularly packed superlattices – either as 2-D arrays or as 3-D solids.[389] Equally, high density films may nevertheless be formed from less monodisperse size distributions also. Such densely packed NC materials generally differ markedly from their NC precursors in their optical and electronic properties and may be usefully exploited for optoelectronic and electronic device applications. Whilst the first reports of ordered metal nanoparticle 2-D arrays[390,391] involved simple TEM grid substrates, some of the first instances of narrow bandgap PbS and PbSe ordered arrays involved *in situ* growth on molecular monolayer substrates[392] and drop casting of NC–toluene solutions onto graphite substrates, where the formation of the ordered solid film was modelled as 2D gas–liquid–solid phase transition.[393] The advent of lead chalcogenide NCs produced *via* the hot injection method with narrow size distribution, capped with long chain ligands, made the formation of high quality ordered arrays on non-ordered substrates far easier and there have been many studies on such films in the last decade, focussed both on understanding the fundamental properties and exploiting the films in solar cells, photodetectors and light emitters. Steckel *et al.*[37] fabricated electroluminescent heterostructured LEDs incorporating PbSe 2D ordered array layers with emission centred at 1495 nm. Hu *et al.*[394] measured the local charge transport in PbSe NC arrays using electrostatic force microscopy, correlating local variations with ordering defects, *etc.* The conduction mechanisms in OA capped PbSe arrays were studied by Romero and Drndić.[395] As deposited their films initially showed Coulomb Blockade insulating behaviour, but on annealing at high temperatures, this gave way to a semiconductor carrier hopping mechanism as the ligand was progressively removed (Fig. 31).

The Nozik group has studied the effect of a number of capping ligands on PbSe NC close packed films, and the effect of treatments to remove oleate ligands from such films.

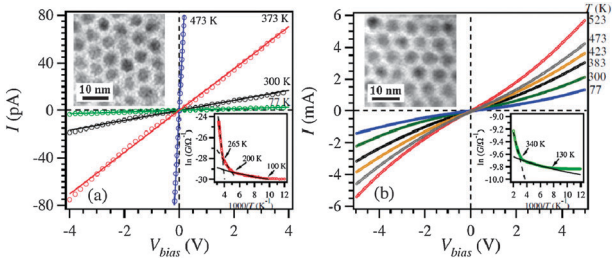

Fig. 31 *I*–V_{bias} characteristics *versus* *T* for a PbSe-NC array vacuum annealed *in situ* at (a) 473 and (b) 523 K. V_{bias} was swept at 100 mV s^{-1}. The solid lines in (a) are linear fits to the data. The lower insets show *G* (in log scale) *versus* the inverse of *T*. Here, the solid and dashed lines are fitted curves. The upper insets are TEM images of PbSe-NC arrays on thin amorphous carbon films, after vacuum annealing at 0.5 K min^{-1}. Reprinted figure with permission from H. E. Romero and M. Drndić, *Phys. Rev. Lett.*, 2005, **95**, 156801 (ref. 395). Copyright 2005 by the American Physical Society.

Table 2 Charging energy (E_c), site energy disorder ($\Delta\alpha$) and carrier mobilities (μ_e, μ_h) of PbSe NC FETs

Diameter (nm)	E_c (meV)	$\Delta\alpha$ (meV)	μ_e (cm^2 V^{-1} s^{-1})	μ_h (cm^2 V^{-1} s^{-1})
3.1	16	159	0.006	0.0002
4.1[a]	11	79	0.016	0.0023
4.8	9	65	0.032	0.0056
5.0	9	55	0.014	0.0039
5.2[b]	9	83	0.058	0.016
5.3[a,b]	9	72	0.054	0.010
5.4[b]	9	101	0.057	0.015
5.6[b]	8	125	0.057	0.012
6.1	7	59	0.070	0.028
6.5[a]	6	68	0.056	0.017
6.9	6	50	0.046	0.021
8.6[a]	4	73	0.025	0.039

[a] NC samples of equal $\Delta\alpha$ but different diameter. [b] NC samples of equal diameter but different $\Delta\alpha$. Reprinted with permission from Y. Liu *et al.*, *Nano Letters*, 2010, **10**, 1960–1969. Copyright 2010 American Chemical Society (ref. 398).

Sub-picosecond photoconductivity measurements for NC arrays with a number of amines (hydrazine, ethylenediamine, butylamine, and aniline) revealed differences in electronic coupling and carrier dynamics, with hydrazine favoured as giving the best balance between electronic coupling and carrier lifetimes for solar cell applications.[120] Further studies examined the efficiency of various treatments to remove oleate ligands (in film) with hydrazine–acetonitrile, hydrazine–ethanol, and pure ethanol. Whilst hydrazine–acetonitrile treated films became high mobility n-type, other treatments resulted in p-type materials.[110] The same group also examined the effect of using ethanedithiol as an insolublizing agent for layer by layer deposited PbSe–oleate capped NC layers, comparing such films with close packed films in which the ethanedithiol was introduced post-deposition. The layer by layer deposited films remained crack-free and had better quality conduction characteristics (p-type under illumination, ambipolar in dark).[111]

Similar studies comparing the effects of a range of dithiol ligands and ethanedithiol and other ligands for PbSe NCs on film conductivity, photovoltaic and photodetector performance have also recently been reported by Kuo *et al.*[396] and Sarasqueta *et al.*[397] Liu *et al.*[398] have conducted a systematic study of the effect of PbSe NC diameter and dithiol linker molecule length on close packed film carrier mobilities for both electrons and holes (Table 2). Fischbein *et al.*[399] combined electrostatic force, transmission electron, and atomic force microscopies (EFM, TEM, and AFM respectively) to visualize charge transport in monolayers and multi-layers of PbSe NC arrays. They were able to image charge densities to visualise the effect of layer thickness, and continuity on local carrier transport. Even without discontinuities, they found that monolayer pathways had substantially suppressed carrier mobility relative to multiple layer regions.

Mentzel *et al.*[116] characterized charge transport in their PbSe NC monolayer FET structures before and after annealing. They found holes to be the majority carriers and modelled their transport in terms of the activation energy to release them from acceptor sites and to further overcome the site disorder barrier. They furthermore extracted a density of states value identical to the degeneracy of the lowest hole state ($1S_h$), validating their approach. Kang *et al.*[400] studied ambipolar PbSe NC films adding an ionic gel gate dielectric (a blend of an ionic liquid, 1-ethyl-3-methylimidazolium bis(trifluoromethylsulfonyl)ide and a styrene, methacrylate block copolymer, see Fig. 32) to improve hole and electron carrier densities in the PbSe films (to $\sim 10^{14}$ cm^{-2}). Densities equivalent to 3 carriers per NC could be achieved at modest (few volt) operating voltages.

Hanrath *et al.*[142] used synchrotron X-ray source scattering techniques to study the degree of spatial coherence in the (orientational) alignment of PbSe NCs deposited by spin coating or drop casting onto single crystal silicon substrates (Fig. 33). They found that the rate of solvent evaporation was a critical factor in allowing NCs to adopt a common alignment on the substrates. Coherence could be improved by reducing the solvent evaporation rate after deposition by holding the films in a solvent vapour atmosphere to reduce drying rates. Furthermore dried films could be annealed by exposure to solvent vapour ambients to allow NC reorientation to take place. However, exposure to ethanedithiol vapour, a commonly used insolublizing bifunctional ligand, resulted in highly disordered films.

Electron tomography has been used by several groups to probe NC shapes and NC stacking geometries in 3-D NC solids, including binary and ternary size combinations (*i.e.* bimodal and trimodal mixed systems). Relatively large cubic and octahedral PbSe NCs were included in the studies by Ahrenkiel *et al.*[402] On a finer scale, Friedrich *et al.*[403] successfully reconstructed the stacking geometry of ordered AB, AB_2 and AB_{13} binary superlattices formed from PbSe, CdSe and Au NC combinations and ternary solids[401] with ABC_4 stacking formed from PbSe (two sizes) and CdSe (single size) mixtures (Fig. 34).

Lee *et al.*[60] have prepared not only ordered films of PbS NCs, but also macroscopic $\sim$100 μm dimension, 3-D crystals of ordered PbS NCs (termed colloidal crystals), with packing order probed by time-resolved small angle X-ray scattering. Careful annealing of their ordered structures allowed conformational relaxation of their OA ligands to form a more contracted structure, but without induced disorder or sintering of adjacent NCs

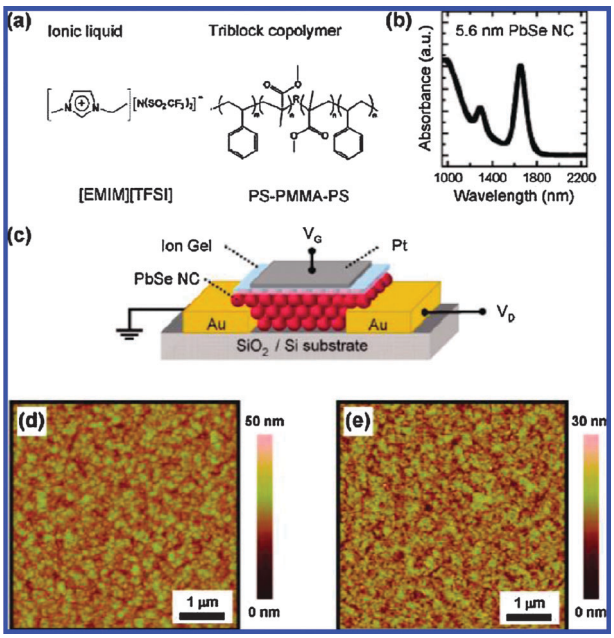

Fig. 32 (a) Chemical structure of the ionic liquid and triblock copolymer ion gel components: 1-ethyl-3-methylimidazolium bis(trifluoromethylsulfonyl)imide ([EMIM][TFSI]) and poly(styrene-*block*-(methyl methacrylate)-*block*-styrene) (PS–PMMA–PS). (b) Optical absorbance spectrum of PbSe NCs in tetrachloroethylene. The lowest energy absorption peak occurs at 1655 nm with a FWHM <50 meV. (c) Schematic diagram in cross section of an ion-gel-gated PbSe NC TFT (not to scale). The device has a channel length of 100 μm and a channel width of 1 mm. (d) AFM height image of a bare PbSe NC film before a hydrazine treatment. The root-mean-square (rms) roughness of the films was 3.2 nm. (e) AFM height image of PbSe NC film after a hydrazine treatment (3 h), which includes two cycles of spin coating and hydrazine dipping. The rms roughness of the film was 2.8 nm. Reprinted with permission from M. S. Kang *et al.*, *Nano Lett.*, 2009, **9**, 3848–3852. Copyright 2009 American Chemical Society (ref. 400).

reported by others with higher temperature treatments. Bodnarchuk *et al.*[51] examined the thermal behaviour of AB_x packing in PbSe–Pd NC binary superlattices as a function of temperature and relative NC proportions and were able to show a wide range of packing types the formation of which was discussed in terms of the interplay between thermodynamic (entropy driven) and interparticle interaction energies (Fig. 35).

Energy transfer in close packed PbS NC films has been investigated by Rinnerbauer *et al.*[404] and Corricelli *et al.*[31] The former group saw enhancement of PL quantum yield at certain NC film densities, attributed to energy transfer from surface states to core, radiative states. Corricelli *et al.* fabricated ordered arrays of both monomodal and bimodal size distribution PbS NCs, the latter exhibiting an AB_6 packing geometry. They saw Förster Resonant Energy Transfer (FRET) in the monomodal close packed film, but packing distances, and energy level alignments in the bimodal film were not optimal for FRET in the bimodal films. Szendrei *et al.*[405] studied the temperature dependence of solar cell parameters and PL decay times in benzenedithiol treated close packed PbS NC films and observed an increase in trap state behaviour in the treated films.

Fabrication of PbTe NC close packed films has been reported by several groups.[170,172,173,177] Lu *et al.*[170] formed regularly packed spherical PbTe NC arrays and mosaic-like arrays of cubic PbTe NCs. Urban *et al.*[172] synthesized a range of different sized monodisperse PbTe NCs, with a range of shapes from spherical to cubic *via* octahedral, and demonstrated films with long-range ordering and some with glassy, disordered packing. In larger (~20 nm) cubic PbTe NCs synthesized with oleylamine ligands, Zhang *et al.*[173] reported hydrolysis of the outer shell in the presence of traces of water to form PbTe–$Pb(OH)_2$ core–shell NCs which could be further heat treated to form PbTe–PbO core–shells. This was accompanied by a change of NC shape (cubic to octahedral) visible in TEM images. Ko and Murray[176] measured the thermopower of dense packed PbTe NC films for several different NC sizes and were able to determine the Fermi level and energy for the onset of carrier transport for each NC diameter (Fig. 36). Wang *et al.*[157] similarly report thermopower and density of states measurements in PbSe NC films.

Yang *et al.*[406] have recently studied organisation in HgS NC layers grown on arachidic acid monolayers at a liquid–air interface. Although the growth method is rather similar to early studies, here the authors realised the packing of organized aggregates of NCs which had regular shape and size. The ~5 nm diameter NCs formed regular sized aggregates which were either circular or at higher densities, hexagonal and which themselves formed regular arrays.

4.7 Summary of coupled nanoparticles, films and self-assembly

In addition to improvements in NC synthesis and characterisation, there have been significant advances in the expertise of assembling NCs into larger scale assemblies,[60,403] a key step towards many types of commercializable electronic and optoelectronic devices. A number of NC deposition techniques are now well explored and are the potential basis for future component manufacturing processes for devices including (but not limited to): field effect transistors[10] (large format/low cost/flexible substrates); IR photodetectors and photo-imaging components;[386] solar cells;[10,22,24] optoelectronic switches, light sources, and optical amplifiers.

Work on narrow bandgap QD sensitized and related types of solar cells[76,90] has been an important driver for studies examining the direct coupling between semiconducting QDs and (wide bandgap) oxide nanoparticles and substrates based on these types of materials. This work led to systematic studies of the properties of various ligands and linker molecules and in particular their influence on carrier transfer efficiency and dynamics.[358] From a materials perspective, this line of enquiry then evolved into the use of heterojunctions between dense thin layers of QDs and primarily inorganic oxide nanoparticle films,[360] or alternatively semiconducting organic polymers, carbon nanotubes, C_{60} or graphenes,[361] but with QDs often still passivated with organic ligands.

Improved carrier transfer could sometimes be obtained with sintered QD films (where this was an option in the fabrication process), or by the use of ligand exchange to substitute with a very short chain ligand (*e.g.* EDT) at the QD surface. The volume contraction upon doing this after film deposition was a

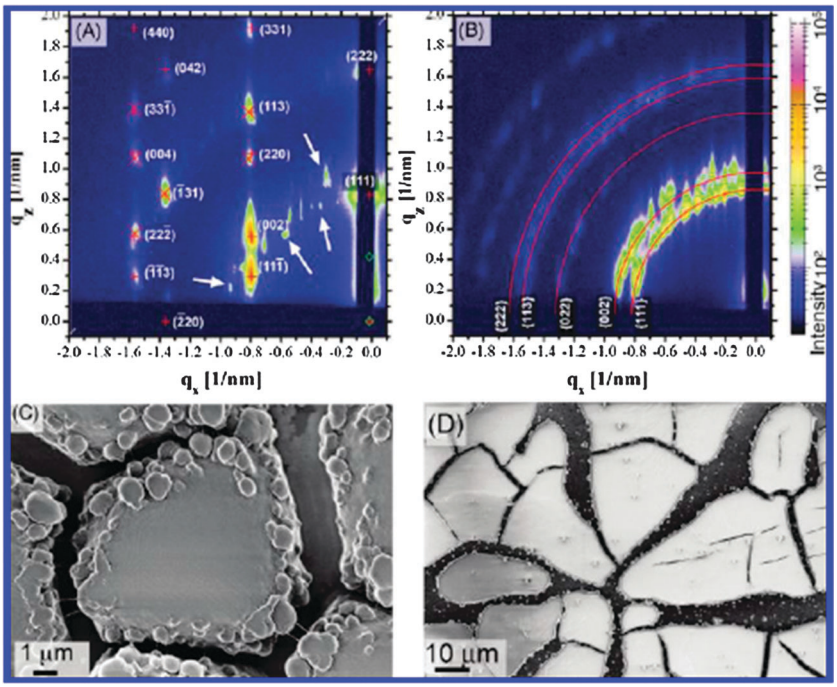

Fig. 33 Drop-cast PbSe NC films. GISAXS patterns of (A) highly oriented NC film on Si and (B) polycrystalline NC film on the ITO substrate. Spot indices (A) for a (111) oriented FCC lattice or FCC powder rings (B) are indicated. (C) SEM image of large NC supracrystal grain on Si and (D) SEM image of cracked NC film on ITO. Reprinted with permission from T. Hanrath *et al.*, *ACS Nano*, 2009, **3**, 2975–2988. Copyright 2009 American Chemical Society (ref. 142).

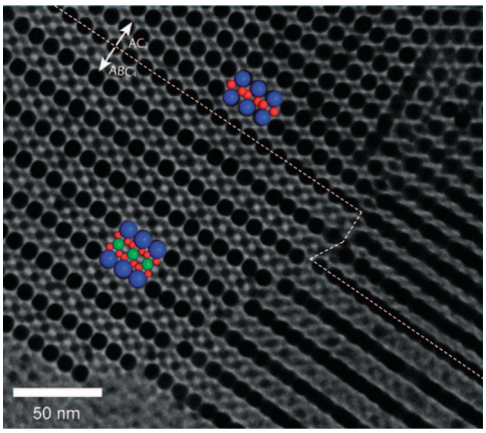

Fig. 34 TEM projection of the ternary ABC_4, that is, [PbSe(l)]-[PbSe(m)][CdSe(s)]$_4$ NC superlattice (l = large, m = medium, s = small) in epitaxial contact with the binary AC_2 superlattice [PbSe(l)]–[CdSe(s)]$_2$. The TEM picture and cartoon show the (100) plane of the ternary superlattice, in which the large PbSe NCs (blue spheres), medium-sized PbSe (green spheres), and small CdSe (red spheres) can be observed individually. The ternary NC superlattice is isostructural with $AlMgB_4$. Reproduced from ref. 401, W. H. Evers *et al.*, *Angew. Chem. Int. Ed.*, 2009, **48**, 9655–9657, © 2009 Wiley-VCH Verlag GmbH & Co. KGaA, Weinheim, with permission from John Wiley & Sons, Inc.

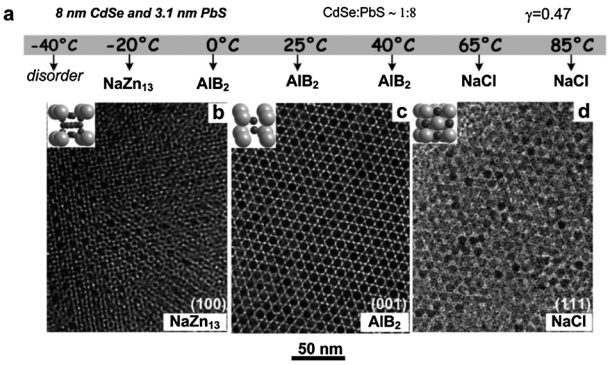

Fig. 35 Effect of temperature on self-assembly of 7.7 nm PbSe and 3.4 nm Pd NCs. (a) Sequence of phase types *vs.* temperature. (b,c) Several examples of binary nanocrystal superlattices self-assembled at different temperatures from solutions of mixed NCs. TEM images of superlattices isostructural with (b) $NaZn_{13}$ intermetallic compound, (c) AlB_2, and (d) NaCl. Reprinted with permission from M. I. Bodnarchuk *et al.*, *J. Am. Chem. Soc.*, 2010, **132**, 11967–11977. Copyright 2010 American Chemical Society (ref. 51).

disadvantage for thin films due to cracking of the film,[399] but the use of multilayer dense films (with ligand exchange on after each deposition cycle) was found to allow for sufficient bridging to reduce the impact of cracks within each layer (*i.e.* there was little tendency for cracks to occur in the same locations in subsequent layers).

Nonetheless, some of the best recent results with randomly packed dense films of QDs have been obtained where organic ligands have been replaced altogether by exchanging the usual growth ligands for very small inorganic molecules or even simple ionic species.[353,355,407] This has been demonstrated both by performing the exchange on deposited films and by carrying out the exchange prior to film deposition, and results in QD film containing devices with better carrier transfer and overall performance.

The evolution of QD doped films[137,368] for applications not involving injection or extraction of charge carriers (*e.g.* for purely optical applications) has progressed from simple dispersion of

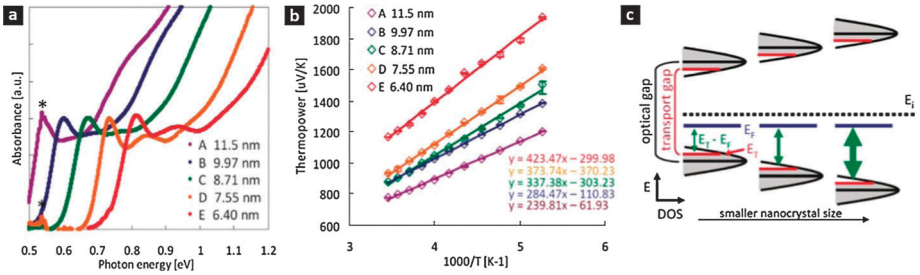

Fig. 36 (a) Optical absorption spectra of PbTe NCs of five different sizes. Two asterisks indicate superimposition of solvent (squalane) and surfactant (OA) absorption peak. (b) Temperature-dependent thermopower measurements on NC solids constructed from various sizes of PbTe NCs. Each solid line is a linear fit to extract slopes which reveal $E_F - E_T$, the difference between the Fermi level energy and the transport level energy respectively. The *y*-intercept comes from three different contributions which include the heat of transport constant. (c) Schematic illustration of $E_F - E_T$ as a function of NC size as measured in temperature-dependent thermopower measurements. Reprinted with permission from D.-K. Ko and C. B. Murray, *ACS Nano*, 2011, **5**, 4810–4817. Copyright 2011 American Chemical Society (ref. 176).

QDs in either water soluble,[161] or organic solvent based polymers to more sophisticated approaches involving covalent linking of QDs to the host network *via* functionalized, reactive ligands.[368] For some applications (*e.g.* the creation of optical waveguide devices), the requirements on the hybrid material are very demanding – even small scale aggregation of QDs or other forms of inhomogeneity in the composite material must be avoided to keep optical scattering over several mm path lengths to an acceptable minimum. Furthermore, the QD surface must remain free of traps in the host film environment to retain the PL quantum yield of the starting QD solution and minimize non-radiative recombination.

While the use of LbL QD/polyelectrolyte deposition techniques[371–374] produces thin films with very high QD content and high optical density, electrical conductivity is limited due in part to the poor carrier mobility of the host polymer and quenching effects appear to limit the PL performance for anything more than a few QD/polymer bilayer thick films for simple structures. In addition, for IR work the presence of CH vibrational absorption features overlapping QD emission in many parts of the spectrum is drawback for many applications. However, such QD/polyelectrolyte films can be made with good optical quality and high QD content and as such have proved very useful in accurately determining optical and dielectric functions for these materials.[376,408] Recent work by Kovalenko *et al.*[354] on QDs dispersed in As_2S_3 sol gel films and similarly by Lhuillier *et al.*[409] on HgTe QD films in As_2S_3 deposited by spin coating may offer a better alternative route to high QD content doped films for these types of application.

The formation of highly ordered superlattice films using monodisperse QDs of one or several different sizes has been impressive. In particular the results reported by Talapin and coworkers[51] and by Evers *et al.*[401] stand out as particularly encouraging, and if effectively coupled with the advances in inorganic ligand capping could lead to very interesting and useful electro-optic materials.

5 Applications

5.1 NC based solar cells

Photovoltaic solar cells making use of narrow bandgap colloidal NCs can be divided into a number of distinct device types: Quantum Dot Sensitized Solar Cells (QDSSCs) – a combination of QDs and wide bandgap (mesoporous or nanotextured) semiconductors; bulk heterojunctions; depleted heterojunctions and Schottky junctions. In addition there have been a number of reports of Tandem (multiple layered) PV cells and the heterojunction cells may include organic–inorganic as well as inorganic–inorganic layer interfaces. Several of these NC cell types are shown schematically in Fig. 37. We have not included in these groups the use of NCs in solar luminescent concentrators, wavelength converters in photon recycling schemes, or down-converters used in conjunction with conventional bulk semiconductor PV cells. Here we concentrate solely on applications where the NCs are themselves directly involved in the photogeneration of charge carriers.

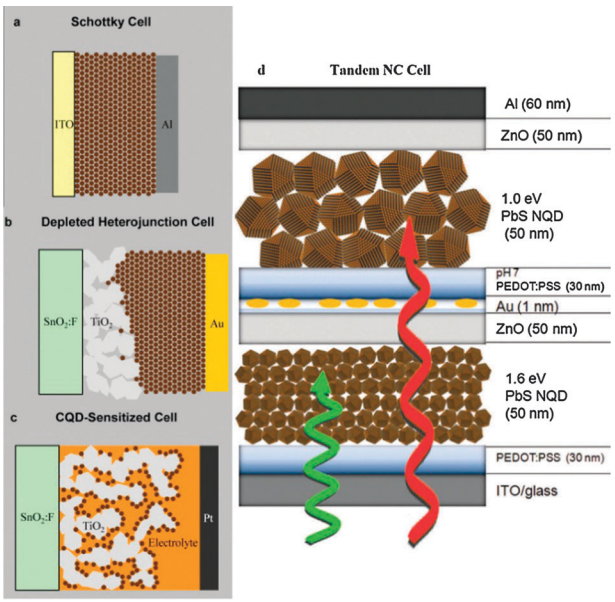

Fig. 37 The schemes of different kinds of NC solar cells. (a) Schottky cell, (b) depleted heterojunction cell, (c) colloidal quantum dot (or NC) sensitized cell, (d) example of a Tandem NC cell. (a)–(c) Reprinted with permission from A. G. Pattantyus-Abraham *et al.*, *ACS Nano*, 2010, **4**, 3374–3380. Copyright 2010 American Chemical Society (ref. 410). (d) Reproduced from ref. 411, J. J. Choi *et al.*, *Adv. Mater.*, 2011, **23**, 3144–3148, © 2011 WILEY-VCH Verlag GmbH & Co. KGaA, Weinheim, with permission from John Wiley & Sons, Inc.

There have been many recent reviews of the NC photovoltaic solar cell sector – for example our own recent review[23] detailing progress in QDSSCs and other cell types. Yang *et al.*[22] also reviewed QDSSCs in general (*i.e.* not restricted to narrow bandgap NCs) and Debnath *et al.*'s[24] 2011 Perspective on solution processed colloidal QD PVs, particularly focussed on the above junction cell types. Whilst NC solar cells still currently lag behind mainstream and even dye sensitized solar cells in the bottom line – power conversion efficiency (PCE), notable progress has recently been seen in the efficiency and durability of heterojunction NC cells with PCEs exceeding 5% and 6%.[349]

Quantum dot sensitized solar cells. Much of the early work on NC based solar cells centered on the replacement of organometallic dyes in Dye Sensitized Solar Cells (DSSCs) with NCs. Whilst NCs offered a great deal of freedom in engineering band alignments and potentially better long term photostability relative to dyes and lower fabrication costs, one of the biggest drawbacks remains to be the difficulty in finding a suitable electrolyte redox pair that does not degrade the NCs. Ideally the electrolyte would also be solid state rather than liquid, though this has not prevented commercial development of DSSCs. CdS–CdSe NCs have been used in conjunction with the S^{2-}/S_x^{2-} polysulfide pair rather than the I^-/I_3^- couple often used with dyes, but many groups report neither to be satisfactory with narrow bandgap NCs such as PbS.[412] Lee *et al.*[413,414] have used an alternate cobalt complex (Co^{2+}–Co^{3+}) based redox couple for their DSSC and QDSSCs.

Despite the electrolyte limitation, other groups have reported progress with PbS/polysulfide QDSSCs, most notably Sambur *et al.*[415] Hossain *et al.*[416] have combined PbS and CdS in a QDSSC with mesoporous SnO_2 and a polysulfide electrolyte, but found it necessary to add a passivation layer of ZnS to improve the air stability of their PbS. They report a PCE of 2.23% for their best configuration. Li *et al.*[417] recently reported an efficiency of 4.2% using a TiO_2–$CuInS_2$ (NCs)–CdS–ZnS photoanode, a polysulfide electrolyte, and a CuS counter electrode structure. By using narrow bandgap $CuInS_2$ NCs they benefited from an extended absorption range to around 800 nm.

At present, around 4% PCE appears to be state of the art for QDSSCs. The limitations of the use of electrolytes, and the complications of the nature of the carrier kinetics across the many interfaces leads naturally to the notion of electrolyte-less, intimately contacted heterostructures between NCs and wide bandgap oxides, and other classes of materials. These may involve direct growth of NCs on other types of semiconductor (oxides, fullerenes) or NCs grown *ex situ* and covalently linked to the latter with short linker molecules, or combined directly in a blend with semiconducting organic polymers. These materials may be coupled in complex structures with a random distributed interface, or in the form of distinct planar layers at which built-in electric fields may be created.

NC junction solar cells

NCs coupled to fullerenes and conjugated polymers. The use of conjugated polymers such as MEH-PPV (poly[2-methoxy-5-(2′-ethyl-hexyloxy)–*p*-phenylene vinylene]), P3HT (poly-3(hexylthiophene)) in conjunction with NCs in general has become commonplace in recent years. Watt *et al.*,[381] combined PbS NCs with MEH-PPV, citing the benefits of more evenly balanced hole and electron mobilities (within the NCs) and long exciton lifetimes (up to around 1 μs being commonly reported by others[418–420]). By growing the NCs within the conducting polymer they were able to form bulk heterostructures directly. Zhu and colleagues[138,385,421] extensively studied PbSe NCs in both bulk and planar heterostructures with P3HT, investigating the optimal NC loading and comparing devices with bulk, planar and planar-bulk heterostructures incorporating a PEDOT:PSS (poly(3,4-ethylene dioxythiophene):poly(styrene sulfonate)) hole transport layer, the latter structure reaching 0.26% PCE. Improvement of the PCE to 0.55% was reported by Noone *et al.*[422] in bulk heterostructure PbS–polymer blends using poly(2,3-didecyl-quinoxaline-5,8-diyl-*alt*-*N*-octyldithieno-[3,2-*b*:2′,3′-*d*]pyrrole) (PDTPQx).

Heiss' group[53,56] has investigated narrow bandgap NC sensitizers blended with (P3HT)–fullerene (PCBM – [6,6]-phenyl-61-butyric acid methyl ester) in solar cell structures. For PbS blends they determined that for NC sizes such that PL emission was below 1300 nm, size dependent electron transfer times between the PbS and conjugated polymer were in the 130–150 ps range and fast enough to allow hot electron transfer to compete with *e.g.* Auger recombination processes. The fullerene was determined to enhance charge transfer speeds as an intermediate between the polymer and NC in the transfer process. Dissanayake *et al.*[361] fabricated discrete heterojunction PbS NC–C_{60} hybrid solar devices with infrared sensitivity extending to over 1600 nm, but only reported low PCE figures of $<0.1\%$. Tsang *et al.*[423] had better success with their PbS–C_{60} heterostructures reporting PCE figures between 1.6% and 2.2%. In their case they treated the PbS layer with benzenedithiol, correlating the latter treatment and combination with a C_{60} layer with almost complete quenching of the PbS luminescence. Zhao *et al.*[424] combined ethanedithiol treated PbS NCs with a layer of fullerene as their electron transporting layer and obtained a PCE figure of 1.3%. Kuo *et al.*[396] used multiple layers of PbSe NCs with ethanedithiol as an insolublizing rinse in between layers, deposited on top of PEDOT:PSS as a hole transport layer and obtained a PCE of 2.45% with their thicker film.

NCs coupled to (wide bandgap) oxides. NC–wide bandgap oxide combinations are most often encountered in QDSSCs which are then treated with polyelectrolyte to complete the device structure. NCs may be synthesized either *in situ* or *ex situ* and then introduced into the mesoporous oxide structure in solution by diffusion or under the action of an electric field. In the *in situ* case the NCs might or might not make very intimate contact with the oxide and thus the junction between the two is not well defined. The use of electrolyte is thus important to ensure another means of contact between the respective elements of the structure. This has led several groups to investigate the use of linker molecules between the NC and porous substrates, or to synthesise the one in direct contact with the other with a well defined interface. These may then be used in cell types other than QDSSCs as well.

Günes *et al.*[425] combined both the NC polymer blend (HgTe (with organic ligands)/P3HT) and a layer of porous TiO_2 coated internally (by soaking) with water soluble HgTe NCs to produce a hybrid cell structure. This was one of the earliest examples other than the lead chalcogenide based devices to show extended IR response.

PbSe NC coated TiO_2 nanorods have been prepared in solution by Acharya *et al.*[105] using a two-stage, one-pot, hot injection synthesis. For NCs below about 5 nm the heterostructure was assumed to be of type II and above this limit, type I. No solar cell device performance was reported, but fluorescence lifetimes were found to be considerably shorter than for pure PbSe NCs (2 ns compared with several hundred ns). This was attributed to fast electron transfer to the TiO_2 rather than carrier trapping. The same group[42] has also extended its *in situ* hot injection method to deposit other lead and cadmium chalcogenides within sintered mesoporous TiO_2 films. Around the resulting directly connected NC sensitized titania hybrid films they fabricated an all-inorganic NC sensitized solar cell as a solid state version of a QDSSC by adding a further layer of MPA capped PbS NCs as a hole transport layer (rather than a sensitizer), and finally a gold electrode layer above that. The best PCE for this cell type was 1.2%. In different layers, PbS QDs acted as both a sensitizer and a hole transport medium.

Krüger *et al.*[61] have investigated the performance of a number of linker molecules used to couple ZnO nanoparticles and PbS NCs. Their study included thioacetic acid, TGA, MPA, hexanedithiol, oxalic acid, and malonic acid. Each of the thioacids is hypothesized to coordinate with the ZnO predominantly *via* their carboxylate groups, and *via* the thiol to the PbS NCs (as shown in Fig. 38). Malonic acid and hexanedithiol have the same carboxylate or thiol group at both ends of the linker. The authors investigated the influence of the linker length and the actual mode of attachment (*i.e.* is the previous coordination hypothesis valid?) on charge transfer.

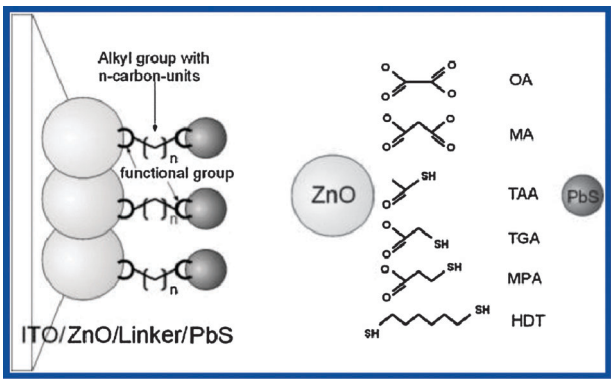

Fig. 38 (Left) Schematic of the ITO/ZnO/linker/PbS substrate used in these studies. The substrate consists of PbS nanoparticles which are bound by a linker molecule to ZnO which has been spin-coated onto ITO glass. The linker molecules vary in their alkyl-chain and functional groups. (Right) Structures representing the linker molecules used in the study: oxalic acid (OA), malonic acid (MA), thioacetic acid (TAA), thioglycolic acid (TGA), mercaptopropionic acid (MPA), and hexanedithiol (HDT). Reprinted with permission from S. Krüger *et al.*, *J. Phys. Chem. C*, 2011, **115**, 13047–13055. Copyright 2011 American Chemical Society (ref. 61).

The use of ethanedithiol as a linker molecule is frequently encountered particularly in connection with layered NC solar cell (hetero)structures. Im *et al.*[387] have also used it to prepare PbS NC coated mesoporous TiO_2 layers where multilayers of the NC are deposited within the porous structure by alternate spin coating cycles of PbS NC solution and dilute ethanedithiol. Up to 25 NC/EDT cycles were applied, and the cell structure then completed by adding a P3HT spin coated hole transport layer, followed by a PEDOT:PSS layer and an evaporated gold top contact, to complete effectively an all-solid state QDSSC. Under 1 sun illumination, a PCE of 2.9% was obtained.

Finally, Etgar *et al.*[360] have combined PbS NCs and layers of TiO_2 nanoplatelets to form a depleted heterojunction solar cell (Fig. 39) with efficiencies ranging up to 4.73% for their smaller 30 nm size nanosheets. Although their NCs and nanoplatelets were not directly coupled as such during synthesis, the fact that the combination performed better than a control with spherical TiO_2 nanoparticles was attributed to the fact that at the junction between the PbS QDs and the TiO_2 sheets, the latter presented preferentially the (001) anatase facet, which has a surface ionic charge higher than other facets and this is believed to improve PbS NC anchoring at the junction.

Schottky junctions. The Sargent group[426] pioneered the use of Schottky junction NC solar cells, making use of the contact formed between NCs and low work function electrodes such as aluminium. Early reports on PbS NCs had PCE values of 1.8% and relative to heterojunction devices showed much improved IR performance, though device stability and lifetime were poorer. The latter was improved substantially by using more elaborate electrode structures – a recent article by the same group[50] identified and reduced the tendency of oxygen and ambient moisture to degrade performance. Sandwiching the Al electrode between blocking layers of (0.8 nm thick) LiF and Ag (Fig. 40) improved device lifetimes by over an order of magnitude, and PCE values of 2% were obtained. PCE values using PbS NCs as high as 3.8% and 3.9% have been obtained by Fu *et al.*[427] and Szendrei *et al.*[428] using similar electrode structures.

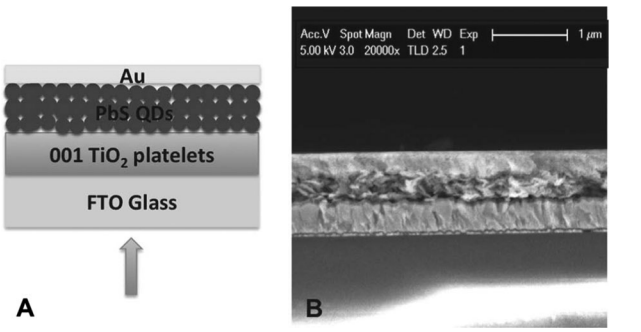

Fig. 39 (A) The architecture of a PbS QD–nanosheet TiO_2 heterojunction photovoltaic device, the light is incident through the FTO glass. (B) Cross sectional HR-SEM of the photovoltaic device. It shows that the PbS QDs form a nanocrystalline layer on top of the TiO_2 film, and only very few QDs penetrate into the nanosheet network of the TiO_2 film. Reproduced from ref. 360, L. Etgar *et al.*, *Adv. Mater.*, 2012, **24**, 2202–2206, © 2012 WILEY-VCH Verlag GmbH & Co. KGaA, Weinheim, with permission from John Wiley & Sons, Inc.

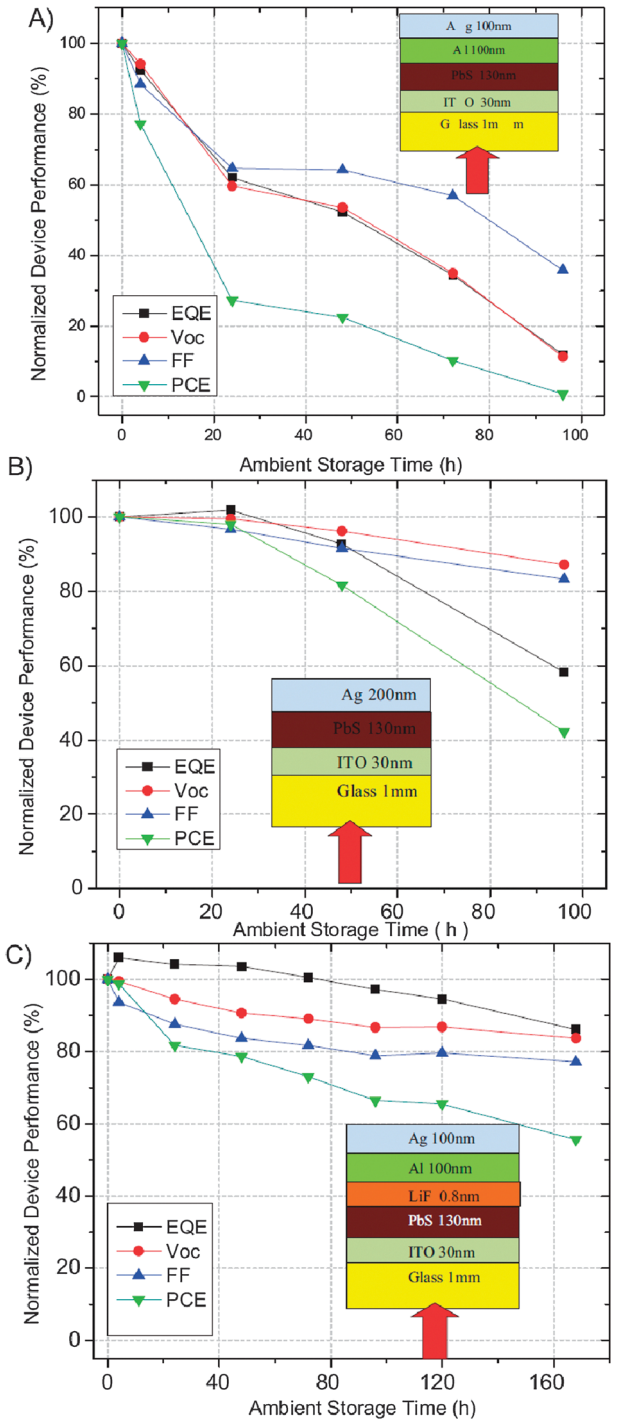

Fig. 40 Normalized device performance (EQE, external quantum efficiency; V_{oc}, open circuit voltage; FF, fill factor; and MPCE, monochromatic power conversion efficiency) as a function of ambient storage time for PbS solar cells using different cathodes: (A) Al–Ag, (B) Ag, and (C) 0.8 nm LiF–Al–Ag. Corresponding device architectures are schematically shown as insets. All devices were tested in air under 120 mW cm^{-2} monochromatic 632-nm-wavelength illumination from the ITO side. The initial absolute EQE, V_{oc}, FF and MPCE of Al–Ag, pure Ag and LiF–Al–Ag devices are: 38.1%, 0.42 V, 48% and 4.1%; 24.5%, 0.24 V, 27% and 0.78%; 40.2%, 0.52 V, 54.5% and 5.8%; respectively. Data shown in each panel are representative of 8 devices tested. Reproduced from ref. 50, J. Tang *et al.*, *Adv. Mater.*, 2010, **22**, 1398–1402, © 2010 WILEY-VCH Verlag GmbH & Co. KGaA, Weinheim, with permission from John Wiley & Sons, Inc.

The latter group[405] has also made a fundamental study of the origins of the temperature dependant optical and electronic properties of their devices (with variations in the treatment of the PbS layers) primarily to try to gain more insight into the conduction mechanisms in such structures. Nozik *et al.*[113] developed a full optical model for their multilayer Schottky devices which took account of light absorption in layers other than the active NC layer. From this they were able to accurately determine internal quantum efficiencies and could potentially determine if carrier multiplication was a factor in cell performance. They also investigated the current voltage characteristics of (multilayer) PbS–ZnO heterojunction cells Schottky contacted by a PbS to metal (Ag, Au) electrode[429] interface as a function of PbS NC size in an attempt to formulate an optimum layer thickness model for different size NCs.

Spatial variation of the photovoltaic performance of PbS–TiO_2 heterojunction Schottky contacted cells has been reported by Turyanska *et al.*[90] who combined PL images and spatially resolved short circuit photocurrent mapping to show anti-correlations between areas that showed peaks in photo-emission and minima in photocurrent output. Similar spatial mapping measurements have also been reported by Madl *et al.*[52] using AFM photocurrent measurements on simple PbS NC films on gold, though in their case both the AFM tip and gold electrodes made Ohmic contacts with the NC layer.

Lin *et al.*[430] have fabricated transparent graphene electrode based PbS Schottky solar cells, showing better IR performance due to the greater long wavelength transparency of graphene relative to that of ITO; however this is somewhat offset in the spectrally integrated performance due to the higher sheet resistivity of the former.

Ma *et al.*[183] compared the performance of PbS, PbSe and PbS_xSe_{1-x} alloy NC Schottky cells, finding the latter to outperform the pure binary NCs (PCEs were 1.7%, 1.4% and 3.3% respectively). This was attributed to simultaneous improvements in both the short circuit current and open circuit voltage. The latter was explained as a consequence of a favourable shift in the NC Fermi level relative to the valence level due to differing trap state densities. The current improvement (at least as far as the alloy relative to PbS) was attributed to a dilation of the Bohr radius and improved coupling between dots as a consequence of the higher degree of quantum confinement. The same group[130] has subsequently studied PbSe NC Schottky cell (ITO/PEDOT/PbSe/Al) performance as a function of NC size and against an accurate optical model taking account of internal reflections from stack layers which superimposes Fabry–Perot cavity features upon the material absorption spectrum, complicating cell optimization. This allowed them to optimize cell performance to a PCE of 4.75% for 2.3 nm PbSe NCs, again with this representing the optimum trade-off point between short circuit current (and other cell performance factors) and open circuit voltage.

Inorganic–inorganic pn-junction cells. In most (but not all cases) II–VI and IV–VI colloidal NCs are synthesized as p-type semiconductors. A number of groups have studied pn junction

hybrid NC materials and devices where the junction is formed at the interface between materials with two different polarities, with other NCs (metal oxides, *etc.*), forming the n-type layer. Device applications include field effect transistors[431,432] and photodetectors[433,434] but there are also potential applications for solar cells, where the limitations of the Schottky cell open circuit voltage can be avoided using the pn junction format. The application to solar cells has been suggested by Pal *et al.*[434] in their demonstration of pn junction NC photodiodes consisting of p-type layers of PbS NCs in contact with n-type layers of either ZnO or TiO_2 NCs. The fabrication and testing of NC pn junction solar cells has been demonstrated by Rath *et al.*[435,436] using p-type PbS and Bi_2S_3 as their n-type NC layer. Initially they tested both regular and inverted discrete junction devices, but subsequently found better performance from devices incorporating an intermediate zone between the two NC layers consisting of a blend of the two types of NC. They termed this structure a Bulk Nano-Heterojunction cell (BNH) and reported PCEs as high as 4.87%, due to an improvement in the carrier lifetimes relative to those in the discrete bilayer device.

Excitonic effects. Choi *et al.*[437] and Leschkies *et al.*[438] almost simultaneously reported PbSe NC excitonic solar cells, with PCEs of 3.4% and 1.6% respectively. In both cases the use of a Schottky NC to metal contact was avoided by sandwiching the NC layer between electron and hole transport (and injection) layers. This leads to far higher open circuit voltages than with Schottky cells. With their designs V_{oc} is determined by the size dependent bandgap of the NCs and Choi *et al.* pointed out that it may be possible to exceed the difference in the workfuntions of the two electrodes in some cases, whilst Schottky cell V_{oc} values are limited to half the bandgap. Choi *et al.* used a ITO/PEDOT:PSS/PbS NC/ZnO NC/Al design, whilst Leschkies *et al.* used Au/α-NPD [*N*,*N*′-bis(1-naphthalenyl)-*N*,*N*′-bis(phenylbenzidine/PbS)] NC/ZnO NC/ITO as their respective electrode/hole transport/excitonic NC/electron transport/electrode stacks. Charge separation in this type of solar cell is driven by a chemical potential gradient at the respective NC/carrier injection layer interfaces with asymmetric transfer kinetics for each carrier, hole transfer favoured at one and electron transfer at the other.[439,440]

Carrier multiplication and hot carriers in NC solar cells. Nozik[441] proposed that NC photovoltaic performance could be enhanced by either hot carrier collection or alternately by carrier multiplication and the subsequent collection of the multiplied carriers before Auger relaxation occurs within the NCs. These effects allow enhancement of V_{oc} or J_{sc} respectively. The cooling of holes is very rapid ($\ll 1$ ps), whilst electron cooling times are typically of the order of a few ps in most cases – Tvrdy *et al.*[442] reported cooling rates of 1.3 eV ps^{-1} for CdSe NCs. Multiplied carriers must be extracted from NCs before non-radiative processes such as Auger relaxation occur. A series of relaxation times may be seen with values scaling as the inverse square of the number of excitons recombining at each stage.[443] Typically the sequence of multiple exponential decay times may be a few ps, of the order of 10 ps and then several tens of ps for the decay to the single exciton state.

Schaller and Klimov[124] reported high efficiency carrier multiplication in PbSe NCs with multiplication values ranging up to 100% and calculated the net potential improvements for solar cells if such multiplication factors could be obtained in solar cell devices. Allan and Delerue[444] investigated the possible mechanisms for carrier multiplication in NCs theoretically, using a tight binding model. They concluded that the multiplication rate for the most likely significant mechanism – impact ionization (the inverse of Auger recombination) should not be significantly enhanced by quantum confinement effects and should be somewhat similar to the same effect in bulk semiconductors – and that the process could be efficient for PbS and PbSe NCs. Other carrier multiplication mechanisms are also possible and have been investigated by a number of groups as summarized in the recent theoretical paper by Velizhanin and Piryatinski.[445]

Klimov[446,447] discussed the mechanisms for generation and recombination of multiplied carriers and the implications for photovoltaic cell improvements. Detailed balance calculations for PbSe NCs predicted a potential improvement from a theoretical 31% efficiency to 36% with a typical threshold energy for multiplication of 3 E_g.

Kim *et al.*[448,449] claimed carrier multiplication in a Tandem organic/PbSe solar cell on the basis of quantum efficiency increases for high excitation photon energies. In a simpler PbSe NC film structure, where the NC film was treated with hydrazine after deposition, they measured charge extraction factors of 210% at excitation energies of 4.4 E_g. Sambur *et al.*[415] saw evidence of carrier multiplication in photocurrent spectroscopy measurements on PbS NC films (with MPA as the ligand) deposited on single crystal TiO_2 substrates. In a range of different NC size samples they calculated absorbed photon to current efficiencies exceeding 100% at excitation photon energies above about 2.5 E_g.

Despite the encouragement of signs of possible enhancement mechanisms, power conversion efficiencies remained low ($\sim <5\%$). Law *et al.*[113] noted the problem in unambiguously identifying carrier multiplication effects especially in multilayer solar cell geometries with complicated transmission spectra (superimposed optical cavity modes, *etc.*). They developed a detailed optical model that could disentangle spectral artifacts due to the formation of optical cavities and in principle show the underlying material spectral efficiency. However they did not see evidence of carrier multiplication with their PbSe NC Schottky cells at that time. The same group (Beard *et al.*[450]) later reported multiple carrier generation in PbSe NC films on the basis of transient absorption measurements, with multiplication factors ranging between 110% and 240% for 3.7 nm NCs and 100% to 220% for 7.4 nm NCs depending on a range of surface treatments applied after deposition of the films (Fig. 41).

Recently Nair *et al.*[462] have made a more sober assessment of carrier multiplication measurement methodology and reanalysed multiplication levels in the literature in the light of variable findings for several common NCs from different groups. For high fluence pump–probe (*e.g.* transient absorption spectroscopy)

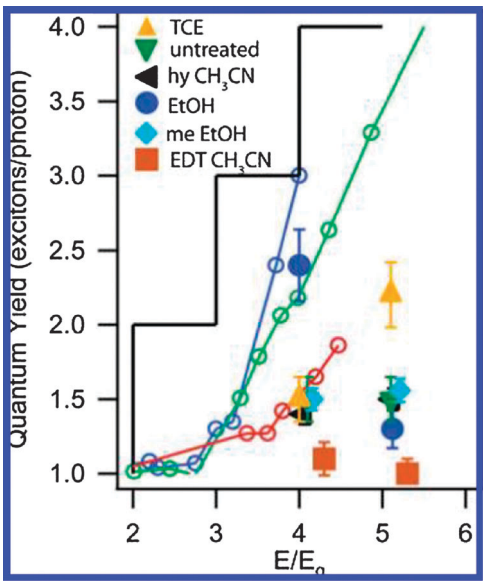

Fig. 41 QYs as determined by Beard *et al.*[450] (solid symbols) overlaid with past QYs of PbSe NCs dispersed in solution from NREL.[451] Blue open circles correspond to results for 4.0 nm NCs in TCE and the red open circles are average results for 4.7 and 5.7 nm NCs in TCE. In the original NREL report some variation on either sample preparation or NC size was observed. The green open circles are reported from LANL.[452] The solid black line represents the maximum possible multiple exciton generation efficiency; achieving *n* excitons at *n* times the band gap energy. Reprinted with permission from M. C. Beard *et al.*, *Nano Lett.*, 2009, **9**, 836–845. Copyright 2009 American Chemical Society (ref. 450).

measurements they point out that prolonged exposure to the pump can result in irreversible degradation which may appear to give misleading evidence of multiplication. They measured carrier multiplication yields for PbS and PbSe, taking precautions to exclude degradation artefacts and compared them with measured values from the literature, casting doubt on the extent of the effect for PbS, PbSe and InAs NCs. With this revised view they calculate a typical PCE enhancement *vs.* NC bandgap curve for a PbSe NC type solar cell (Fig. 42), suggesting at best a modest 14% improvement.

Binks[463] also discussed the carrier multiplication measurement controversy in a recent Royal Society of Chemistry Perspective article and described how accurate pump–probe measurement techniques can be made to avoid the appearance of artefacts masquerading as multiplication signals. As in the Nair *et al.* assessment relatively modest benefits from carrier multiplication in the present understanding are implied, but recent developments such as retarded electron cooling rates[464] are highlighted as being of possible benefit to enhance carrier multiplication in the future.

The development of transient absorption measurements and measurement methodology to screen misleading artefacts is also the focus of a recent article by Gdor *et al.*[465] who studied PbSe NCs in the IR in a transient absorption pump–probe experiment with a probe wavelength range from 90 to 1600 nm. Their measurement technique had sub-ps resolution allowing electron cooling to be observed, whilst their transient analysis allowed single, double and triple exciton contributions to be resolved.

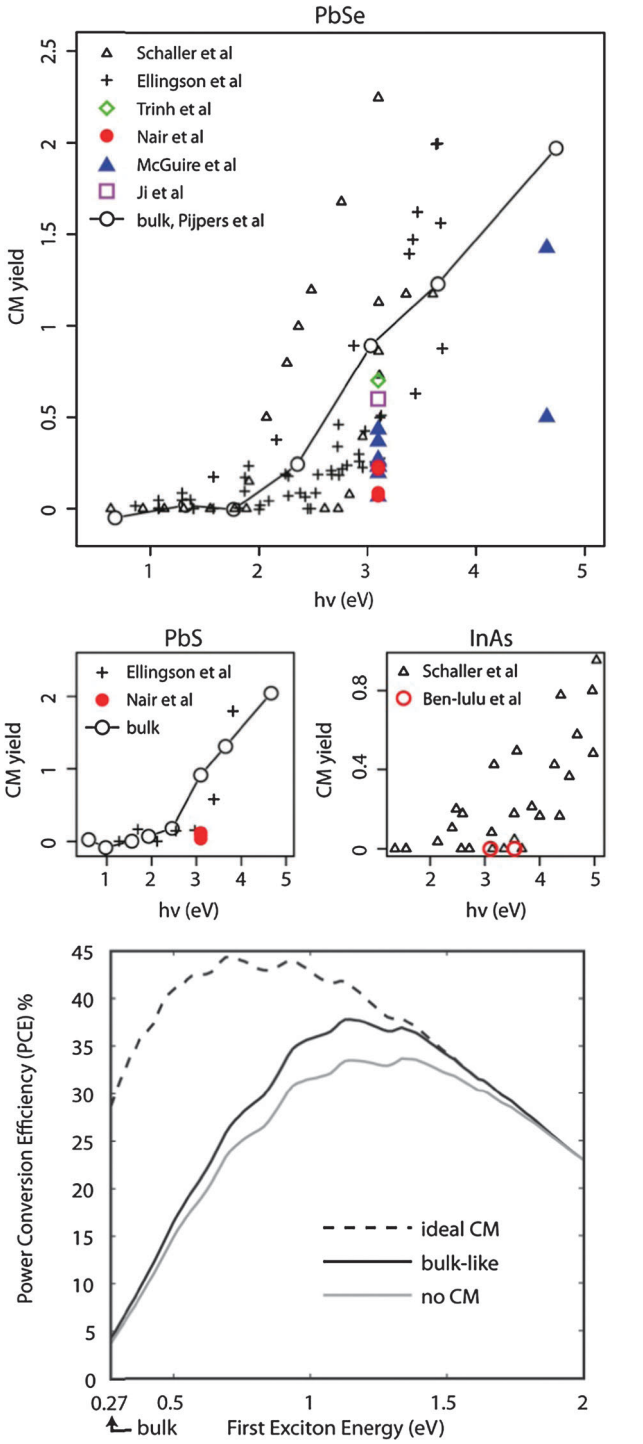

Fig. 42 Summary of carrier multiplication (CM) data in the literature for liquid dispersions of (a) PbSe,[114,124,451,453–456] (b) PbS,[114,451] and (c) InAs-based[452,457] NCs. A retracted InAs NC CM report is not plotted.[458,459] The Nair *et al.*[114] and McGuire *et al.*[454] reports (solid symbols) used stirring to minimize artifacts from sample degradation. The CM yield is defined as the average number of additional electron–hole pairs generated by absorption of a single photon. The solid lines for PbSe and PbS are the Bulk CM profiles measured by Pijpers *et al.*[460] (d) Calculated maximum theoretical solar power conversion efficiency for a single junction PbSe NC-based cell at normal incidence under AM1.5 illumination using reported methods[461] as a function of the NC size-dependent optical bandgap E_{X0}, *i.e.*, the first exciton energy. The dashed, solid black, and solid gray lines correspond to ideal CM, bulk-like CM and no CM. Reprinted with permission from G. Nair *et al.*, *Nano Lett.*, 2011, **11**, 2145–2151. Copyright 2011 American Chemical Society (ref. 462).

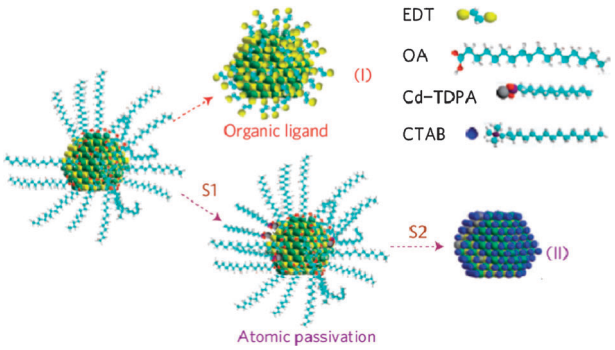

Fig. 43 Organic and atomic passivation strategies. PbS QDs having a Pb^{2+}-rich surface are initially capped with deprotonated OA. In the organic route, ethanedithiol (EDT) substitutes the long OA ligands and binds to Pb^{2+} on the surface. In the atomic ligand route described herein, a cadmium–tetradecylphosphonic acid (Cd–TDPA) complex was first introduced to the PbS QD surface to passivate the exposed S^{2-} anions (S1). A solid-state halide anion treatment, such as that employing cetyltrimethylammonium bromide (CTAB), introduced Br^- to cap the surface cations (S2), forming all-inorganic, halide anion-passivated PbS QDs. The molecular structures of EDT, OA, Cd–TDPA and CTAB are shown as insets. Colours are green (lead), yellow (sulphur), cyan (carbon), white (hydrogen), red (oxygen), grey (cadmium), blue (bromine) and purple (nitrogen). Adapted by permission from Macmillan Publishers Ltd: J. Tang *et al.*, *Nat. Mater.*, 2011, **10**, 765–771, copyright 2011 (ref. 349).

They were unable to observe any sign of multiple exciton generation for excitation energies up to 3.7 E_g in either InAs or PbSe NC samples and attributed this tentatively to possible differences in sample treatments between their materials and those reported in the literature.

Narrow bandgap NC solar cell – state of the art. At the time of writing, the highest PCE for a narrow bandgap colloidal NC solar cell stands at 6% and is held by Tang *et al.*[349] from the Sargent group. Their heterostructure, FTO–TiO2–PbS–Au–Ag, incorporated PbS NCs passivated with an inorganic rather than organic surface layer: PbS NCs grown by hot injection were subsequently treated with a $CdCl_2$ TDPA–OLA solution to enrich the surface layer of the PbS NCs with cadmium ions. During the layer by layer dot deposition to form the NC layer in their solar cells, after spin coating the PbS solution, an additional step – spin coating a layer of organo–halide solution – was included. Several of these were used in the study – cetyltrimethylammonium bromide (CTAB), hexadecyltrimethylammonium chloride (HTAC), tetrabutylammonium iodide (TBAI) and tetrabutylammonium thiocyanate (TBAT). This strategy results in a halide passivation layer with the displacement of the prior Cd–TDPA ligand (Fig. 43) that is far more compact than organic ligands, facilitating charge transfer processes.

For slightly wider bandgap materials, which nonetheless extend just into the IR, recent reports by Mulvaney and co-workers[466,467] using Depleted Heterojunction devices based layer by layer deposited CdTe and $CdSe_xTe_{1-x}$ sintered QDs have cited PCE values as high as 7.3%. Their use of $CdSe_xTe_{1-x}$ alloy QDs brings the benefit of a bandgap lower than that of CdTe by up to about 0.1 eV for compositions around $x = 0.4$ as the result of the alloy's bowing parameter. They also used a $CdCl_2$ treatment after deposition of each QD layer to effectively replace the organic passivating ligand used during synthesis with an inorganic halide layer as Tang *et al.* did (above). Multiple deposition cycles of QD layers with sequential graded composition and therefore favourably stepped conduction and valence band energy levels were also used to improve carrier separation and transfer. Tuning the composition and using a post-deposition sintering process allowed the edge in the device's absorption spectrum to be shifted further into the IR (typically up to a bulk-like 800 nm with high temperature sintering).

Table 3 Power conversion efficiencies reported for a range of narrow bandgap NC solar cells

NC type	Cell type	PCE (%)
CdTe	QDSSC[468]	2.0
CdHgTe–CdTe	QDSSC[469]	2.2
PbS	Schottky[48]	1.8
PbS	Schottky[470]	2.2
PbS	Schottky[471]	3.6
PbS	Schottky[427]	3.8
PbS	Schottky[428]	3.9
CdTe	Schottky[472]	5
PbS	Heterojunction[473]	0.7
PbSe	Heterojunction[438]	1.6
PbS	Heterojunction[423]	2.2
PbS	Heterojunction[58]	3
PbS	Heterojunction[474]	3.5
PbS	Heterojunction[24]	3.5
PbS	Heterojunction[410]	5.1
PbS	Heterojunction[475]	5.7
PbSe	Bulk Heterojunction[476]	2
PbSe	Bulk Heterojunction[477]	5.5
PbS–PbS	Tandem[411]	1.3
PbS–PbS	Tandem[478]	4.2
CdSe–CdTe	Schottky[479]	2.9
HgTe	Heterojunction[425]	0.4
PbS	Heterojunction[480]	0.02
Cu_2S	Heterojunction[481]	1.6
$CuInSe_2$	Heterojunction[482]	2.8
PbSe	Schottky[483]	3.6
PbSe	Schottky[484]	2.1
PbS	Schottky[426]	4.2
$PbSe_xS_{1-x}$	Schottky[183]	3.3

The values listed are a narrow bandgap NC material subset of those tabulated in the reviews by Yang *et al.*,[22] Debnath *et al.*[24] and Talapin *et al.*[10]

Table 3 lists a selection of PCE values reported for other narrow bandgap NCs and other cell types to date.

5.2 Biological applications

Magnetic, metallic and in general fluorescent inorganic nanoparticles have attracted considerable interest for applications in bio-sensing, bio-assay and drug delivery applications. In this review we restrict the discussion to a selection of narrow bandgap colloidal semiconductor nanoparticles. Reviews of biological applications of the wider range of inorganic nanomaterials have been given by Blanco-Andujar *et al.*,[25] concentrating on synthetic methods to prepare biocompatible and bioconjugated nanoparticles and by Wang and Su[26,] focussing on magnetic and fluorescent bifunctional composite nanoparticles and their uses in *in vitro* assay and drug delivery. Sperling and Parak's[27] recent Royal Society of London article

comprehensively reviews current knowledge on techniques of surface modification, functionalization and bioconjugation methods applied to colloidal nanoparticles and includes descriptions of methods to add polymer or silica shells to NCs to reduce cytotoxicity. Rogach and Ogris[485] specifically addressed the applicability of near-IR emitting semiconductor QDs for tumor imaging and targeting.

Formation of IR emitting NC-based bioconjugates. Gaponik *et al.*[350] fabricated microcapsules composed of chitosan membranes designed to contain drugs for targeted delivery within patients. HgCdTe or HgTe NCs were absorbed into the capsules, preferentially within the capsule walls as a method to introduce a fluorescent tagging agent to highlight the microcapsule's location within tissue. NC emission wavelengths were chosen to be within the so-called IR tissue transparency window around 750 nm. Etgar *et al.*[158,159] conjugated PbSe NCs to superparamagnetic γ-Fe_2O_3, making use of hydrogen bonding interactions between 2-aminoethanethiol on the PbSe NCs and polyhedral silsesquioxane (PSS) hydrate octakis ligands on the magnetic NCs to form networks of interconnected PbSe–Fe_2O_3 particles. They showed that the IR emitting material retained its luminescence whilst conjugation with the magnetic NCs provided a method in principle to localise the conjugates in tissue within a magnetic field gradient.

Zhao *et al.*[93] coated PbS–CdS core–shell particles with a further shell of amphiphilic copolymer (poly(maleic anhydride)-*alt*-1-octadecene-*co*-poly(ethylene glycol), (PMAO–PEG)) and showed improved stability of the NC fluorescence polymers under physiological conditions. In the presence of saline buffers, the NC–polymer colloids did not show any tendency to aggregate (''salt-out'').

***In vitro* examples.** Rather than using PbS NCs as fluorescent bio-markers Liu *et al.*[87,486] demonstrated an electrochemical detection method. A range of different group II metal sulfide NCs including PbS synthesized with hexadecylxanthate ligands were conjugated to different antibodies, by first exchanging the ligands for 1,1-carbonyl diimidazole ligands and coupling *via* a carbamate linkage to the antibodies. Coupling with specific antigen sites bound to magnetic nanoparticle–antibody complexes was assayed down to femtomolar concentrations by dissolving the II–VI nanoparticles and measuring stripping voltammograms on the resulting solutions. This allowed for multiplexed metal ion detection, lead, zinc and cadmium sulfide bound antibody–antigen recognition events could be detected simultaneously. A similar voltammographic method was used by Zhu *et al.*[78] They prepared mercaptoacetic acid capped PbS NCs and again using imidazole, coupled these to amine functionalised oligonucleotides. Hybridization of the PbS–oligonucleotide particles with an immobilized DNA target was again detected after dissolution of the bound PbS. Chiang *et al.*[487] have similarly used HgTe QDs for ultra-high sensitivity detection of peptides, proteins, and protein–drug complexes by using surface-assisted laser desorption, ionization mass spectrometry (SALDI-MS) rather than making use of the optical properties of the HgTe NCs.

The use of CdSSe–CdS alloy core–shell NCs with different alloy compositions to enable multiplexed fluorescence detection of two separately labelled populations of HeLa cells was reported by Jiang *et al.*[298] They conjugated their alloy NCs with transferrin and bovine serum albumin the former acting as an agent to transfer their NC partner into the interior of the cells. Optical filtering of images of multiple cells with filters appropriate to the respective NC emission spectra allowed separation of the respective cell populations and showed localization of the NC uptake within the cells (Fig. 44).

Turyanska *et al.*[488,489] have prepared IR emitting apoferritin capped PbS NCs, where the hollow pH sensitive apoferritin was used as a nanoreactor in which the NCs were grown. They compared the cytotoxicity of capped and uncapped PbS QDs on healthy and cancerous cell lines. Interestingly, they found healthy cells to be unaffected by the uptake of apoferritin capped NCs whilst in tumorigenic apoptotic cells death was triggered above a certain dose.

***In vivo* examples.** There have been a number of examples of *in vitro* demonstrations of IR fluorescence imaging in mice, taking advantage of the ability to tune narrow bandgap NC emission into the NIR tissue transparency window. Qian *et al.*[490] demonstrated subcutaneous imaging using CdHgTe–CdS alloy core–shells (shown in Fig. 45). Zhang *et al.*[244] used HgTe–CdSe core–shell NCs with dihydrolipoic acid stabilizer ligands. In their case the NC emission was slightly longer than the usual tissue transparency region (1050 nm). The use of longer wavelengths can be an advantage in separating NC emission from tissue autofluorescence and in gated detection systems, the long NC emission lifetimes can also be advantageous in this respect.

Gu *et al.*[312] have attempted to address the issue of heavy metal cytotoxicity through the use of IR emitting Ag_2Se NCs. Several types of cell were exposed to Ag_2Se for 24 hours and their ability to continue to metabolise 3-[4,5-dimethylthiazol-2-yl]-2,5-diphenyltetrazolium bromide (MTT) (a standard cell viability assay) examined, and cell viabilities ranged from 96% to 100%. With NCs emitting around 820 nm they furthermore imaged regions of a mouse abdominal cavity injected with an NC solution with fluorescence visible from either front or back of the mouse body (see Fig. 46). Li *et al.*[491] similarly used $CuInS_2$–ZnS core–shell fluorophores for cadmium/lead-free *in vitro* imaging, with NC emission at wavelengths up to 815 nm and quantum efficiencies up to 60%.

Zintchenko *et al.*[492] utilized NIR emitting, MPA coated CdTe QDs to follow the biodistribution of polymeric gene carriers *in vivo* in real time. QDs bearing a net negative charge due to terminal carboxy groups were incorporated into polyplexes by virtue of electrostatic interactions with polycationic polyethylenimine and negatively charged plasmid DNA, resulting in what have been termed 'quantoplexes', approximately 250 nm in size. The *in vivo* biodistribution of quantoplexes in mice has been followed from 15 seconds after intravenous injection for up to one week. In contrast to bare QDs which accumulated within vessel-like structures in the liver and spleen, quantoplexes immediately accumulated in the lungs. In a subcutaneous murine neuroblastoma model, only PEGylated quantoplexes were retained in the tumor tissue after systemic injection,

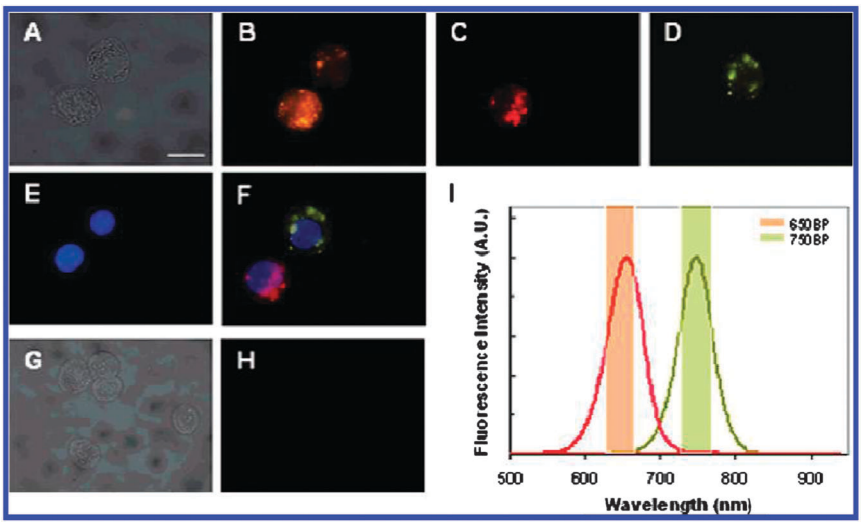

Fig. 44 Multiplexed *in vitro* imaging of HeLa cells stained with near-infrared-emitting QDs. Two different populations of HeLa cells were incubated with 660 nm emitting (pseudo-colored red) and 750 nm emitting (pseudo-colored green) near-IR-emitting QDs (A–F) with or (G–H) without conjugation to transferrin. Upon trypsinization and mixing of the two cell populations into a single culture dish, DIC (A, G) and fluorescence (B–F, H) images were taken. Spectral resolution and sorting of HeLa cells labeled with transferrin-conjugated near-infrared-emitting Qdots is demonstrated by taking fluorescence images (B–D) using (B) 650 LP (long pass), (C) 650/40 BP (band pass), and (D) 750/40 BP emission filters. (E) Image of HeLa cell nuclei stained with DAPI, taken using a 460/50 BP emission filter. (F) Superimposed image of (C–G) demonstrating that transferrin-conjugated near-IR-emitting QDs are located in perinuclear regions within the HeLa cells. (G) Control DIC and (H) fluorescence image of two HeLa cell populations incubated with near IR emitting QDs without transferrin conjugation (B–F). (I) Fluorescence spectra of near IR emitting QDs and emission filter selection corresponding to fluorescence images (C, D). Scale bar = 10 μm. Reprinted with permission from W. Jiang *et al.*, *Chem. Mater.*, 2006, **18**, 4845–4854. Copyright 2006 American Chemical Society (ref. 298).

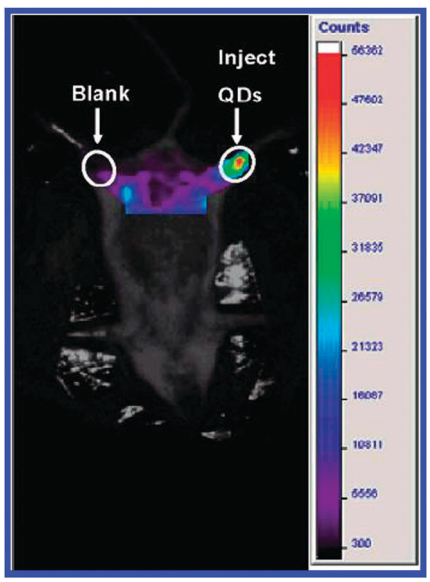

Fig. 45 Fluorescence *in vivo* imaging of a mouse after the injection of CdHg(20%)Te/CdS in the right leg. Reprinted with permission from H. Qian *et al.*, *J. Phys. Chem. C*, 2007, **111**, 16852–16857. Copyright 2007 American Chemical Society (ref. 490).

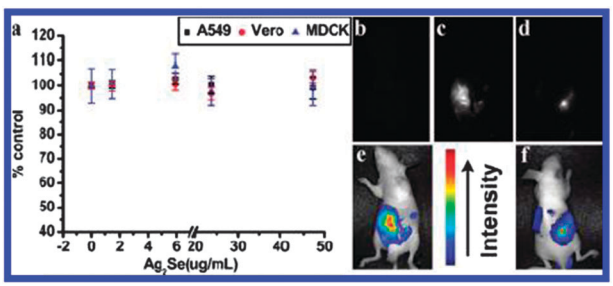

Fig. 46 MTT assay and NIR images of a living nude mouse after injection of Ag_2Se QDs: (a) MTT assay on A549, Vero, and MDCK cells exposed to Ag_2Se QDs at different concentrations from 0 to 47.4 μg mL^{-1} for 24 h; (b) fluorescence image of the nude mouse; (c) fluorescence imaging from the abdominal cavity of the nude mouse with Ag_2Se QDs injected into the abdominal cavity; (d) fluorescence imaging on the back side of the nude mouse with Ag_2Se QDs injected into the abdominal cavity; (e,f) merged images of the bright-field and the threshold false color of (c) and (d), respectively. Reprinted with permission from Y.-P Gu *et al.*, *J. Am. Chem. Soc.*, 2011, **134**, 79–82. Copyright 2011 American Chemical Society (ref. 312).

and a short circulation in blood was clearly observed. In sharp contrast, without PEG quantoplexes immediately accumulated in the lungs without reaching the circulation system or the tumor.

The final biological application we have chosen is an example of the potential therapeutic use of narrow bandgap NC–titania nanocomposites more commonly found in solar application research. Ratanatawanate *et al.*[493] have combined 3.6 nm diameter PbS nanoparticles with titania nanotubes and the biomolecule *S*-nitrosocysteine. Under NIR illumination this combination produces nitric oxide which can then lead to the production of singlet oxygen within tissues to destroy tumorous cells. The authors proposed that this would form the basis of a photodynamic therapy, without the need for high energy photon exposure, and with the benefit of deep tissue penetration at the long wavelengths used to excite the NCs. Of course in

this case the use of lead based NCs would be a barrier to clinical use.

5.3 Applications summary

Notwithstanding the great strides in the synthesis and device fabrication technologies, there are still great challenges, both technical and commercial that remain to be solved. Whilst good quality materials with correspondingly high quantum yields can be grown, this is not yet something that can be achieved across the board. Maintaining material quality such that larger diameter, long wavelength emitting NCs[243,248] (*e.g.* >2 μm wavelengths) fluoresce much more efficiently than at present is a synthetic challenge. For these materials and even many shorter wavelength NC materials, the elimination of trap states, particularly at NC surfaces and ligand sites, can be further improved.

In the FET, LED and solar cell fields, improvements in carrier mobilities of NC films[10] and more efficient charge transfer between NC and the surrounding dielectric is bringing these devices closer to commercially viable performance. However, the control of non-radiative processes such as Auger recombination[443] remains a problem in solar cell and opto-electronic applications.[446] In the former case in particular, either a means to suppress Auger processes or to extract photogenerated carriers before non-radiative recombination can occur, are desirable to combat this problem. For excitation well above the bandgap energy (as in photovoltaic solar cells), fast transfer of hot carriers (hot electrons)[441] or the use of slowed carrier cooling are promising areas of research in this respect in that they avoid the simultaneous presence of multiple excitons within NCs. Auger recombination is one of the main limitations for optoelectronic devices such as lasers or optical amplifiers. In order to invert the population of degenerate excited states in semiconductor NCs, multiple excitons must be created within each particle during the exciton lifetimes. Whilst this may be achieved on short timescales, it remains a challenge to obtain steady state gain, with the excited state population being depleted by fast non-radiative recombination (which is more rapid the more excitons that are needed to coexist). The exploration of methods to lift the degeneracy of NC excited states, perhaps by using anisotropic structures, may be a potential way to reduce the required excitation level. Equally, selecting materials with lower inherent degeneracy is also an obvious method to minimise the necessary excitation level and therefore reduce the rate of non-radiative recombination, though this will still remain a difficult barrier to overcome.

The understanding of the carrier multiplication process in NCs has improved in the light of better measurement techniques and methodology.[450,462] Whilst several possible mechanisms have been proposed, a primary contender, the inverse of Auger recombination, impact ionization,[444,445] seems the most significant. Impact ionization in NCs (and Auger relaxation[494] itself) is believed to differ little from that in the corresponding bulk material, so it is sensible to borrow from established bulk semiconductor materials technology to try to enhance this process. That said, the benefits of carrier multiplication for solar cell technology have had a more sober re-assessment recently.[447,462,463] It is perhaps of even greater importance to continue to focus upon the improvement of carrier extraction and transport efficiencies in NC solar cell devices.

For optoelectronic devices, optical scattering and loss (both self-absorption and absorption due to any host dielectric medium), particularly in the IR, limit some of the potential applications. This compares with rare earth ions doped into silica fibre (as a gain medium), where optical paths of 10–20 metres have been used, thanks to the very low absorption and scattering losses of the host material. Whilst the much greater oscillator strengths for QDs transitions probably implies that such long optical paths are unlikely to be required for QD devices in most cases, for some applications it may still be helpful to have good host transparency on say wafer length scales, and perhaps moderate transparency on say the metre or so length scale. Here further improvements in the assembly of large scale ordered NC superlattices, or perhaps the inclusion of NCs in non-hydrocarbon or hydroxyl group containing hosts may prove to be useful.

6 Conclusion and outlook

Over the last two decades, the field of narrow bandgap colloidal QDs has evolved from moderately simple syntheses of QD solutions to the fabrication of NC materials with precisely controlled particle size (diameters and size distributions), semiconductor compositions and particle shapes. Heterostructures with both discrete shells and graded compositions can be made in many material systems, and for most materials there are a range of synthesis methods that give the flexibility to tailor the QDs to a broad set of applications. The role of the ligands during synthesis and in subsequent processing stages where the NCs are combined with other types of material or assembled into QD films or ordered solids has been studied in great detail and there are now many methods to reliably exchange ligands at various stages, *e.g.* QDs may be grown in organic solvents at high temperatures using long chain organo-phosphorous stabilizers for optimum synthetic control, and these later replaced by small inorganic molecules (*e.g.* MMCs) better suited for the target application. There is a wide variety of ligand types – water soluble ionic compounds, covalently bound organic molecules, small inorganic molecules or ionic species (serving as capping layer or ligands) and molecules combining both surface binding groups and other (reactive) functional groups to allow complex covalently bound structures (with other QDs or particular substrates) to be formed. In addition, for monodisperse QDs it is also possible to assemble larger scale complex but regularly packed (periodic) superlattice films and solids that may be used as the basis for electronic or photonic bandgap materials.

At the individual QD level, there is now much better understanding of the role of surface species as carrier traps and how best to reduce their impact on the performance of QDs. The role of other non-radiative processes, largely internal to the NCs (*e.g.* Auger relaxation), is likewise better understood and a number of approaches (*e.g.* use of heterostructures, or fast hot carrier transfer) are emerging to likewise combat their effect.

One of the most enduring challenges at this stage however remains – how to commercialize NC technology. Though the potential applications for narrow bandgap NCs are clearly identified, it is still difficult to attract serious corporate or venture capital funding for many of these. Largely the problem is down to the perceived time to market, and that in most of the applications for narrow bandgap NCs the materials are 'playing catch-up' in performance with well established technologies: for LEDs and displays NCs trail LCDs, OLEDs and other bulk semiconductors; in IR optoelectronics InGaAs dominates telecom component technologies; in solar cells NC devices trail even DSSCs and mainstream silicon photovoltaics by a wide margin; in FET applications carrier mobilities still lag by orders of magnitude behind conventional semiconductors. To enter established markets new technologies must either exceed the performance of the incumbents or bring a feature not already offered – low cost, better integratability, wider operation range, *etc.* Moreover a startup company launching such technology must typically be able to demonstrate commercial viability in less than 3 years – a difficult prospect without prior commercial experience.

Debatably the best prospects lie in the commercialization of NCs for solar cell applications. Government backed funding initiatives are presently the main source of early stage funding which may fill the gap until performance or other differentiators rise to levels that excite corporate or venture capital funding to pull the technology to market. Talapin *et al.*[10] have suggested that with moderate improvements in carrier mobility, NC FETs for microelectronic applications may be able to gain a foothold on the strength of potential low cost (materials costs perhaps less than 1 US$ g^{-1}), and compatibility with flexible substrates for niche applications. For smaller revenue markets, NC sensors, biosensors or bio-assay applications might have shorter development timescales (at least for *in vitro* applications) and may be a better option to build materials competence and a commercial track-record for NCs and indeed several university spin-out companies (most notably Quantum Dot Corporation in the USA, now part of Invitrogen) have already explored this option.

In spite of these challenges, however, the NC materials research effort worldwide is making tremendous progress and the next few years are sure to be exciting and rewarding as the material science of narrow bandgap NCs in particular improves still further, bringing commercializable optoelectronic and other applications within reach.

Acknowledgements

This work was supported by an Applied Research Grant of City University of Hong Kong (9667067), and by a grant from the Research Grants Council of the Hong Kong S.A.R., China (project CityU 102412).

References

1 M. Shim and P. Guyot-Sionnest, *Nature*, 2000, **407**, 981–983.
2 J. L. Blackburn, R. J. Ellingson, O. I. Mićić and A. J. Nozik, *J. Phys. Chem. B*, 2002, **107**, 102–109.
3 C. Wang, M. Shim and P. Guyot-Sionnest, *Science*, 2001, **291**, 2390–2392.
4 C. Wang, M. Shim and P. Guyot-Sionnest, *Appl. Phys. Lett.*, 2002, **80**, 4–6.
5 P. Guyot-Sionnest and M. A. Hines, *Appl. Phys. Lett.*, 1998, **72**, 686–688.
6 A. Eychmüller, *J. Phys. Chem. B*, 2000, **104**, 6514–6528.
7 B. L. Cushing, V. L. Kolesnichenko and C. J. O'Connor, *Chem. Rev.*, 2004, **104**, 3893–3946.
8 C. Burda, X. Chen, R. Narayanan and M. A. El-Sayed, *Chem. Rev.*, 2005, **105**, 1025–1102.
9 A. L. Rogach, A. Eychmüller, S. G. Hickey and S. V. Kershaw, *Small*, 2007, **3**, 536–557.
10 D. V. Talapin, J.-S. Lee, M. V. Kovalenko and E. V. Shevchenko, *Chem. Rev.*, 2009, **110**, 389–458.
11 N. Gaponik and A. L. Rogach, *Phys. Chem. Chem. Phys.*, 2010, **12**, 8685–8693.
12 J. Yang, J. Y. Lee and J. Y. Ying, *Chem. Soc. Rev.*, 2011, **40**, 1672–1696.
13 M. D. Regulacio and M.-Y. Han, *Acc. Chem. Res.*, 2010, **43**, 621–630.
14 Z. Zhuang, Q. Peng and Y. Li, *Chem. Soc. Rev.*, 2011, **40**, 5492–5513.
15 P. D. Cozzoli, T. Pellegrino and L. Manna, *Chem. Soc. Rev.*, 2006, **35**, 1195–1208.
16 C. de Mello Donegá, *Chem. Soc. Rev.*, 2011, **40**, 1512–1546.
17 Y. Xia and Z. Tang, *Chem. Commun.*, 2012, **48**, 6320–6336.
18 R. Ghosh Chaudhuri and S. Paria, *Chem. Rev.*, 2011, **112**, 2373–2433.
19 H. Althues, J. Henle and S. Kaskel, *Chem. Soc. Rev.*, 2007, **36**, 1454–1465.
20 E. Holder, N. Tessler and A. L. Rogach, *J. Mater. Chem.*, 2008, **18**, 1064–1078.
21 M. Afzaal and P. O'Brien, *J. Mater. Chem.*, 2006, **16**, 1597–1602.
22 Z. Yang, C.-Y. Chen, P. Roy and H.-T. Chang, *Chem. Commun.*, 2011, **47**, 9561–9571.
23 F. Hetsch, X. Xu, H. Wang, S. V. Kershaw and A. L. Rogach, *J. Phys. Chem. Lett.*, 2011, **2**, 1879–1887.
24 R. Debnath, O. Bakr and E. H. Sargent, *Energy Environ. Sci.*, 2011, **4**, 4870–4881.
25 C. Blanco-Andujar, L. D. Tung and N. T. K. Thanh, *Annu. Rep. Prog. Chem., Sect. A*, 2010, **106**, 553–568.
26 G. Wang and X. Su, *Analyst*, 2011, **136**, 1783–1798.
27 R. A. Sperling and W. J. Parak, *Philos. Trans. R. Soc. London, Ser. A*, 2010, **368**, 1333–1383.
28 S. Sortino, *J. Mater. Chem.*, 2012, **22**, 301–318.
29 C. B. Murray, C. R. Kagan and M. G. Bawendi, *Annu. Rev. Mater. Sci.*, 2000, **30**, 545–610.
30 M. A. Hines and G. D. Scholes, *Adv. Mater.*, 2003, **15**, 1844–1849.
31 M. Corricelli, F. Enrichi, D. Altamura, L. De Caro, C. Giannini, A. Falqui, A. Agostiano, M. L. Curri and M. Striccoli, *J. Phys. Chem. C*, 2012, **116**, 6143–6152.
32 M. Corricelli, D. Altamura, L. De Caro, A. Guagliardi, A. Falqui, A. Genovese, A. Agostiano, C. Giannini,

M. Striccoli and M. L. Curri, *CrystEngComm*, 2011, **13**, 3988–3997.
33 D. Altamura, L. De Caro, M. Corricelli, A. Falqui, M. Striccoli, M. L. Curri and C. Giannini, *Cryst. Growth Des.*, 2012, **12**, 1970–1976.
34 D. J. Asunskis, I. L. Bolotin, J. E. Haley, A. Urbas and L. Hanley, *J. Phys. Chem. C*, 2009, **113**, 19824–19829.
35 D. J. Asunskis, I. L. Bolotin and L. Hanley, *J. Phys. Chem. C*, 2008, **112**, 9555–9558.
36 D. J. Asunskis, I. L. Bolotin, A. T. Wroble, A. M. Zachary and L. Hanley, *Macromol. Symp.*, 2008, **268**, 33–37.
37 J. S. Steckel, S. Coe-Sullivan, V. Bulović and M. G. Bawendi, *Adv. Mater.*, 2003, **15**, 1862–1866.
38 I. L. Bolotin, D. J. Asunskis, A. M. Jawaid, Y. Liu, P. T. Snee and L. Hanley, *J. Phys. Chem. C*, 2010, **114**, 16257–16262.
39 S. J. Baik, K. Kim, K. S. Lim, S. Jung, Y.-C. Park, D. G. Han, S. Lim, S. Yoo and S. Jeong, *J. Phys. Chem. C*, 2010, **115**, 607–612.
40 M. V. Kovalenko, M. I. Bodnarchuk, J. Zaumseil, J.-S. Lee and D. V. Talapin, *J. Am. Chem. Soc.*, 2010, **132**, 10085–10092.
41 K. P. Acharya, N. N. Hewa-Kasakarage, T. R. Alabi, I. Nemitz, E. Khon, B. Ullrich, P. Anzenbacher and M. Zamkov, *J. Phys. Chem. C*, 2010, **114**, 12496–12504.
42 K. P. Acharya, E. Khon, T. O'Conner, I. Nemitz, A. Klinkova, R. S. Khnayzer, P. Anzenbacher and M. Zamkov, *ACS Nano*, 2011, **5**, 4953–4964.
43 S. A. McDonald, P. W. Cyr, L. Levina and E. H. Sargent, *Appl. Phys. Lett.*, 2004, **85**, 2089–2091.
44 E. J. D. Klem, L. Levina and E. H. Sargent, *Appl. Phys. Lett.*, 2005, **87**, 053101.
45 G. Konstantatos, C. Huang, L. Levina, Z. Lu and E. H. Sargent, *Adv. Funct. Mater.*, 2005, **15**, 1865–1869.
46 S. Zhang, P. W. Cyr, S. A. McDonald, G. Konstantatos and E. H. Sargent, *Appl. Phys. Lett.*, 2005, **87**, 233101.
47 S. Hinds, L. Levina, E. J. D. Klem, G. Konstantatos, V. Sukhovatkin and E. H. Sargent, *Adv. Mater.*, 2008, **20**, 4398–4402.
48 K. W. Johnston, A. G. Pattantyus-Abraham, J. P. Clifford, S. H. Myrskog, D. D. MacNeil, L. Levina and E. H. Sargent, *Appl. Phys. Lett.*, 2008, **92**, 151115.
49 K. S. Jeong, J. Tang, H. Liu, J. Kim, A. W. Schaefer, K. Kemp, L. Levina, X. Wang, S. Hoogland, R. Debnath, L. Brzozowski, E. H. Sargent and J. B. Asbury, *ACS Nano*, 2011, **6**, 89–99.
50 J. Tang, X. Wang, L. Brzozowski, D. A. R. Barkhouse, R. Debnath, L. Levina and E. H. Sargent, *Adv. Mater.*, 2010, **22**, 1398–1402.
51 M. I. Bodnarchuk, M. V. Kovalenko, W. Heiss and D. V. Talapin, *J. Am. Chem. Soc.*, 2010, **132**, 11967–11977.
52 M. Madl, W. Brezna, G. Strasser, P. Klang, A. M. Andrews, M. I. Bodnarchuk, M. V. Kovalenko, M. Yarema, W. Heiss and J. Smoliner, *Phys. Status Solidi C*, 2011, **8**, 426–428.
53 G. Itskos, A. Othonos, T. Rauch, S. F. Tedde, O. Hayden, M. V. Kovalenko, W. Heiss and S. A. Choulis, *Adv. Energy Mater.*, 2011, **1**, 802–812.
54 M. Böberl, M. V. Kovalenko, G. Pillwein, G. Brunthaler and W. Heiss, *Appl. Phys. Lett.*, 2008, **92**, 261113.
55 K. Szendrei, F. Cordella, M. V. Kovalenko, M. Böberl, G. Hesser, M. Yarema, D. Jarzab, O. V. Mikhnenko, A. Gocalinska, M. Saba, F. Quochi, A. Mura, G. Bongiovanni, P. W. M. Blom, W. Heiss and M. A. Loi, *Adv. Mater.*, 2009, **21**, 683–687.
56 A. Gocalińska, M. Saba, F. Quochi, M. Marceddu, K. Szendrei, J. Gao, M. A. Loi, M. Yarema, R. Seyrkammer, W. Heiss, A. Mura and G. Bongiovanni, *J. Phys. Chem. Lett.*, 2010, **1**, 1149–1154.
57 J. Roither, M. V. Kovalenko and W. Heiss, *Nanotechnology*, 2008, **19**, 355205.
58 J. M. Luther, J. Gao, M. T. Lloyd, O. E. Semonin, M. C. Beard and A. J. Nozik, *Adv. Mater.*, 2010, **22**, 3704–3707.
59 S. M. Rupich, E. V. Shevchenko, M. I. Bodnarchuk, B. Lee and D. V. Talapin, *J. Am. Chem. Soc.*, 2009, **132**, 289–296.
60 B. Lee, P. Podsiadlo, S. Rupich, D. V. Talapin, T. Rajh and E. V. Shevchenko, *J. Am. Chem. Soc.*, 2009, **131**, 16386–16388.
61 S. Krüger, S. G. Hickey, S. Tscharntke and A. Eychmüller, *J. Phys. Chem. C*, 2011, **115**, 13047–13055.
62 T.-Y. Liu, M. Li, J. Ouyang, M. B. Zaman, R. Wang, X. Wu, C.-S. Yeh, Q. Lin, B. Yang and K. Yu, *J. Phys. Chem. C*, 2009, **113**, 2301–2308.
63 H. Li, D. Chen, L. Li, F. Tang, L. Zhang and J. Ren, *CrystEngComm*, 2010, **12**, 1127–1133.
64 J. Akhtar, M. Azad Malik, P. O'Brien, K. G. U. Wijayantha, R. Dharmadasa, S. J. O. Hardman, D. M. Graham, B. F. Spencer, S. K. Stubbs, W. R. Flavell, D. J. Binks, F. Sirotti, M. El Kazzi and M. Silly, *J. Mater. Chem.*, 2010, **20**, 2336–2344.
65 D. Berhanu, K. Govender, D. Smyth-Boyle, M. Archbold, D. P. Halliday and P. O'Brien, *Chem. Commun.*, 2006, 4709–4711.
66 T. Trindade, P. O'Brien, X.-m. Zhang and M. Motevalli, *J. Mater. Chem.*, 1997, **7**, 1011–1016.
67 L. Bakueva, I. Gorelikov, S. Musikhin, X. S. Zhao, E. H. Sargent and E. Kumacheva, *Adv. Mater.*, 2004, **16**, 926–929.
68 M. J. Fernée, A. Watt, J. Warner, S. Cooper, N. Heckenberg and H. Rubinsztein-Dunlop, *Nanotechnology*, 2003, **14**, 991.
69 M. J. Ferné, A. Watt, J. Warner, N. Heckenberg and H. Rubinsztein-Dunlop, *Nanotechnology*, 2004, **15**, 1328.
70 M. T. Nenadovic, M. I. Comor, V. Vasic and O. I. Micic, *J. Phys. Chem.*, 1990, **94**, 6390–6396.
71 J. H. Warner, A. A. R. Watt and R. D. Tilley, *Nanotechnology*, 2005, **16**, 2381.
72 A. L. Brazeau and N. D. Jones, *J. Phys. Chem. C*, 2009, **113**, 20246–20251.
73 A. Stavrinadis, R. Beal, J. M. Smith, H. E. Assender and A. A. R. Watt, *Adv. Mater.*, 2008, **20**, 3105–3109.
74 D. J. Keeble, E. A. Thomsen, A. Stavrinadis, I. D. W. Samuel, J. M. Smith and A. A. R. Watt, *J. Phys. Chem. C*, 2009, **113**, 17306–17312.
75 K. Biswas and C. N. R. Rao, *Chem.–Eur. J.*, 2007, **13**, 6123–6129.

76 Y. Sun, E. Hao, X. Zhang, B. Yang, M. Gao and J. Shen, *Chem. Commun.*, 1996, 2381–2382.
77 A. L. P. Cornacchio and N. D. Jones, *J. Mater. Chem.*, 2006, **16**, 1171–1177.
78 N. Zhu, A. Zhang, Q. Wang, P. He and Y. Fang, *Electroanalysis*, 2004, **16**, 577–582.
79 P. Jiang, Z.-F. Liu and S.-M. Cai, *J. Appl. Phys.*, 2001, **90**, 2039–2041.
80 Z. Hens, D. Vanmaekelbergh, E. J. A. J. Stoffels and H. van Kempen, *Phys. Rev. Lett.*, 2002, **88**, 236803.
81 B. Jia, D. Buso, J. van Embden, J. Li and M. Gu, *Adv. Mater.*, 2010, **22**, 2463–2467.
82 D. Buso, L. Palmer, V. Bello, G. Mattei, M. Post, P. Mulvaney and A. Martucci, *J. Mater. Chem.*, 2009, **19**, 2051–2057.
83 D. Buso, P. Falcaro, S. Costacurta, M. Guglielmi, A. Martucci, P. Innocenzi, L. Malfatti, V. Bello, G. Mattei, C. Sada, H. Amenitsch, I. Gerdova and A. Haché, *Chem. Mater.*, 2005, **17**, 4965–4970.
84 A. H. Khan, Q. Ji, K. Ariga, U. Thupakula and S. Acharya, *J. Mater. Chem.*, 2011, **21**, 5671–5676.
85 A. H. Khan, Q. Ji, K. Ariga, B. Das, D. D. Sarma and S. Acharya, *Chem. Commun.*, 2011, **47**, 8421–8423.
86 J. M. Clark, G. Kociok-Kohn, N. J. Harnett, M. S. Hill, R. Hill, K. C. Molloy, H. Saponia, D. Stanton and A. Sudlow, *Dalton Trans.*, 2011, **40**, 6893–6900.
87 G. Liu, J. Wang, J. Kim, M. R. Jan and G. E. Collins, *Anal. Chem.*, 2004, **76**, 7126–7130.
88 J. H. Choi, K. H. Chen, J.-H. Han, A. M. Chaffee and M. S. Strano, *Small*, 2009, **5**, 672–675.
89 D. Deng, W. Zhang, X. Chen, F. Liu, J. Zhang, Y. Gu and J. Hong, *Eur. J. Inorg. Chem.*, 2009, 3440–3446.
90 L. Turyanska, O. Makarovsky, U. Elfurawi, A. Patané, M. W. Fay, J. W. Bowers and H. M. Upadhyaya, *Phys. Status Solidi A*, 2011, **208**, 2450–2453.
91 L. Turyanska, A. Patane, M. Henini, B. Hennequin and N. R. Thomas, *Appl. Phys. Lett.*, 2007, **90**, 101913.
92 H. Zhao, M. Chaker and D. Ma, *Phys. Chem. Chem. Phys.*, 2010, **12**, 14754–14761.
93 H. Zhao, M. Chaker and D. Ma, *J. Mater. Chem.*, 2011, **21**, 17483–17491.
94 H. Zhao, D. Wang, M. Chaker and D. Ma, *J. Phys. Chem. C*, 2011, **115**, 1620–1626.
95 C. Li, Y. Zhao, F. Li, Z. Shi and S. Feng, *Chem. Mater.*, 2010, **22**, 1901–1907.
96 H.-Y. Si, D. Yuan, J.-S. Chen and G.-M. Chow, *RSC Adv.*, 2011, **1**, 817–822.
97 C. Zhang, Z. Kang, E. Shen, E. Wang, L. Gao, F. Luo, C. Tian, C. Wang, Y. Lan, J. Li and X. Cao, *J. Phys. Chem. B*, 2005, **110**, 184–189.
98 T. Ding, J.-R. Zhang, S. Long and J.-J. Zhu, *Microelectron. Eng.*, 2003, **66**, 46–52.
99 T. Ding and J.-J. Zhu, *Mater. Sci. Eng., B*, 2003, **100**, 307–313.
100 K. M. Freny Joy, N. Victor Jaya and J.-J. Zhu, *Mod. Phys. Lett. B*, 2006, **20**, 963–970.
101 B. Deng, S.-L. Zhong, D.-H. Wang, S.-S. Wang, T.-K. Zhang, W.-G. Qu and A.-W. Xu, *Nanoscale*, 2011, **3**, 1014–1021.
102 L. Jankovic, K. Dimos, J. Bujdak, I. Koutselas, J. Madejova, D. Gournis, M. A. Karakassides and P. Komadel, *Phys. Chem. Chem. Phys.*, 2010, **12**, 14236–14244.
103 A. V. Lukashin, A. A. Eliseev, N. G. Zhuravleva, A. A. Vertegel, Y. D. Tretyakov, O. I. Lebedev and G. V. Tendeloo, *Mendeleev Commun.*, 2004, **14**, 174–176.
104 R. Koole, G. Allan, C. Delerue, A. Meijerink, D. Vanmaekelbergh and A. J. Houtepen, *Small*, 2008, **4**, 127–133.
105 K. P. Acharya, T. R. Alabi, N. Schmall, N. N. Hewa-Kasakarage, M. Kirsanova, A. Nemchinov, E. Khon and M. Zamkov, *J. Phys. Chem. C*, 2009, **113**, 19531–19535.
106 Z. Hens, E. S. Kooij, G. Allan, B. Grandidier and D. Vanmaekelbergh, *Nanotechnology*, 2005, **16**, 339–343.
107 Z. Hens, D. Vanmaekelbergh, E. S. Kooij, H. Wormeester, G. Allan and C. Delerue, *Phys. Rev. Lett.*, 2004, **92**, 026808.
108 B. Grandidier, *J. Phys.: Condens. Matter*, 2004, **16**, S161–S170.
109 C. B. Murray, S. Sun, W. Gaschler and H. Doyle, *et al.*, *IBM J. Res. Dev.*, 2001, **45**, 47–56.
110 M. Law, J. M. Luther, Q. Song, B. K. Hughes, C. L. Perkins and A. J. Nozik, *J. Am. Chem. Soc.*, 2008, **130**, 5974–5985.
111 J. M. Luther, M. Law, Q. Song, C. L. Perkins, M. C. Beard and A. J. Nozik, *ACS Nano*, 2008, **2**, 271–280.
112 P. Liljeroth, P. A. Z. van Emmichoven, S. G. Hickey, H. Weller, B. Grandidier, G. Allan and D. Vanmaekelbergh, *Phys. Rev. Lett.*, 2005, **95**, 086801.
113 M. Law, M. C. Beard, S. Choi, J. M. Luther, M. C. Hanna and A. J. Nozik, *Nano Lett.*, 2008, **8**, 3904–3910.
114 G. Nair, S. M. Geyer, L.-Y. Chang and M. G. Bawendi, *Phys. Rev. B: Condens. Matter Mater. Phys.*, 2008, **78**, 125325.
115 Y. K. Olsson, G. Chen, R. Rapaport, D. T. Fuchs, V. C. Sundar, J. S. Steckel, M. G. Bawendi, A. Aharoni and U. Banin, *Appl. Phys. Lett.*, 2004, **85**, 4469–4471.
116 T. S. Mentzel, V. J. Porter, S. Geyer, K. MacLean, M. G. Bawendi and M. A. Kastner, *Phys. Rev. B: Condens. Matter Mater. Phys.*, 2008, **77**, 075316.
117 O. Solomeshch, A. Kigel, A. Saschiuk, V. Medvedev, A. Aharoni, A. Razin, Y. Eichen, U. Banin, E. Lifshitz and N. Tessler, *J. Appl. Phys.*, 2005, **98**, 074310.
118 I. Moreels, K. Lambert, D. De Muynck, F. Vanhaecke, D. Poelman, J. C. Martins, G. Allan and Z. Hens, *Chem. Mater.*, 2007, **19**, 6101–6106.
119 R. B. Vasiliev, S. G. Dorofeev, D. N. Dirin, D. A. Belov and T. A. Kuznetsova, *Mendeleev Commun.*, 2004, **14**, 169–171.
120 J. E. Murphy, M. C. Beard and A. J. Nozik, *J. Phys. Chem. B*, 2006, **110**, 25455–25461.
121 D. Yu, C. Wang and P. Guyot-Sionnest, *Science*, 2003, **300**, 1277–1280.
122 A. J. Houtepen, R. Koole, D. Vanmaekelbergh, J. Meeldijk and S. G. Hickey, *J. Am. Chem. Soc.*, 2006, **128**, 6792–6793.
123 J. Joo, J. M. Pietryga, J. A. McGuire, S.-H. Jeon, D. J. Williams, H.-L. Wang and V. I. Klimov, *J. Am. Chem. Soc.*, 2009, **131**, 10620–10628.
124 R. D. Schaller and V. I. Klimov, *Phys. Rev. Lett.*, 2004, **92**, 186601.

125 R. D. Schaller, J. M. Pietryga, S. V. Goupalov, M. A. Petruska, S. A. Ivanov and V. I. Klimov, *Phys. Rev. Lett.*, 2005, **95**, 196401.
126 J. M. Pietryga, K. K. Zhuravlev, M. Whitehead, V. I. Klimov and R. D. Schaller, *Phys. Rev. Lett.*, 2008, **101**, 217401.
127 G. R. Maskaly, M. A. Petruska, J. Nanda, I. V. Bezel, R. D. Schaller, H. Htoon, J. M. Pietryga and V. I. Klimov, *Adv. Mater.*, 2006, **18**, 343–347.
128 L. A. Padilha, I. Robel, D. C. Lee, P. Nagpal, J. M. Pietryga and V. I. Klimov, *ACS Nano*, 2011, **5**, 5045–5055.
129 J. M. Pietryga, R. D. Schaller, D. Werder, M. H. Stewart, V. I. Klimov and J. A. Hollingsworth, *J. Am. Chem. Soc.*, 2004, **126**, 11752–11753.
130 W. Ma, S. L. Swisher, T. Ewers, J. Engel, V. E. Ferry, H. A. Atwater and A. P. Alivisatos, *ACS Nano*, 2011, **5**, 8140–8147.
131 Q. Dai, Y. Wang, X. Li, Y. Zhang, D. J. Pellegrino, M. Zhao, B. Zou, J. Seo, Y. Wang and W. W. Yu, *ACS Nano*, 2009, **3**, 1518–1524.
132 Q. Dai, Y. Wang, Y. Zhang, X. Li, R. Li, B. Zou, J. Seo, Y. Wang, M. Liu and W. W. Yu, *Langmuir*, 2009, **25**, 12320–12324.
133 Q. Dai, Y. Zhang, Y. Wang, M. Z. Hu, B. Zou, Y. Wang and W. W. Yu, *Langmuir*, 2010, **26**, 11435–11440.
134 Q. Dai, Y. Zhang, Y. Wang, Y. Wang, B. Zou, W. W. Yu and M. Z. Hu, *J. Phys. Chem. C*, 2010, **114**, 16160–16167.
135 W. W. Yu, J. C. Falkner, B. S. Shih and V. L. Colvin, *Chem. Mater.*, 2004, **16**, 3318–3322.
136 J. G. Tischler, T. A. Kennedy, E. R. Glaser, A. L. Efros, E. E. Foos, J. E. Boercker, T. J. Zega, R. M. Stroud and S. C. Erwin, *Phys. Rev. B: Condens. Matter Mater. Phys.*, 2010, **82**, 245303.
137 K. Roy Choudhury, Y. Sahoo and P. N. Prasad, *Adv. Mater.*, 2005, **17**, 2877–2881.
138 T. Zhu, A. Berger, Z. Tan, D. Cui, J. Xu, P. Khanchaitit and Q. Wang, *J. Appl. Phys.*, 2008, **104**, 044306.
139 J. Li, B. Jia, G. Zhou, C. Bullen, J. Serbin and M. Gu, *Adv. Mater.*, 2007, **19**, 3276–3280.
140 Y. C. Ou, S. F. Cheng and W. B. Jian, *Nanotechnology*, 2009, **20**, 285401.
141 X. Liu, T. Iimori, R. Ohshima, T. Nakabayashi and N. Ohta, *Appl. Phys. Lett.*, 2011, **98**, 161911–161913.
142 T. Hanrath, J. J. Choi and D.-M. Smilgies, *ACS Nano*, 2009, **3**, 2975–2988.
143 T. Hanrath, D. Veldman, J. J. Choi, C. G. Christova, M. M. Wienk and R. A. J. Janssen, *ACS Appl. Mater. Interfaces*, 2009, **1**, 244–250.
144 E. E. Foos, T. J. Zega, J. G. Tischler, R. M. Stroud and J. E. Boercker, *J. Mater. Chem.*, 2011, **21**, 2616–2623.
145 M. A. Sliem, A. Chemseddine, U. Bloeck and R. A. Fischer, *CrystEngComm*, 2011, **13**, 483–488.
146 O. Chen, X. Chen, Y. Yang, J. Lynch, H. Wu, J. Zhuang and Y. C. Cao, *Angew. Chem., Int. Ed.*, 2008, **120**, 8766–8769.
147 D. K. Kim, T. R. Vemulkar, S. J. Oh, W.-K. Koh, C. B. Murray and C. R. Kagan, *ACS Nano*, 2011, **5**, 3230–3236.
148 W. Shi, Y. Sahoo, H. Zeng, Y. Ding, M. T. Swihart and P. N. Prasad, *Adv. Mater.*, 2006, **18**, 1889–1894.
149 J. Zeng, J. Huang, C. Liu, C. H. Wu, Y. Lin, X. Wang, S. Zhang, J. Hou and Y. Xia, *Adv. Mater.*, 2010, **22**, 1936–1940.
150 K.-T. Yong, Y. Sahoo, K. R. Choudhury, M. T. Swihart, J. R. Minter and P. N. Prasad, *Nano Lett.*, 2006, **6**, 709–714.
151 A. C. Bartnik, A. L. Efros, W. K. Koh, C. B. Murray and F. W. Wise, *Phys. Rev. B: Condens. Matter Mater. Phys.*, 2010, **82**, 195313.
152 S. Acharya, U. K. Gautam, T. Sasaki, Y. Bando, Y. Golan and K. Ariga, *J. Am. Chem. Soc.*, 2008, **130**, 4594–4595.
153 A. Sashchiuk, L. Langof, R. Chaim and E. Lifshitz, *J. Cryst. Growth*, 2002, **240**, 431–438.
154 B. L. Wehrenberg, C. Wang and P. Guyot-Sionnest, *J. Phys. Chem. B*, 2002, **106**, 10634–10640.
155 D. V. Talapin, C. T. Black, C. R. Kagan, E. V. Shevchenko, A. Afzali and C. B. Murray, *J. Phys. Chem. C*, 2007, **111**, 13244–13249.
156 K.-S. Cho, D. V. Talapin, W. Gaschler and C. B. Murray, *J. Am. Chem. Soc.*, 2005, **127**, 7140–7147.
157 R. Y. Wang, J. P. Feser, J.-S. Lee, D. V. Talapin, R. Segalman and A. Majumdar, *Nano Lett.*, 2008, **8**, 2283–2288.
158 L. Etgar, E. Lifshitz and R. Tannenbaum, *J. Phys. Chem. C*, 2007, **111**, 6238–6244.
159 L. Etgar, G. Leitus, L. Fradkin, Y. G. Assaraf, R. Tannenbaum and E. Lifshitz, *ChemPhysChem*, 2009, **10**, 2235–2241.
160 M. Brumer, A. Kigel, L. Amirav, A. Sashchiuk, O. Solomesch, N. Tessler and E. Lifshitz, *Adv. Funct. Mater.*, 2005, **15**, 1111–1116.
161 W. E. Mahmoud, *Polym. Adv. Technol.*, 2011, **22**, 2550–2555.
162 R. Cui, Y.-P. Gu, Z.-L. Zhang, Z.-X. Xie, Z.-Q. Tian and D.-W. Pang, *J. Mater. Chem.*, 2012, **22**, 3713–3716.
163 A. Kumar and B. Singh, *Chem. Commun.*, 2011, **47**, 4144–4146.
164 N. F. Borrelli and D. W. Smith, *J. Non-Cryst. Solids*, 1994, **180**, 25–31.
165 R. Espiau de Lamaestre, J. Majimel, F. Jomard and H. Bernas, *J. Phys. Chem. B*, 2005, **109**, 19148–19155.
166 E. I. Rogacheva, O. N. Nashchekina, A. V. Meriuts, S. G. Lyubchenko, M. S. Dresselhaus and G. Dresselhaus, *Appl. Phys. Lett.*, 2005, **86**, 063103.
167 M. V. Kovalenko, B. Spokoyny, J.-S. Lee, M. Scheele, A. Weber, S. Perera, D. Landry and D. V. Talapin, *J. Am. Chem. Soc.*, 2010, **132**, 6686–6695.
168 S. V. Kershaw, M. Harrison, A. L. Rogach and A. Kornowski, *IEEE J. Sel. Top. Quantum Electron.*, 2000, **6**, 534–543.
169 K. S. Cho, K. L. Stokes and C. B. Murray, *Abstr. Paper. Am. Chem. Soc.*, 2003, **225**, U74.
170 W. Lu, J. Fang, K. L. Stokes and J. Lin, *J. Am. Chem. Soc.*, 2004, **126**, 11798–11799.
171 J. E. Murphy, M. C. Beard, A. G. Norman, S. P. Ahrenkiel, J. C. Johnson, P. Yu, O. I. Mićić, R. J. Ellingson and A. J. Nozik, *J. Am. Chem. Soc.*, 2006, **128**, 3241–3247.
172 J. J. Urban, D. V. Talapin, E. V. Shevchenko and C. B. Murray, *J. Am. Chem. Soc.*, 2006, **128**, 3248–3255.
173 J. Zhang, A. Kumbhar, J. He, N. C. Das, K. Yang, J.-Q. Wang, H. Wang, K. L. Stokes and J. Fang, *J. Am. Chem. Soc.*, 2008, **130**, 15203–15209.

174 I. R. Franchini, G. Bertoni, A. Falqui, C. Giannini, L. W. Wang and L. Manna, *J. Mater. Chem.*, 2010, **20**, 1357–1366.
175 G. Tai, W. Guo and Z. Zhang, *Cryst. Growth Des.*, 2008, **8**, 2906–2911.
176 D.-K. Ko and C. B. Murray, *ACS Nano*, 2011, **5**, 4810–4817.
177 Z. Lin, M. Wang, L. Zhang, Y. Xue, X. Yao, H. Cheng and J. Bai, *J. Mater. Chem.*, 2012, **22**, 9082–9085.
178 A. T. Fafarman, W.-k. Koh, B. T. Diroll, D. K. Kim, D.-K. Ko, S. J. Oh, X. Ye, V. Doan-Nguyen, M. R. Crump, D. C. Reifsnyder, C. B. Murray and C. R. Kagan, *J. Am. Chem. Soc.*, 2011, **133**, 15753–15761.
179 C. Erk, A. Berger, J. H. Wendorff and S. Schlecht, *Dalton Trans.*, 2010, **39**, 11248–11254.
180 E. Kaufmann, T. Schwarzl, H. Groiss, G. Hesser, F. Schaffler, L. Palmetshofer, G. Springholz and W. Heiss, *J. Appl. Phys.*, 2009, **106**, 043105.
181 I. U. Arachchige and M. G. Kanatzidis, *Nano Lett.*, 2009, **9**, 1583–1587.
182 J. O. Dimmock, I. Melngailis and A. J. Strauss, *Phys. Rev. Lett.*, 1966, **16**, 1193–1196.
183 W. Ma, J. M. Luther, H. Zheng, Y. Wu and A. P. Alivisatos, *Nano Lett.*, 2009, **9**, 1699–1703.
184 Q. Zhang, T. Sun, F. Cao, M. Li, M. Hong, J. Yuan, Q. Yan, H. H. Hng, N. Wu and X. Liu, *Nanoscale*, 2010, **2**, 1256–1259.
185 S. Bals, M. Casavola, M. A. van Huis, S. Van Aert, K. J. Batenburg, G. Van Tendeloo and D. l. Vanmaekelbergh, *Nano Lett.*, 2011, **11**, 3420–3424.
186 D. Grodzińska, W. H. Evers, R. Dorland, J. van Rijssel, M. A. van Huis, A. Meijerink, C. de Mello Donegá and D. Vanmaekelbergh, *Small*, 2011, **7**, 3493–3501.
187 D. Grodzinska, F. Pietra, M. A. van Huis, D. Vanmaekelbergh and C. de Mello Donegá, *J. Mater. Chem.*, 2011, **21**, 11556–11565.
188 T. H. Nguyen, J. Habinshuti, Y. Justo, R. Gomes, G. Mahieu, S. Godey, J. P. Nys, S. Carrillo, Z. Hens, O. Robbe, S. Turrell and B. Grandidier, *Phys. Rev. B: Condens. Matter Mater. Phys.*, 2011, **84**, 195133.
189 E. Lifshitz, M. Brumer, A. Kigel, A. Sashchiuk, M. Bashouti, M. Sirota, E. Galun, Z. Burshtein, A. Q. Le Quang, I. Ledoux-Rak and J. Zyss, *J. Phys. Chem. B*, 2006, **110**, 25356–25365.
190 J. M. Pietryga, D. J. Werder, D. J. Williams, J. L. Casson, R. D. Schaller, V. I. Klimov and J. A. Hollingsworth, *J. Am. Chem. Soc.*, 2008, **130**, 4879–4885.
191 H. Zhao, M. Chaker, N. Wu and D. Ma, *J. Mater. Chem.*, 2011, **21**, 8898–8904.
192 J. M. Luther, H. Zheng, B. Sadtler and A. P. Alivisatos, *J. Am. Chem. Soc.*, 2009, **131**, 16851–16857.
193 P. K. Jain, L. Amirav, S. Aloni and A. P. Alivisatos, *J. Am. Chem. Soc.*, 2010, **132**, 9997–9999.
194 J. Xu, D. Cui, T. Zhu, G. Paradee, Z. Liang, Q. Wang, S. Xu and A. Y. Wang, *Nanotechnology*, 2006, **17**, 5428–5434.
195 J. J. Li, Y. A. Wang, W. Guo, J. C. Keay, T. D. Mishima, M. B. Johnson and X. Peng, *J. Am. Chem. Soc.*, 2003, **125**, 12567–12575.
196 J. H. Warner, A. R. Watt, M. J. Fernee, N. R. Heckenberg and H. Rubinsztein-Dunlop, *Nanotechnology*, 2005, **16**, 479–483.
197 A. Falqui, G. Bertoni, A. Genovese, S. Marras, M. Malerba, I. R. Franchini and L. Manna, *Microsc. Res. Tech.*, 2010, **73**, 944–951.
198 J. Yang, J. Peng, Q. Zhang, F. Peng, H. Wang and H. Yu, *Angew. Chem.*, 2009, **121**, 4051–4055.
199 J.-S. Lee, E. V. Shevchenko and D. V. Talapin, *J. Am. Chem. Soc.*, 2008, **130**, 9673–9675.
200 B. Mukherjee, A. Peterson and V. Subramanian, *Chem. Commun.*, 2012, **48**, 2415–2417.
201 A. L. Rogach, A. Eychmüller, J. Rockenberger, A. Kornowski, H. Weller, L. Troger, M. Y. Gao, M. T. Harrison, S. V. Kershaw and M. G. Burt, *MRS Online Proc. Libr.*, 1998, **536**, 365.
202 A. L. Rogach, L. Katsikas, A. Kornowski, D. Su, A. Eychmüller and H. Weller, *Ber. Bunsen-Ges. Phys. Chem.*, 1996, **100**, 1772–1778.
203 N. Gaponik, D. V. Talapin, A. L. Rogach, K. Hoppe, E. V. Shevchenko, A. Kornowski, A. Eychmüller and H. Weller, *J. Phys. Chem. B*, 2002, **106**, 7177–7185.
204 N. Gaponik, D. V. Talapin, A. L. Rogach, A. Eychmüller and H. Weller, *Nano Lett.*, 2002, **2**, 803–806.
205 S. F. Wuister, I. Swart, F. van Driel, S. G. Hickey and C. de Mello Donegá, *Nano Lett.*, 2003, **3**, 503–507.
206 D. V. Talapin, S. Haubold, A. L. Rogach, A. Kornowski, M. Haase and H. Weller, *J. Phys. Chem. B*, 2001, **105**, 2260–2263.
207 A. Shavel, N. Gaponik and A. Eychmüller, *J. Phys. Chem. B*, 2006, **110**, 19280–19284.
208 H. Liu, J. S. Owen and A. P. Alivisatos, *J. Am. Chem. Soc.*, 2006, **129**, 305–312.
209 L. Efrat and E. Alexander, *J. Cluster Sci.*, 2007, **18**, 5–18.
210 A. L. Rogach, T. Franzl, T. A. Klar, J. Feldmann, N. Gaponik, V. Lesnyak, A. Shavel, A. Eychmüller, Y. P. Rakovich and J. F. Donegan, *J. Phys. Chem. C*, 2007, **111**, 14628–14637.
211 D. Zhao, Z. He, W. H. Chan and M. M. F. Choi, *J. Phys. Chem. C*, 2008, **113**, 1293–1300.
212 S. Xu, C. Wang, H. Zhang, Q. Sun, Z. Wang and Y. Cui, *J. Mater. Chem.*, 2012, **22**, 9216–9221.
213 H. Zhang, Z. Zhou, B. Yang and M. Gao, *J. Phys. Chem. B*, 2002, **107**, 8–13.
214 Z. Wang, H. Song, H. Zhao and Y. Lv, *Luminescence*, 2012, DOI: 10.1002/bio.2371 (online).
215 Y.-F. Liu and J.-S. Yu, *J. Colloid Interface Sci.*, 2009, **333**, 690–698.
216 Y. Li, L. Jing, R. Qiao and M. Gao, *Chem. Commun.*, 2011, **47**, 9293–9311.
217 V. Lesnyak, S. V. Voitekhovich, P. N. Gaponik, N. Gaponik and A. Eychmüller, *ACS Nano*, 2010, **4**, 4090–4096.
218 V. Lesnyak, A. Wolf, A. Dubavik, L. Borchardt, S. V. Voitekhovich, N. Gaponik, S. Kaskel and A. Eychmüller, *J. Am. Chem. Soc.*, 2011, **133**, 13413–13420.
219 V. Kloper, R. Osovsky, J. Kolny-Olesiak, A. Sashchiuk and E. Lifshitz, *J. Phys. Chem. C*, 2007, **111**, 10336–10341.

220 M.-O. M. Piepenbrock, T. Stirner, M. O'Neill and S. M. Kelly, *J. Am. Chem. Soc.*, 2007, **129**, 7674–7679.
221 K. A. Higginson, M. Kuno, J. Bonevich, S. B. Qadri, M. Yousuf and H. Mattoussi, *J. Phys. Chem. B*, 2002, **106**, 9982–9985.
222 M. Kuno, K. A. Higginson, S. B. Qadri, M. Yousuf, S. H. Lee, B. L. Davis and H. Mattoussi, *J. Phys. Chem. B*, 2003, **107**, 5758–5767.
223 S. B. Qadri, M. Kuno, C. R. Feng, B. B. Rath and M. Yousuf, *Appl. Phys. Lett.*, 2003, **83**, 4011–4013.
224 A. K. Mahapatra and A. K. Dash, *Physica E*, 2006, **35**, 9–15.
225 B. K. Patel, S. Rath, S. N. Sarangi and S. N. Sahu, *Appl. Phys. A: Mater. Sci. Process.*, 2007, **86**, 447–450.
226 J. G. Winiarz, L. Zhang, J. Park and P. N. Prasad, *J. Phys. Chem. B*, 2002, **106**, 967–970.
227 P. S. Nair, T. Radhakrishnan, N. Revaprasadu, G. A. Kolawole and P. O'Brien, *J. Mater. Chem.*, 2004, **14**, 581–584.
228 X. Zhang, Y. Xie, Q. Zhao and Y. Tian, *New J. Chem.*, 2003, **27**, 827–830.
229 J.-F. Zhu, Y.-J. Zhu, M.-G. Ma, L.-X. Yang and L. Gao, *J. Phys. Chem. C*, 2007, **111**, 3920–3926.
230 W. Xu, S. Lou, S. Li, H. Wang, H. Shen, J. Z. Niu, Z. Du and L. S. Li, *Colloids Surf., A: Physicochemical and Engineering Aspects*, 2009, **341**, 68–72.
231 B. B. Pejova, M. Z. Najdoski, I. S. Grozdanov and S. K. Dey, *J. Mater. Chem.*, 1999, **9**, 2889–2892.
232 D. J. Crouch, P. M. Hatton, M. Helliwell, P. O'Brien and J. Raftery, *Dalton Trans.*, 2003, 2761–2766.
233 A. M. M. Abeykoon, M. Castro-Colin, E. V. Anokhina, M. N. Iliev, W. Donner, A. J. Jacobson and S. C. Moss, *Phys. Rev. B: Condens. Matter Mater. Phys.*, 2008, **77**, 075333.
234 P. Howes, M. Green, C. Johnston and A. Crossley, *J. Mater. Chem.*, 2008, **18**, 3474–3480.
235 J. Jang, K. Cho, J. Yun and S. Kim, *Microelectron. Eng.*, 2009, **86**, 2030–2033.
236 S. V. Kershaw, M. Burt, M. Harrison, A. Rogach, H. Weller and A. Eychmüller, *Appl. Phys. Lett.*, 1999, **75**, 1694–1696.
237 A. Rogach, S. V. Kershaw, M. Burt, M. T. Harrison, A. Kornowski, A. Eychmüller and H. Weller, *Adv. Mater.*, 1999, **11**, 552–555.
238 A. L. Rogach, M. T. Harrison, S. V. Kershaw, A. Kornowski, M. G. Burt, A. Eychmüller and H. Weller, *Phys. Status Solidi B*, 2001, **224**, 153–158.
239 M. T. Harrison, S. V. Kershaw, M. G. Burt, A. Rogach, A. Eychmüller and H. Weller, *J. Mater. Chem.*, 1999, **9**, 2721–2722.
240 S. V. Kershaw, M. T. Harrison and M. G. Burt, *Philos. Trans. R. Soc. London, Ser. A*, 2003, **361**, 331–343.
241 V. A. Fishman, V. I. Lainer and I. G. Erusalimchik, *Sov. Electrochem.*, 1969, **5**, 530–536.
242 L. M. Dennis and R. P. Anderson, *J. Am. Chem. Soc.*, 1914, **36**, 822–827.
243 M. V. Kovalenko, E. Kaufmann, D. Pachinger, J. Roither, M. Huber, J. Stangl, G. Hesser, F. Schäffler and W. Heiss, *J. Am. Chem. Soc.*, 2006, **128**, 3516–3517.
244 W.-H. Zhang, J. Yang and J.-S. Yu, *J. Mater. Chem.*, 2012, **22**, 6383–6388.
245 M. Green, G. Wakefield and P. J. Dobson, *J. Mater. Chem.*, 2003, **13**, 1076–1078.
246 M. Green, *Patent*, *WO*0234757, 2002.
247 S. Keuleyan, E. Lhuillier, V. Brajuskovic and P. Guyot-Sionnest, *Nat. Photonics*, 2011, **5**, 489–493.
248 S. Keuleyan, E. Lhuillier and P. Guyot-Sionnest, *J. Am. Chem. Soc.*, 2011, **133**, 16422–16424.
249 S. Kim, T. Kim, S. H. Im, S. I. Seok, K. W. Kim, S. Kim and S.-W. Kim, *J. Mater. Chem.*, 2011, **21**, 15232–15236.
250 M.-O. M. Piepenbrock, T. Stirner, S. M. Kelly and M. O'Neill, *J. Am. Chem. Soc.*, 2006, **128**, 7087–7090.
251 L. S. Li, H. Wang, Y. Liu, S. Lou, Y. Wang and Z. Du, *J. Colloid Interface Sci.*, 2007, **308**, 254–257.
252 A. Priyam, D. E. Blumling and K. L. Knappenberger, *Langmuir*, 2010, **26**, 10636–10644.
253 H. Song, K. Cho, H. Kim, J. S. Lee, B. Min, H. S. Kim, S. W. Kim, T. Noh and S. Kim, *J. Cryst. Growth*, 2004, **269**, 317–323.
254 S. Rath, A. K. Dash, S. N. Sahu and S. Nozaki, *Int. J. Nanosci.*, 2004, **3**, 393–401.
255 S. Rath and S. N. Sahu, *Europhys. Lett.*, 2004, **67**, 294–300.
256 S. Rath and S. N. Sahu, *Surf. Sci.*, 2006, **600**, L110–L115.
257 S. Rath, G. B. N. Chainy, S. Nozaki and S. N. Sahu, *Physica E*, 2005, **30**, 182–185.
258 S. Rath, S. N. Sarangi and S. N. Sahu, *Nanotechnology*, 2008, **19**, 15606.
259 A. M. P. Hussain, S. N. Sarangi and S. N. Sahu, *J. Appl. Phys.*, 2009, **106**, 094306–094311.
260 R. Dornhaus and G. Nimtz, *Narrow-Gap Semiconductors: The Properties and Applications of the Hg1-xCdxTe Alloy System*, Springer-Verlag, Berlin, 1983.
261 A. Rogalski, *Rep. Prog. Phys.*, 2005, **68**, 2267–2326.
262 S. Perkowitz, D. Rajavel, I. K. Sou, J. Reno, J. P. Faurie, C. E. Jones, T. Casselman, K. A. Harris, J. W. Cook and J. F. Schetzina, *Appl. Phys. Lett.*, 1986, **49**, 806–808.
263 A. Tardot, A. Hamoudi, N. Magnea, P. Gentile and J. L. Pautrat, *Appl. Phys. Lett.*, 1993, **62**, 2548–2550.
264 D. Schooss, A. Mews, A. Eychmüller and H. Weller, *Phys. Rev. B: Condens. Matter Mater. Phys.*, 1994, **49**, 17072–17078.
265 S. Haizhu, Z. Hao, J. Jie, Z. Junhu, Q. Gang, W. Chunlei, Y. Bai and W. Zhi Yuan, *Chem. Mater.*, 2008, **20**, 6764–6769.
266 V. Lesnyak, A. Lutich, N. Gaponik, M. Grabolle, A. Plotnikov, U. Resch-Genger and A. Eychmüller, *J. Mater. Chem.*, 2009, **19**, 9147–9152.
267 J. Yang, Y. Zhou, S. Zheng, X. Liu, X. Qiu, Z. Tang, R. Song, Y. He, C. W. Ahn and J. W. Kim, *Chem. Mater.*, 2009, **21**, 3177–3182.
268 B. Tang, F. Yang, Y. Lin, L. Zhuo, J. Ge and L. Cao, *Chem. Mater.*, 2007, **19**, 1212–1214.
269 A. M. Smith and S. Nie, *J. Am. Chem. Soc.*, 2011, **133**, 24–26.
270 S. Taniguchi and M. Green, *J. Mater. Chem.*, 2011, **21**, 11592–11598.
271 S. Taniguchi, M. Green and T. Lim, *J. Am. Chem. Soc.*, 2011, **133**, 3328–3331.

272 B. A. Korgel and H. G. Monbouquette, *Langmuir*, 2000, **16**, 3588–3594.
273 J. D. Doll, G. Pilania, R. Ramprasad and F. Papadimitrakopoulos, *Nano Lett.*, 2010, **10**, 680–685.
274 A. Prudnikau, M. Artemyev, M. Molinari, M. Troyon, A. Sukhanova, I. Nabiev, A. V. Baranov, S. A. Cherevkov and A. V. Fedorov, *Mater. Sci. Eng., B*, 2012, **177**, 744–749.
275 E. Turner, H. Rösner, Y. Huang and J. Corrigan, *J. Cluster Sci.*, 2007, **18**, 764–771.
276 R. E. Bailey and S. Nie, *J. Am. Chem. Soc.*, 2003, **125**, 7100–7106.
277 N. P. Gurusinghe, N. N. Hewa-Kasakarage and M. Zamkov, *J. Phys. Chem. C*, 2008, **112**, 12795–12800.
278 N. Piven, A. S. Susha, M. Döblinger and A. L. Rogach, *J. Phys. Chem. C*, 2008, **112**, 15253–15259.
279 A. Mews, A. Eychmüller, M. Giersig, D. Schooss and H. Weller, *J. Phys. Chem.*, 1994, **98**, 934–941.
280 E. Lifshitz, H. Porteanu, A. Glozman, H. Weller, M. Pflughoefft and A. Eychmüller, *J. Phys. Chem. B*, 1999, **103**, 6870–6875.
281 H. Borchert, D. Dorfs, C. McGinley, S. Adam, T. Möller, H. Weller and A. Eychmüller, *J. Phys. Chem. B*, 2003, **107**, 7486–7491.
282 L. Fradkin, L. Langof, E. Lifshitz, A. Rogach, N. Gaponik, H. Weller and A. Eychmüller, *ChemPhysChem*, 2003, **4**, 1203–1210.
283 L. Fradkin, L. Langof, E. Lifshitz, N. Gaponik, A. Rogach, A. Eychmüller, H. Weller, O. I. Micic and A. J. Nozik, *Physica E*, 2005, **26**, 9–13.
284 A. Mews, U. Banin, A. V. Kadavanich and A. P. Alivisatos, *Ber. Bunsen-Ges. Phys. Chem.*, 1997, **101**, 1621–1625.
285 V. F. Kamalov, R. Little, S. L. Logunov and M. A. El-Sayed, *J. Phys. Chem.*, 1996, **100**, 6381–6384.
286 R. B. Little, C. Burda, S. Link, S. Logunov and M. A. El-Sayed, *J. Phys. Chem. A*, 1998, **102**, 6581–6584.
287 D. Dorfs, H. Henschel, J. Kolny and A. Eychmüller, *J. Phys. Chem. B*, 2004, **108**, 1578–1583.
288 D. Dorfs and A. Eychmüller, *Nano Lett.*, 2001, **1**, 663–665.
289 M. Braun, C. Burda and M. A. El-Sayed, *J. Phys. Chem. A*, 2001, **105**, 5548–5551.
290 D. Dorfs, H. Henschel, J. Kolny and A. Eychmüller, *J. Phys. Chem. B*, 2004, **108**, 1578–1583.
291 A. W. Schill and M. A. El-Sayed, *J. Phys. Chem. B*, 2004, **108**, 13619–13625.
292 M. T. Harrison, S. V. Kershaw, A. L. Rogach, A. Kornowski, A. Eychmüller and H. Weller, *Adv. Mater.*, 2000, **12**, 123–125.
293 O. Schöps, N. Le Thomas, U. Woggon and M. V. Artemyev, *J. Phys. Chem. B*, 2006, **110**, 2074–2079.
294 M. T. Harrison, S. V. Kershaw, M. G. Burt, A. Eychmüller, H. Weller and A. L. Rogach, *Mater. Sci. Eng., B*, 2000, **69–70**, 355–360.
295 S. Kim, B. Fisher, H.-J. Eisler and M. Bawendi, *J. Am. Chem. Soc.*, 2003, **125**, 11466–11467.
296 D.-W. Kim, K. Cho, H. Kim, B. Park, M. Young Sung and S. Kim, *Solid State Commun.*, 2006, **140**, 215–218.
297 J. M. Tsay, M. Pflughoefft, L. A. Bentolila and S. Weiss, *J. Am. Chem. Soc.*, 2004, **126**, 1926–1927.
298 W. Jiang, A. Singhal, J. Zheng, C. Wang and W. C. W. Chan, *Chem. Mater.*, 2006, **18**, 4845–4854.
299 T. Pons, N. Lequeux, B. Mahler, S. Sasnouski, A. Fragola and B. Dubertret, *Chem. Mater.*, 2009, **21**, 1418–1424.
300 V. Buschmann, G. Van Tendeloo, P. Monnoyer and J. B. Nagy, *Langmuir*, 1998, **14**, 1528–1531.
301 X. Jiang, Y. Xie, J. Lu, L. Zhu, W. He and Y. Qian, *J. Mater. Chem.*, 2001, **11**, 584–588.
302 Y. Jiang, B. Xie, J. Wu, S. Yuan, Y. Wu, H. Huang and Y. Qian, *J. Solid State Chem.*, 2002, **167**, 28–33.
303 N. Belman, Y. Golan and A. Berman, *Cryst. Growth Des.*, 2004, **5**, 439–443.
304 J. Liu, P. Raveendran, Z. Shervani and Y. Ikushima, *Chem. Commun.*, 2004, 2582–2583.
305 H. Shi, X. Fu, X. Zhou and Z. Hu, *J. Mater. Chem.*, 2006, **16**, 2097–2101.
306 H. Tan, S. Li and W. Y. Fan, *J. Phys. Chem. B*, 2006, **110**, 15812–15816.
307 Q. Tang, H. J. Song, H. R. Byon, H. J. Yang and H. C. Choi, *Langmuir*, 2007, **23**, 2800–2804.
308 D. Wang, T. Xie, Q. Peng and Y. Li, *J. Am. Chem. Soc.*, 2008, **130**, 4016–4022.
309 D.-S. Wang, W. Zheng, C.-H. Hao, Q. Peng and Y.-D. Li, *Chem.–Eur. J.*, 2009, **15**, 1870–1875.
310 Y.-Y. Kim and D. Walsh, *Nanoscale*, 2010, **2**, 240–247.
311 A. Sahu, A. Khare, D. D. Deng and D. J. Norris, *Chem. Commun.*, 2012, **48**, 5458–5460.
312 Y.-P. Gu, R. Cui, Z.-L. Zhang, Z.-X. Xie and D.-W. Pang, *J. Am. Chem. Soc.*, 2011, **134**, 79–82.
313 J. Yang and J. Y. Ying, *Chem. Commun.*, 2009, 3187–3189.
314 J. Zhu, Y. Shen, A. Xie and L. Zhu, *J. Mater. Chem.*, 2009, **19**, 8871–8875.
315 J. Qu, H. Liu, Y. Wei, X. Wu, R. Yue, Y. Chen and J. Yang, *J. Mater. Chem.*, 2011, **21**, 11750–11753.
316 F. Jiang, Q. Tian, M. Tang, Z. Chen, J. Yang and J. Hu, *CrystEngComm*, 2011, **13**, 7189–7193.
317 A. Sahu, L. Qi, M. S. Kang, D. Deng and D. J. Norris, *J. Am. Chem. Soc.*, 2011, **133**, 6509–6512.
318 M. Yarema, S. Pichler, M. Sytnyk, R. Seyrkammer, R. T. Lechner, G. Fritz-Popovski, D. Jarzab, K. Szendrei, R. Resel, O. Korovyanko, M. A. Loi, O. Paris, G. Hesser and W. Heiss, *ACS Nano*, 2011, **5**, 3758–3765.
319 L. Han, Y. Lv, A. M. Asiri, A. O. Al-Youbi, B. Tu and D. Zhao, *J. Mater. Chem.*, 2012, **22**, 7274–7279.
320 Z. Zhuang, X. Lu, Q. Peng and Y. Li, *Chem.–Eur. J.*, 2011, **17**, 10445–10452.
321 D. H. Son, S. M. Hughes, Y. Yin and A. P. Alivisatos, *Science*, 2004, **306**, 1009–1012.
322 E. M. Chan, M. A. Marcus, S. Fakra, M. El Naggar, R. A. Mathies and A. P. Alivisatos, *J. Phys. Chem. A*, 2007, **111**, 12210–12215.
323 B. Sadtler, D. O. Demchenko, H. Zheng, S. M. Hughes, M. G. Merkle, U. Dahmen, L.-W. Wang and A. P. Alivisatos, *J. Am. Chem. Soc.*, 2009, **131**, 5285–5293.

324 R. D. Robinson, B. Sadtler, D. O. Demchenko, C. K. Erdonmez, L.-W. Wang and A. P. Alivisatos, *Science*, 2007, **317**, 355–358.
325 S.-B. Wang, B. Hu, C.-C. Liu and S.-H. Yu, *J. Colloid Interface Sci.*, 2008, **325**, 351–355.
326 A. Dorn, P. M. Allen, D. K. Harris and M. G. Bawendi, *Nano Lett.*, 2010, **10**, 3948–3951.
327 P. Zuo, S. Zhang, B. Jin, Y. Tian and J. Yang, *J. Phys. Chem. C*, 2008, **112**, 14825–14829.
328 G. D. Moon, S. Ko, Y. Xia and U. Jeong, *ACS Nano*, 2010, **4**, 2307–2319.
329 W. Zhu, W. Wang and J. Shi, *J. Phys. Chem. B*, 2006, **110**, 9785–9790.
330 P. H. C. Camargo, Y. H. Lee, U. Jeong, Z. Zou and Y. Xia, *Langmuir*, 2007, **23**, 2985–2992.
331 R. Vogel, P. Hoyer and H. Weller, *J. Phys. Chem.*, 1994, **98**, 3183–3188.
332 R. Suarez, P. K. Nair and P. V. Kamat, *Langmuir*, 1998, **14**, 3236–3241.
333 E. E. Foos, R. M. Stroud and A. D. Berry, *Nano Lett.*, 2001, **1**, 693–695.
334 C. L. Bowes and G. A. Ozin, *J. Mater. Chem.*, 1998, **8**, 1281–1289.
335 M. V. Kovalenko, W. Heiss, E. V. Shevchenko, J.-S. Lee, H. Schwinghammer, A. P. Alivisatos and D. V. Talapin, *J. Am. Chem. Soc.*, 2007, **129**, 11354–11355.
336 M. V. Kovalenko, D. V. Talapin, M. A. Loi, F. Cordella, G. Hesser, M. I. Bodnarchuk and W. Heiss, *Angew. Chem., Int. Ed.*, 2008, **47**, 3029–3033.
337 J. Ning, K. Men, G. Xiao, B. Zou, L. Wang, Q. Dai, B. Liu and G. Zou, *CrystEngComm*, 2010, **12**, 4275–4279.
338 J. Ning, G. Xiao, T. Jiang, L. Wang, Q. Dai, B. Zou, B. Liu, Y. Wei, G. Chen and G. Zou, *CrystEngComm*, 2011, **13**, 4161–4166.
339 Y. Xu, N. Al-Salim, J. M. Hodgkiss and R. D. Tilley, *Cryst. Growth Des.*, 2011, **11**, 2721–2723.
340 A. Stavrinadis, J. M. Smith, C. A. Cattley, A. G. Cook, P. S. Grant and A. A. R. Watt, *Nanotechnology*, 2010, **21**, 185202.
341 S. G. Hickey, C. Waurisch, B. Rellinghaus and A. Eychmüller, *J. Am. Chem. Soc.*, 2008, **130**, 14978–14980.
342 P. M. Allen and M. G. Bawendi, *J. Am. Chem. Soc.*, 2008, **130**, 9240–9241.
343 S. L. Castro, S. G. Bailey, R. P. Raffaelle, K. K. Banger and A. F. Hepp, *Chem. Mater.*, 2003, **15**, 3142–3147.
344 R. Xie, M. Rutherford and X. Peng, *J. Am. Chem. Soc.*, 2009, **131**, 5691–5697.
345 L. Tian, M. T. Ng, N. Venkatram, W. Ji and J. J. Vittal, *Cryst. Growth Des.*, 2010, **10**, 1237–1242.
346 S. Peng, S. Zhang, S. G. Mhaisalkar and S. Ramakrishna, *Phys. Chem. Chem. Phys.*, 2012, **14**, 8523–8529.
347 S. Liu, H. Zhang, Y. Qiao and X. Su, *RSC Adv.*, 2012, **2**, 819–825.
348 S. Li, Z. Zhao, Q. Liu, L. Huang, G. Wang, D. Pan, H. Zhang and X. He, *Inorg. Chem.*, 2011, **50**, 11958–11964.
349 J. Tang, K. W. Kemp, S. Hoogland, K. S. Jeong, H. Liu, L. Levina, M. Furukawa, X. Wang, R. Debnath, D. Cha, K. W. Chou, A. Fischer, A. Amassian, J. B. Asbury and E. H. Sargent, *Nat. Mater.*, 2011, **10**, 765–771.
350 N. Gaponik, I. L. Radtchenko, M. R. Gerstenberger, Y. A. Fedutik, G. B. Sukhorukov and A. L. Rogach, *Nano Lett.*, 2003, **3**, 369–372.
351 A. Pourret, P. Guyot-Sionnest and J. W. Elam, *Adv. Mater.*, 2009, **21**, 232–235.
352 R. Ihly, J. Tolentino, Y. Liu, M. Gibbs and M. Law, *ACS Nano*, 2011, **5**, 8175–8186.
353 M. V. Kovalenko, M. Scheele and D. V. Talapin, *Science*, 2009, **324**, 1417–1420.
354 M. V. Kovalenko, R. D. Schaller, D. Jarzab, M. A. Loi and D. V. Talapin, *J. Am. Chem. Soc.*, 2012, **134**, 2457–2460.
355 A. Nag, M. V. Kovalenko, J.-S. Lee, W. Liu, B. Spokoyny and D. V. Talapin, *J. Am. Chem. Soc.*, 2011, **133**, 10612–10620.
356 O. E. Semonin, J. C. Johnson, J. M. Luther, A. G. Midgett, A. J. Nozik and M. C. Beard, *J. Phys. Chem. Lett.*, 2010, **1**, 2445–2450.
357 H. Liu and P. Guyot-Sionnest, *J. Phys. Chem. C*, 2010, **114**, 14860–14863.
358 B.-R. Hyun, A. C. Bartnik, L. Sun, T. Hanrath and F. W. Wise, *Nano Lett.*, 2011, **11**, 2126–2132.
359 C. Wang, R. L. Thompson, P. Ohodnicki, J. Baltrus and C. Matranga, *J. Mater. Chem.*, 2011, **21**, 13452–13457.
360 L. Etgar, W. Zhang, S. Gabriel, S. G. Hickey, M. K. Nazeeruddin, A. Eychmüller, B. Liu and M. Grätzel, *Adv. Mater.*, 2012, **24**, 2202–2206.
361 D. M. N. M. Dissanayake, R. A. Hatton, T. Lutz, C. E. Giusca, R. J. Curry and S. R. P. Silva, *Appl. Phys. Lett.*, 2007, **91**, 133506.
362 K. K. Manga, J. Wang, M. Lin, J. Zhang, M. Nesladek, V. Nalla, W. Ji and K. P. Loh, *Adv. Mater.*, 2012, **24**, 1697–1702.
363 M. Gao, Y. Yang, B. Yang, F. Bian and J. Shen, *J. Chem. Soc., Chem. Commun.*, 1994, 2779–2780.
364 M. Gao, Y. Yang, B. Yang, J. Shen and X. Ai, *J. Chem. Soc., Faraday Trans.*, 1995, **91**, 4121–4125.
365 Z. Qiao, Y. Xie, Y. Zhu and Y. Qian, *J. Mater. Chem.*, 1999, **9**, 1001–1002.
366 Z.-P. Qiao, G. Xie, J.-M. Huang, S.-Y. Zhao and X.-M. Chen, *J. Mater. Chem.*, 2002, **12**, 611–613.
367 X.-F. Qian, J. Yin, S. Feng, S.-H. Liu and Z.-K. Zhu, *J. Mater. Chem.*, 2001, **11**, 2504–2506.
368 H. Sun, H. Zhang, J. Ju, J. Zhang, G. Qian, C. Wang, B. Yang and Z. Y. Wang, *Chem. Mater.*, 2008, **20**, 6764–6769.
369 W. Chunxia, J. Roither, R. Kirschschlager, M. V. Kovalenko, M. Brehm, T. Fromherz, K. Qiang, T. Pingheng, L. Jian, C. Hongda and W. Heiss, *Appl. Phys. Lett.*, 2009, **95**, 053107.
370 L. M. Bronstein and Z. B. Shifrina, *Chem. Rev.*, 2011, **111**, 5301–5344.
371 G. Decher, *Science*, 1997, **277**, 1232–1237.
372 D. Wang, A. L. Rogach and F. Caruso, *Chem. Mater.*, 2003, **15**, 2724–2729.
373 A. L. Rogach, D. S. Koktysh, M. Harrison and N. A. Kotov, *Chem. Mater.*, 2000, **12**, 1526–1528.
374 A. L. Rogach, N. A. Kotov, D. S. Koktysh, A. S. Susha and F. Caruso, *Colloids Surf., A: Physicochemical and Engineering Aspects*, 2002, **202**, 135–144.

375 V. Rinnerbauer, K. Hingerl, M. Kovalenko and W. Heiss, *Appl. Surf. Sci.*, 2007, **254**, 291–294.
376 V. Rinnerbauer, K. Hingerl, M. Kovalenko and W. Heiss, *Appl. Phys. Lett.*, 2006, **89**, 193114.
377 P. Olk, B. C. Buchler, V. Sandoghdar, N. Gaponik, A. Eychmüller and A. L. Rogach, *Appl. Phys. Lett.*, 2004, **84**, 4732–4734.
378 J. Roither, M. V. Kovalenko, S. Pichler, T. Schwarzl and W. Heiss, *Appl. Phys. Lett.*, 2005, **86**, 241104.
379 S. I. Shopova, G. Farca, A. T. Rosenberger, W. M. S. Wickramanayake and N. A. Kotov, *Appl. Phys. Lett.*, 2004, **85**, 6101–6103.
380 J. H. Warner, A. R. Watt, E. Thomsen, N. Heckenberg, P. Meredith and H. Rubinsztein-Dunlop, *J. Phys. Chem. B*, 2005, **109**, 9001–9005.
381 A. Watt, T. Eichmann, H. Rubinsztein-Dunlop and P. Meredith, *Appl. Phys. Lett.*, 2005, **87**, 253109.
382 L. Bakueva, G. Konstantatos, L. Levina, S. Musikhin and E. H. Sargent, *Appl. Phys. Lett.*, 2004, **84**, 3459–3461.
383 L. Bakueva, S. Musikhin, M. A. Hines, T.-W. F. Chang, M. Tzolov, G. D. Scholes and E. H. Sargent, *Appl. Phys. Lett.*, 2003, **82**, 2895–2897.
384 D. K. Chambers, Z. Zhang, F. Khatkhatay, S. Karanam, O. Kizilkaya, Y. B. Losovyj and S. Z. Selmic, *J. Phys.: Condens. Matter*, 2008, **20**, 382202.
385 Z. Tan, T. Zhu, M. Thein, S. Gao, A. Cheng, F. Zhang, C. Zhang, H. Su, J. Wang, R. Henderson, J.-i. Hahm, Y. Yang and J. Xu, *Appl. Phys. Lett.*, 2009, **95**, 063510–063513.
386 T. Rauch, M. Boberl, S. F. Tedde, J. Furst, M. V. Kovalenko, G. Hesser, U. Lemmer, W. Heiss and O. Hayden, *Nat. Photonics*, 2009, **3**, 332–336.
387 S. H. Im, H.-J. Kim, S. W. Kim, S.-W. Kim and S. I. Seok, *Energy Environ. Sci.*, 2011, **4**, 4181–4186.
388 J. H. Warner, *Adv. Mater.*, 2008, **20**, 784–787.
389 A. L. Rogach, *Angew. Chem., Int. Ed.*, 2004, **43**, 148–149.
390 C. J. Kiely, J. Fink, M. Brust, D. Bethell and D. J. Schiffrin, *Nature*, 1998, **396**, 444–446.
391 C. J. Kiely, J. Fink, J. G. Zheng, M. Brust, D. Bethell and D. J. Schiffrin, *Adv. Mater.*, 2000, **12**, 640–643.
392 F. C. Meldrum, J. Flath and W. Knoll, *J. Mater. Chem.*, 1999, **9**, 711–723.
393 J. Tang, G. Ge and L. E. Brus, *J. Phys. Chem. B*, 2002, **106**, 5653–5658.
394 Z. Hu, M. D. Fischbein and M. Drndić, *Nano Lett.*, 2005, **5**, 1463–1468.
395 H. E. Romero and M. Drndić, *Phys. Rev. Lett.*, 2005, **95**, 156801.
396 C.-Y. Kuo, M.-S. Su, C.-S. Ku, S.-M. Wang, H.-Y. Lee and K.-H. Wei, *J. Mater. Chem.*, 2011, **21**, 11605–11612.
397 G. Sarasqueta, K. R. Choudhury and F. So, *Chem. Mater.*, 2010, **22**, 3496–3501.
398 Y. Liu, M. Gibbs, J. Puthussery, S. Gaik, R. Ihly, H. W. Hillhouse and M. Law, *Nano Lett.*, 2010, **10**, 1960–1969.
399 M. D. Fischbein, M. Puster and M. Drndić, *Nano Lett.*, 2010, **10**, 2155–2161.
400 M. S. Kang, J. Lee, D. J. Norris and C. D. Frisbie, *Nano Lett.*, 2009, **9**, 3848–3852.
401 W. H. Evers, H. Friedrich, L. Filion, M. Dijkstra and D. Vanmaekelbergh, *Angew. Chem., Int. Ed.*, 2009, **48**, 9655–9657.
402 S. P. Ahrenkiel, P. R. Yu, J. E. Murphy, J. M. Nedeljković and B. S. Donohoe, *J. Microsc.*, 2008, **230**, 382–387.
403 H. Friedrich, C. J. Gommes, K. Overgaag, J. D. Meeldijk, W. H. Evers, B. d. Nijs, M. P. Boneschanscher, P. E. de Jongh, A. J. Verkleij, K. P. de Jong, A. van Blaaderen and D. Vanmaekelbergh, *Nano Lett.*, 2009, **9**, 2719–2724.
404 V. Rinnerbauer, H. J. Egelhaaf, K. Hingerl, P. Zimmer, S. Werner, T. Warming, A. Hoffmann, M. Kovalenko, W. Heiss, G. Hesser and F. Schaffler, *Phys. Rev. B: Condens. Matter Mater. Phys.*, 2008, **77**, 085322.
405 K. Szendrei, M. Speirs, W. Gomulya, D. Jarzab, M. Manca, O. V. Mikhnenko, M. Yarema, B. J. Kooi, W. Heiss and M. A. Loi, *Adv. Funct. Mater.*, 2012, **22**, 1598–1605.
406 Y.-G. Yang, H.-G. Liu, L.-J. Chen, K.-C. Chen, H.-P. Ding and J. Hao, *Langmuir*, 2010, **26**, 14879–14884.
407 E. Lhuillier, S. Keuleyan, P. Rekemeyer and P. Guyot-Sionnest, *J. Appl. Phys.*, 2011, **110**, 033110.
408 V. Rinnerbauer, M. Kovalenko, V. Lavchiev, G. Kocher, J. Roither, W. Heiss and K. Hingerl, *Physica E*, 2006, **32**, 104–107.
409 E. Lhuillier, S. Keuleyan, P. Zolotavin and P. Guyot-Sionnest, *Adv. Mater.*, 2012, **25**, 137–141.
410 A. G. Pattantyus-Abraham, I. J. Kramer, A. R. Barkhouse, X. Wang, G. Konstantatos, R. Debnath, L. Levina, I. Raabe, M. K. Nazeeruddin, M. Grätzel and E. H. Sargent, *ACS Nano*, 2010, **4**, 3374–3380.
411 J. J. Choi, W. N. Wenger, R. S. Hoffman, Y.-F. Lim, J. Luria, J. Jasieniak, J. A. Marohn and T. Hanrath, *Adv. Mater.*, 2011, **23**, 3144–3148.
412 B. Ma, L. Wang, H. Dong, R. Gao, Y. Geng, Y. Zhu and Y. Qiu, *Phys. Chem. Chem. Phys.*, 2011, **13**, 2656–2658.
413 H. J. Lee, J.-H. Yum, H. C. Leventis, S. M. Zakeeruddin, S. A. Haque, P. Chen, S. I. Seok, M. Grätzel and M. K. Nazeeruddin, *J. Phys. Chem. C*, 2008, **112**, 11600–11608.
414 H. Lee, M. Wang, P. Chen, D. R. Gamelin, S. M. Zakeeruddin, M. Grätzel and M. K. Nazeeruddin, *Nano Lett.*, 2009, **9**, 4221–4227.
415 J. B. Sambur, T. Novet and B. A. Parkinson, *Science*, 2010, **330**, 63–66.
416 M. A. Hossain, Z. Y. Koh and Q. Wang, *Phys. Chem. Chem. Phys.*, 2012, **14**, 7367–7374.
417 T.-L. Li, Y.-L. Lee and H. Teng, *Energy Environ. Sci.*, 2012, **5**, 5315–5324.
418 I. Moreels, K. Lambert, D. Smeets, D. De Muynck, T. Nollet, J. C. Martins, F. Vanhaecke, A. Vantomme, C. Delerue, G. Allan and Z. Hens, *ACS Nano*, 2009, **3**, 3023–3030.
419 A. Kigel, M. Brumer, G. Maikov, A. Sashchiuk and E. Lifshitz, *Superlattices Microstruct.*, 2009, **46**, 272–276.
420 D. Oron, A. Aharoni, C. de Mello Donegá, J. van Rijssel, A. Meijerink and U. Banin, *Phys. Rev. Lett.*, 2009, **102**, 177402.
421 D. Cui, J. Xu, T. Zhu, G. Paradee, S. Ashok and M. Gerhold, *Appl. Phys. Lett.*, 2006, **88**, 183111–183113.

422 K. M. Noone, E. Strein, N. C. Anderson, P.-T. Wu, S. A. Jenekhe and D. S. Ginger, *Nano Lett.*, 2010, **10**, 2635–2639.
423 S. W. Tsang, H. Fu, R. Wang, J. Lu, K. Yu and Y. Tao, *Appl. Phys. Lett.*, 2009, **95**, 183505.
424 N. Zhao, T. P. Osedach, L.-Y. Chang, S. M. Geyer, D. Wanger, M. T. Binda, A. C. Arango, M. G. Bawendi and V. Bulovic, *ACS Nano*, 2010, **4**, 3743–3752.
425 S. Günes, H. Neugebauer, N. S. Sariciftci, J. Roither, M. Kovalenko, G. Pillwein and W. Heiss, *Adv. Funct. Mater.*, 2006, **16**, 1095–1099.
426 K. W. Johnston, A. G. Pattantyus-Abraham, J. P. Clifford, S. H. Myrskog, S. Hoogland, H. Shukla, E. J. D. Klem, L. Levina and E. H. Sargent, *Appl. Phys. Lett.*, 2008, **92**, 122111.
427 H. Fu, S.-W. Tsang, Y. Zhang, J. Ouyang, J. Lu, K. Yu and Y. Tao, *Chem. Mater.*, 2011, **23**, 1805–1810.
428 K. Szendrei, W. Gomulya, M. Yarema, W. Heiss and M. A. Loi, *Appl. Phys. Lett.*, 2010, **97**, 203501–203503.
429 J. Gao, J. M. Luther, O. E. Semonin, R. J. Ellingson, A. J. Nozik and M. C. Beard, *Nano Lett.*, 2011, **11**, 1002–1008.
430 C.-C. Lin, D.-Y. Wang, K.-H. Tu, Y.-T. Jiang, M.-H. Hsieh, C.-C. Chen and C.-W. Chen, *Appl. Phys. Lett.*, 2011, **98**, 263509.
431 D.-W. Kim, J. Jang, H. Kim, K. Cho and S. Kim, *Thin Solid Films*, 2008, **516**, 7715–7719.
432 K. Hyunsuk, C. Kyoungah, K. Dong-Won, L. Hye-Ryoung and K. Sangsig, *Appl. Phys. Lett.*, 2006, **89**, 173107.
433 S. Hojun, C. Kyoungah, Y. Junggwon, K. Kiyeol, J. J. Hyung and K. Sangsig, *Solid State Sci.*, 2010, **12**, 1328–1331.
434 B. N. Pal, I. Robel, A. Mohite, R. Laocharoensuk, D. J. Werder and V. I. Klimov, *Adv. Funct. Mater.*, 2012, **22**, 1741–1748.
435 A. K. Rath, M. Bernechea, L. Martinez and G. Konstantatos, *Adv. Mater.*, 2011, **23**, 3712–3717.
436 A. K. Rath, M. Bernechea, L. Martinez, F. P. G. de Arquer, J. Osmond and G. Konstantatos, *Nat. Photonics*, 2012, **6**, 529–534.
437 J. J. Choi, Y.-F. Lim, M. E. B. Santiago-Berrios, M. Oh, B.-R. Hyun, L. Sun, A. C. Bartnik, A. Goedhart, G. G. Malliaras, H. D. Abruña, F. W. Wise and T. Hanrath, *Nano Lett.*, 2009, **9**, 3749–3755.
438 K. S. Leschkies, T. J. Beatty, M. S. Kang, D. J. Norris and E. S. Aydil, *ACS Nano*, 2009, **3**, 3638–3648.
439 B. A. Gregg, *J. Phys. Chem. B*, 2003, **107**, 4688–4698.
440 B. A. Gregg and M. C. Hanna, *J. Appl. Phys.*, 2003, **93**, 3605–3614.
441 A. J. Nozik, *Physica E*, 2002, **14**, 115–120.
442 K. Tvrdy, P. A. Frantsuzov and P. V. Kamat, *Proc. Nat. Acad. Sci. U. S. A.*, 2011, **108**, 29–34.
443 V. I. Klimov, A. A. Mikhailovsky, D. W. McBranch, C. A. Leatherdale and M. G. Bawendi, *Science*, 2000, **287**, 1011–1013.
444 G. Allan and C. Delerue, *Phys. Rev. B: Condens. Matter Mater. Phys.*, 2006, **73**, 205423.
445 K. A. Velizhanin and A. Piryatinski, *Phys. Rev. Lett.*, 2011, **106**, 207401.
446 V. I. Klimov, *J. Phys. Chem. B*, 2006, **110**, 16827–16845.
447 V. I. Klimov, *Appl. Phys. Lett.*, 2006, **89**, 123118.
448 S. J. Kim, W. J. Kim, A. N. Cartwright and P. N. Prasad, *Appl. Phys. Lett.*, 2008, **92**, 191107.
449 S. J. Kim, W. J. Kim, Y. Sahoo, A. N. Cartwright and P. N. Prasad, *Appl. Phys. Lett.*, 2008, **92**, 031107.
450 M. C. Beard, A. G. Midgett, M. Law, O. E. Semonin, R. J. Ellingson and A. J. Nozik, *Nano Lett.*, 2009, **9**, 836–845.
451 R. J. Ellingson, M. C. Beard, J. C. Johnson, P. Yu, O. I. Micic, A. J. Nozik, A. Shabaev and A. L. Efros, *Nano Lett.*, 2005, **5**, 865–871.
452 R. D. Schaller, J. M. Pietryga and V. I. Klimov, *Nano Lett.*, 2007, **7**, 3469–3476.
453 R. D. Schaller, M. Sykora, J. M. Pietryga and V. I. Klimov, *Nano Lett.*, 2006, **6**, 424–429.
454 J. A. McGuire, J. Joo, J. M. Pietryga, R. D. Schaller and V. I. Klimov, *Acc. Chem. Res.*, 2008, **41**, 1810–1819.
455 M. T. Trinh, A. J. Houtepen, J. M. Schins, T. Hanrath, J. Piris, W. Knulst, A. P. L. M. Goossens and L. D. A. Siebbeles, *Nano Lett.*, 2008, **8**, 1713–1718.
456 M. Ji, S. Park, S. T. Connor, T. Mokari, Y. Cui and K. J. Gaffney, *Nano Lett.*, 2009, **9**, 1217–1222.
457 M. Ben-Lulu, D. Mocatta, M. Bonn, U. Banin and S. Ruhman, *Nano Lett.*, 2008, **8**, 1207–1211.
458 J. J. H. Pijpers, E. Hendry, M. T. W. Milder, R. Fanciulli, J. Savolainen, J. L. Herek, D. Vanmaekelbergh, S. Ruhman, D. Mocatta, D. Oron, A. Aharoni, U. Banin and M. Bonn, *J. Phys. Chem. C*, 2007, **111**, 4146–4152.
459 J. J. H. Pijpers, E. Hendry, M. T. W. Milder, R. Fanciulli, J. Savolainen, J. L. Herek, D. Vanmaekelbergh, S. Ruhman, D. Mocatta, D. Oron, A. Aharoni, U. Banin and M. Bonn, *J. Phys. Chem. C*, 2008, **112**, 4783–4784.
460 J. J. H. Pijpers, R. Ulbricht, K. J. Tielrooij, A. Osherov, Y. Golan, C. Delerue, G. Allan and M. Bonn, *Nat. Phys.*, 2009, **5**, 811–814.
461 M. C. Hanna and A. J. Nozik, *J. Appl. Phys.*, 2006, **100**, 074510.
462 G. Nair, L.-Y. Chang, S. M. Geyer and M. G. Bawendi, *Nano Lett.*, 2011, **11**, 2145–2151.
463 D. J. Binks, *Phys. Chem. Chem. Phys.*, 2011, **13**, 12693–12704.
464 A. Pandey and P. Guyot-Sionnest, *Science*, 2008, **322**, 929–932.
465 I. Gdor, H. Sachs, A. Roitblat, D. B. Strasfeld, M. G. Bawendi and S. Ruhman, *ACS Nano*, 2012, **6**, 3269–3277.
466 J. Jasieniak, B. I. MacDonald, S. E. Watkins and P. Mulvaney, *Nano Lett.*, 2011, **11**, 2856–2864.
467 B. I. MacDonald, A. Martucci, S. Rubanov, S. E. Watkins, P. Mulvaney and J. J. Jasieniak, *ACS Nano*, 2012, **6**, 5995–6004.
468 G.-Y. Lan, Z. Yang, Y.-W. Lin, Z.-H. Lin, H.-Y. Liao and H.-T. Chang, *J. Mater. Chem.*, 2009, **19**, 2349–2355.
469 Z. Yang and H.-T. Chang, *Solar Energy Mater. Solar Cells*, 2010, **94**, 2046–2051.
470 J. Tang, L. Brzozowski, D. A. R. Barkhouse, X. Wang, R. Debnath, R. Wolowiec, E. Palmiano, L. Levina, A. G. Pattantyus-Abraham, D. Jamakosmanovic and E. H. Sargent, *ACS Nano*, 2010, **4**, 869–878.

471 R. Debnath, J. Tang, D. A. Barkhouse, X. Wang, A. G. Pattantyus-Abraham, L. Brzozowski, L. Levina and E. H. Sargent, *J. Am. Chem. Soc.*, 2010, **132**, 5952–5953.
472 J. D. Olson, Y. W. Rodriguez, L. D. Yang, G. B. Alers and S. A. Carter, *Appl. Phys. Lett.*, 2010, **96**, 242103.
473 B. Sun, A. T. Findikoglu, M. Sykora, D. J. Werder and V. I. Klimov, *Nano Lett.*, 2009, **9**, 1235–1241.
474 R. Debnath, M. T. Greiner, I. J. Kramer, A. Fischer, J. Tang, D. A. R. Barkhouse, X. Wang, L. Levina, Z.-H. Lu and E. H. Sargent, *Appl. Phys. Lett.*, 2010, **97**, 023109.
475 H. Liu, J. Tang, I. J. Kramer, R. Debnath, G. I. Koleilat, X. Wang, A. Fisher, R. Li, L. Brzozowski, L. Levina and E. H. Sargent, *Adv. Mater.*, 2011, **23**, 3832–3837.
476 K. S. Leschkies, A. G. Jacobs, D. J. Norris and E. S. Aydil, *Appl. Phys. Lett.*, 2009, **95**, 193103.
477 D. A. R. Barkhouse, R. Debnath, I. J. Kramer, D. Zhitomirsky, A. G. Pattantyus-Abraham, L. Levina, L. Etgar, M. Grätzel and E. H. Sargent, *Adv. Mater.*, 2011, **23**, 3134–3138.
478 X. Wang, G. I. Koleilat, J. Tang, H. Liu, I. J. Kramer, R. Debnath, L. Brzozowski, D. A. R. Barkhouse, L. Levina, S. Hoogland and E. H. Sargent, *Nat. Photonics*, 2011, **5**, 480–484.
479 I. Gur, N. A. Fromer, M. L. Geier and A. P. Alivisatos, *Science*, 2005, **310**, 462–465.
480 K. P. Fritz, S. Guenes, J. Luther, S. Kumar, N. S. Sariciftci and G. D. Scholes, *J. Photochem. Photobiol., A*, 2008, **195**, 39–46.
481 Y. Wu, C. Wadia, W. Ma, B. Sadtler and A. P. Alivisatos, *Nano Lett.*, 2008, **8**, 2551–2555.
482 Q. Guo, S. J. Kim, M. Kar, W. N. Shafarman, R. W. Birkmire, E. A. Stach, R. Agrawal and H. W. Hillhouse, *Nano Lett.*, 2008, **8**, 2982–2987.
483 G. I. Koleilat, L. Levina, H. Shukla, S. H. Myrskog, S. Hinds, A. G. Pattantyus-Abraham and E. H. Sargent, *ACS Nano*, 2008, **2**, 833–840.
484 J. M. Luther, M. Law, M. C. Beard, Q. Song, M. O. Reese, R. J. Ellingson and A. J. Nozik, *Nano Lett.*, 2008, **8**, 3488–3492.
485 M. Ogris and A. L. Rogach, *Curr. Opin. Mol. Ther.*, 2010, **12**, 331–339.
486 G. Liu, T. M. H. Lee and J. Wang, *J. Am. Chem. Soc.*, 2004, **127**, 38–39.
487 C.-K. Chiang, Z. Yang, Y. W. Lin, W. T. Chen, H.-J. Lin and H.-T. Chang, *Anal. Chem.*, 2010, **82**, 4543–4550.
488 L. Turyanska, T. D. Bradshaw, J. Sharpe, M. Li, S. Mann, N. R. Thomas and A. Patanè, *Small*, 2009, **5**, 1738–1741.
489 L. Turyanska, T. D. Bradshaw, M. Li, P. Bardelang, W. C. Drewe, M. W. Fay, S. Mann, A. Patane and N. R. Thomas, *J. Mater. Chem.*, 2012, **22**, 660–665.
490 H. Qian, C. Dong, J. Peng, X. Qiu, Y. Xu and J. Ren, *J. Phys. Chem. C*, 2007, **111**, 16852–16857.
491 L. Li, T. J. Daou, I. Texier, T. T. Kim Chi, N. Q. Liem and P. Reiss, *Chem. Mater.*, 2009, **21**, 2422–2429.
492 A. Zintchenko, A. S. Susha, M. Concia, J. Feldmann, E. Wagner, A. L. Rogach and M. Ogris, *Mol. Ther.*, 2009, **17**, 1849–1856.
493 C. Ratanatawanate, A. Chyao and K. J. Balkus, *J. Am. Chem. Soc.*, 2011, **133**, 3492–3497.
494 B. Cho, W. K. Peters, R. J. Hill, T. L. Courtney and D. M. Jonas, *Nano Lett.*, 2010, **10**, 2498–2505.